Università degli Studi di Bergamo

DEPARTMENT OF ENGINEERING AND APPLIED SCIENCES
Ph.D. program in engineering and applied sciences
Technologies for computer science, automation, electronic engineering and mechatronics

Novel wearable sensor systems for cardiovascular monitoring

Relatore
Prof. Valerio Re

Candidato
Andrea Pedrana

Correlatore
Prof. Gianluca Traversi

Academic Year 2019/2020

Contents

List of Figures

List of Tables

Introduction

According to the World Health Organization (WHO), ischemic heart disease is the world's biggest killer in the last 15 years [1]. This kind of heart diseases represents a concern not only for high-income and middle-income economies, but also for low-income and lower-middle-income countries. Heart diseases arise not only as consequences of wrong lifestyles and food habits, but also for the lack of prevention behaviors. In this framework, the early diagnosis plays a key role and may be possible by means of targeted screenings on high-risk patients. Thanks to advances in semiconductor and microelectronic technologies, with utmost achievements in embedded digital and signal processing, RF communication, and power management, we are beholding the increasing diffusion of wearable devices able to detect physiological signals. This kind of systems has to meet several requirements in terms of miniaturization, for an easy to use and non-invasive design, and power consumption, for a higher longevity of the system without the need of being frequently recharged.

This thesis presents the results of the design and the development of two wearable systems which can be used to monitor the cardiovascular system. The presented devices are based on two different techniques: the ECG (Electrocardiogram), used to record the heart electrical activity, and the PPG (Photoplethysmography), an electro-optical method used to detect blood volume variations. The electronic platforms are completed by specific applications that allow to easily interact with the systems without having deep knowledge of their functioning.

Chapter 1 provides a description of some basic concepts of the human cardiovascular system. Moreover, the two techniques used in this research are analyzed in depth. The signals' characteristics and the measurement methods provide an information background useful for a better comprehension about the operation of the presented wearable systems.

In Chapter 2, the development of the wearable platform for ECG measurement is described. The system was designed in order to provide a device capable to record multiple leads in a small form factor. The main aspects of the hardware components and the functioning of the implemented firmware are reported. A custom Android application completes the system providing a simple mean of interaction. Several characterization measurements carried out to assess the performances of the system are presented and a prototype of a t-shirt made with smart-textiles is shown. Finally, a comparison between the system proposed in this work and several state-of-the-art solutions is performed.

Chapter 3 shows the developed in-ear system able to acquire, store and transmit PPG signals. The system was characterized in order to determine the best configuration leading to a good trade-off between power consumption and signal quality. Different algorithms capable of extracting relevant parameters are presented and the results of the validation are shown. Finally, the features of the developed wearable system are compared with the state-of-the-art devices.

Chapter 1

Cardiovascular system and heart monitoring techniques

This chapter describes some basic concepts about the functioning of the cardiovascular system and the heart. Moreover, for the purpose of the current project of research, two different monitoring techniques are presented: the electrocardiogram (ECG) and the photoplethysmography (PPG). The characteristics of the acquired signals and the techniques used for their measurements are useful for a better comprehension of the next chapters.

1.1 The cardiovascular system

In basic terms, the cardiovascular system is made up by different structures: pipes (the blood vessels) filled with fluid (the blood) and connected to a pump (the heart). The pressure generated by the heart causes the blood to flow through the system continuously. The blood picks up the oxygen at the lung alveoli and nutrients in the intestinal epithelium.

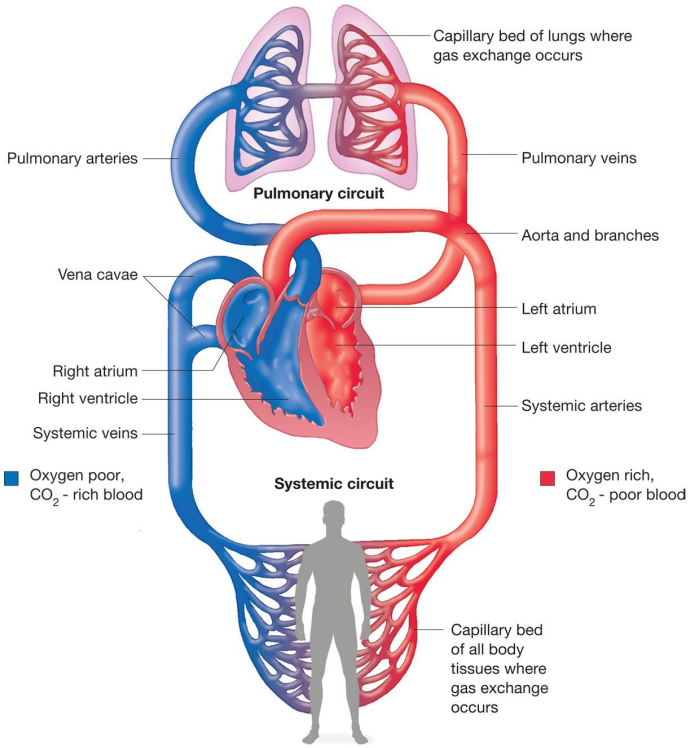

Figure 1.1 – Overview of the cardiovascular system.

The purpose of the blood flow is to distribute, to each biological tissue, all the substances required by the many metabolic activities and, at the same time, to rid the body of catabolites and waste products generated by the cellular metabolism. A steady supply of oxygen is crucial, as many cells, if deprived of it, get irreparably damaged in a very short period of time. Cell-to-cell communication is another key function achieved by means of the cardiovascular system. For example, hormones secreted by the endocrine glands travel in the blood to their specific targets. In general, substances moving in the cardiovascular system can be classified in three categories:

- Nutrients, water and gases coming from the external environment.
- Substances moving from cell to cell inside the body.
- Waste products, such as carbon dioxide and metabolic wastes that are transported to the lungs or kidneys for excretion.

Concerning the blood vessels, they are divided into two types: arteries and veins, both with their respective branches. The term artery denotes all the vessels that deliver the blood from the heart to the periphery, either in the case of the pulmonary circuit and the systemic one. The word vein, on the contrary, indicates the vessels that follow the opposite path. A schematic overview of the cardiovascular system structure is depicted in Figure 1.1.

1.1.1 Physiology of the cardiovascular system

The heart is a muscular organ divided by a central wall, called septum, in left and right halves. Each half functions as an independent pump that consists of an atrium and a ventricle. The atrium receives blood returning from the circulation, whereas the ventricle ejects blood into the blood vessels [2]. The circulation starts from the right atrium that receives, from the superior and inferior vena cava, the blood coming from peripheral tissues. Then the fluid goes, through the ostium of the tricuspid valve, to the right ventricle and it is pumped into the pulmonary artery, that originates at this point. In the following step, the pulmonary artery carries the blood into smaller vessels as arterioles, alveolar capillaries and venules that constitute the pulmonary or small circulation. Then the four pulmonary veins bring the oxygenated blood back to the heart, precisely to the left atrium. From the latter, the fluid flows to the left ventricle via the ostium of the bicuspid (or mitral) valve. The left ventricle now pumps the blood into the aorta that, thanks to its branches, allows the perfusion of all organs and tissues. The transition from the right ventricle to the pulmonary artery takes place at the ostium of the pulmonary valve, whereas the passage from the left ventricle to the aorta occurs through the ostium of the aortic valve. From a functional point of view, the blood that flows into the right atrium via the two venae cavae (superior and inferior) is low oxygenated blood loaded with carbon dioxide. In this form, it passes into the right ventricle and therefore into the pulmonary artery. When the fluid crosses the alveolar capillaries, it becomes arterial, since it acquires oxygen and releases carbon dioxide. Conventionally, as depicted by Figure 1.1, in schematic representations of the cardiovascular system, the well oxygenated blood is represented in red, whereas the blood flowing in the right side of the heart is shown in blue. In living people, the oxygenated blood is bright red, and low-oxygenated blood is darker. Under specific conditions, the low-oxygenated blood can impact the color of certain areas such as fingernails. This condition, known as cyanosis, is the reason why blue is used in drawings. In Figure 1.1 it is also possible to observe how the aorta, the biggest artery, has different

divisions as it leaves the left ventricle. The first branch is represented by the coronary arteries which provide blood supply to the cardiac muscle. The fluid flows into capillaries, then into the coronary veins, which empty directly in the coronary sinus. Ascending branches of the aorta are directed to the arms, head and brain. Descending branches go to the legs and the internal organs such as liver, digestive tract and kidneys.

1.1.2 Anatomy of the heart

The heart is a hollow, uneven and asymmetric organ (Figure 1.2). Typically, it is 12 cm tall, 9 cm wide, and it weights approximately 250-300 g. It lays behind the sternum, on the diaphragmatic muscle, but the main part of it is located in the left hemitorax. For this reason, the left lung has two lobes, instead of three, since part of the space is occupied by the heart [3].

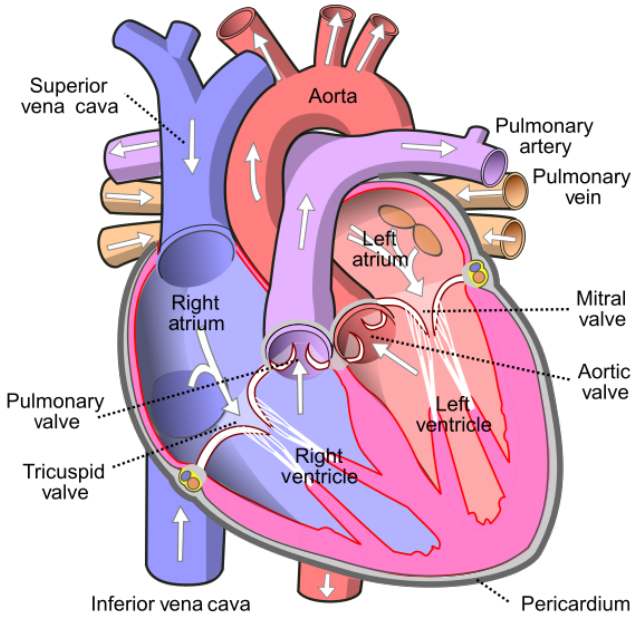

Figure 1.2 – Anatomical view of the human heart [4].

Anatomically, it is divided into two atria (left and right) and two ventricles (left and right). Functionally, there is the distinction between right and left heart. The last differentiation is given by the inflow tract and the outflow tract. The heart consists of several layers:

- Pericardium - it is not exactly a cardiac tissue, because it is like a membranous bag, but it is fundamental in the heart's natural motion. It encompasses a virtual space filled with liquid between two layers (fibrous, external, and serous, visceral). The fluid inside the pericardium lubricates the external surface of the heart as it beats within the sac. Inflammation of the pericardium (pericarditis) may reduce the lubrication to the point that the heart rub against the pericardium causing a sound called friction rub. A hole in this membrane can cause a cardiac tamponade, a common symptom of tuberculosis.
- Epicardium - it covers entirely the external surface of the heart and it is comprised of a layer of adipose tissue and another one called "subepicardial", where the coronaries run.

- Myocardium - it is the main component of the heart and it consists of a muscle, the cardiac muscle, with, in addition, external and internal layers of epithelium and connective tissue. It is an involuntary muscle even if it is striated.

- Endocardium - it is a thin layer of tissue covering the internal surface of the heart. It can be divided into three more layer represented by the endothelium, the lamina propria, and the subendocardic layer.

The atria are the upper chambers, thin walled and separated by the atrial septum. The right side of the septum presents the fossa ovalis cordis, remnant of the embryonic foramen ovale. The right atrium receives blood from the periphery, while the left one from the lungs. The ventricles constitute the main part of the mass of the heart. The left ventricle is 2-3 fold larger than the right one and thicker too. Due to the different shape and function, even the way of contraction is different. Furthermore, they are separated by the interventricular septum.

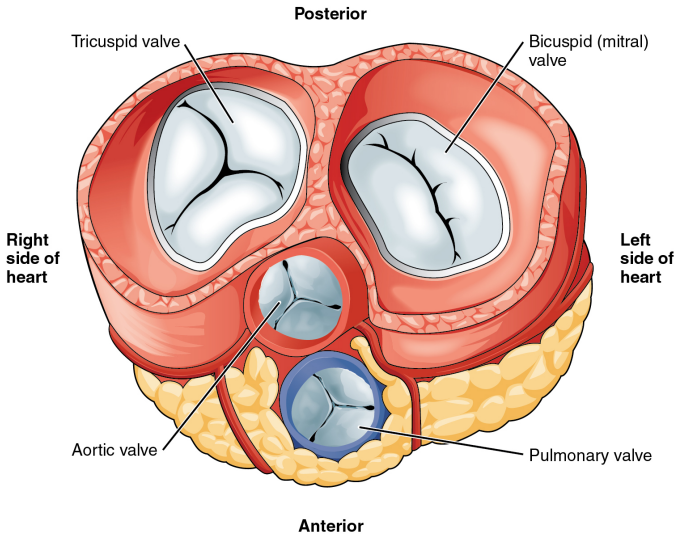

Figure 1.3 – Top view of the heart highlighting cardiac valves [5].

The heart is also equipped with two series of valves that ensure the unidirectionality of the flow. The first ones, the so called atrioventricular (AV) valves, are located, as the name suggests, between the atria and the ventricles. The second series, named semilunar valves, can be found between the ventricles and the arteries. Although these two groups are structurally distinct, they have the same function, since they both avoid the retrograde flow of the blood. The atrioventricular valves are made of thin leaflets of tissue linked at the baseline to a ring of connective tissue. The leaflets are connected to the ventricular side through tendons full of collagen (tendon cords). The valves open and close passively, when they are pushed from the bloodflow. The AV valves are not identical, because the one that separates the right atrium is characterized by three leaflets and therefore is called tricuspid valve, while the one that acts on the left side has only two leaflets and, for this reason, is called bicuspid or mitral valve (because of the resemblance to the tall headdress, known as mitre, worn by bishops). As for the semilunar valves, they are divided into aortic and pulmonary valves and they work on the left and on the right side respectively. Due to their shape (both made with three leaflets), they don't need tendons of connective tissue unlike the AV valves.

1.1.3 Pressure, volume and resistance

Fluids are able to flow from one point to another only if the pressure gradient (ΔP) condition is satisfied, which means that they can move only whether the starting pressure is higher than the ending one [3]. When the heart contracts, the pressure generated is very high and therefore the blood exits from the cardiac organ and goes to the vessels, where the pressure is considerably lower. Due to the friction between the fluid and the vessels wall, a pressure drop occurs and this implies a decreased value along the system. The highest value can be found at the level of the aorta and the systemic arteries once the blood is pumped from the left ventricle. Instead, the lowest pressure lies in the left and right vena cava just before the influx of the blood in the right atrium. The pressure gradient in the systemic circulation is graphically represented in Figure 1.4.

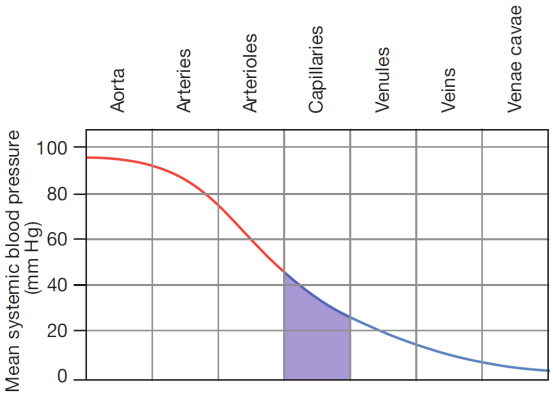

Figure 1.4 – Representation of the pressure gradient in the systemic circulation.

The pressure generated in the ventricles is called "push pressure" because it represents the force that pushes the blood through the blood vessels. As mentioned before, the blood requires a pressure gradient in order to move and this is explained by the following expression:

$$Flow \propto \Delta P \tag{1.1}$$

The relationship shows that there is a direct proportionality between the two quantities, and this implies that the higher is ΔP, the greater is the blood flow. The blood flow, during its pathway, is influenced by the friction performed by the vessels wall which constitutes an obstacle to the flow. The tendency of an hydraulic system in doing that is called resistance (R). An increase of R leads to a reduction of the blood flow in the region when this event happens. In other words, the flow is inversely proportional to the resistance, as shown below:

$$Flow \propto \frac{1}{R} \tag{1.2}$$

R is influenced by three parameters: the radius of the vessel (r), the length of the vessel (L) and the blood viscosity (η). The following equation, derived by the French physician Jean Leonard Marie Poiseuille and known as Poiseuille's law, shows the relationship of these quantities:

$$R = \frac{8L\eta}{\pi r^4} \tag{1.3}$$

Since $^{8}/_{\pi}$ is constant, this factor can be removed from the equation, and the relationship can be rewritten as:

$$R \propto \frac{L\eta}{r^4} \tag{1.4}$$

This expression explains that the resistance to the fluid offered by a tube increases as the length of the tube increases, resistance increases as the viscosity of the fluid increases, whereas there is a resistance reduction when the radius increases. Assuming that the length of the circulatory system remains constant and there is a negligible viscosity change, the radius of the tube has the greatest effect on resistance. If only resistance (R) and radius (r) are considered, it is possible to write the following expression:

$$R \propto \frac{1}{r^4} \tag{1.5}$$

As consequence, a small change in the radius of a blood vessel has a large effect on the resistance to blood flow offered by that vessel. A decrease in the blood vessel radius is known as vasoconstriction, whereas an increase in the blood vessel diameter is called vasodilation. Vasoconstriction decreases blood flow through a vessel, and vasodilation increases it. By combining the results of Equation (1.1) and Equation (1.2) it is possible to obtain the following expression:

$$Flow \propto \frac{\Delta P}{R} \tag{1.6}$$

With the term blood flow, we usually indicate the volume of fluid that crosses a given point of the system in the unit of time. The measuring unit is expressed in L/min or mL/min. Typical values of flow at the aorta level in a male individual of 70 kg are around 5 L/min. The flow must not be confused with the idea of velocity, which is the distance that a given volume of fluid covers in the unit of time. A relationship among these parameters links them with the cross-section of the vessel:

$$v = \frac{Q}{A} \tag{1.7}$$

where v is the velocity, Q is the blood flow, and A is the area of the cross-section of the vessel. The smaller is A and the higher will be the velocity.

1.1.4 Heart contraction and action potential

As regards the ability of the heart to contract, the main part of the cardiac muscle is contractile, but about 1 % of myocardial cells is specialized in the spontaneous generation of action potentials. These cells provide the heart with the unique property of being able to contract without any external stimulus. The considered organ can start the contraction without any connection with other parts of the body because the signal related to the mechanical activity is myogenic, which means that the signal originates inside the cardiac muscle. The cells involved in this kind of activity are a specific type of myocardial cells called autorhythmic or pacemaker cells, since they regulate the heart rate. These cells are anatomically different from the contractile typology, because they are smaller and contain fewer contractile fibers. The cardiac action potential is a brief voltage variation across the cell membrane of heart cells. The mechanism at the base of this potential is the movement of ions (sodium Na^+, potassium K^+, calcium Ca^{2+}) across the inside and the outside of the cell of ions through proteins called ion channels. In a different way with respect to the skeletal muscle cells, the action potential of the cardiac cells is not initiated by the

nervous activity. Action potential activity of the heart can be acquired and recorded in order to produce an electrocardiogram (ECG). Similarly to the skeletal muscle cells, the resting membrane potential due to the different concentration of ions in contractile cells is around −90 mV. When fully depolarized it reaches +20 mV [6]. The cardiac action potential, represented in Figure 1.5, is composed by different phases which determine its shape depicted in :

- **Phase 4: resting membrane potential**. Myocardial contractile cells are characterized by a stable resting potential of −90 mV.
- **Phase 0: rapid depolarization.** Fast sodium channels are responsible of the rapid shift in membrane potential from −90 mV to +20 mV. These channels allow the rapid influx of positive Na^+ ions which cause the depolarization of the membrane potential in a very small amount of time, around 1-2 ms. However, these channels also quickly close and the sodium ions influx is stopped when maximum depolarization of +20 mV is achieved.
- **Phase 1: initial repolarization**. When sodium channels close, a partial repolarization happens due to a brief flow of K^+ ions out of the cell through potassium channels.
- **Phase 2: the plateau.** The action potential flattens into a plateau as the result of two different events: a decrease in K^+ permeability and increase in Ca^{2+} permeability. The combination of Ca^{2+} influx and K^+ efflux determine the action potential plateau phase.
- **Phase 3: rapid repolarization.** The plateau phase ends when the Ca^{2+} channels close and the permeability of K^+ increases once more. During this phase potassium ions have a rapid efflux and the cell returns to its resting potential.

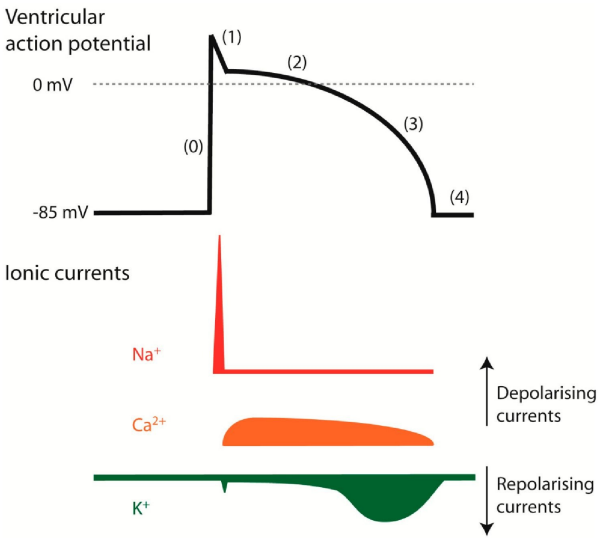

Figure 1.5 – Action potential of cardiac contractile cells [7].

A cardiomyocyte cannot be restimulated by an action potential if it's not yet fully depolarized. This is a key feature of cardiomyocytes known as refractory period. The refractory period in cardiac muscles allows complete emptying of the ventricles prior the next

contraction. It is important to notice that the pacemaker cells, which generate the heart electrical stimulus, have a substantially different behavior with respect to the contractile cells. They are not characterized by a true resting potential, but they generate regular, spontaneous action potentials starting from a membrane potential of about −60 mV.

1.1.5 Electrical conduction

Electrical communication in the heart begins with an action potential generated by an autorhythmic cell and the depolarization spreads rapidly to adjacent cells. The depolarization wave is followed by a contraction wave that passes across the atria, then moves to the ventricles. It generates from the sinoatrial node (SA node), a group of autorhythmic cells located in the right atrium next to the junction of the superior vena cava that represents the main cardiac pacemaker. The depolarization wave spreads rapidly through a conduction system made of non-contractile autorhythmic fibers. A branched internodal pathway connects the SA node to the atrioventricular node (AV node), a group of autorhythmic cells near the floor of the right atrium. From the AV node, the depolarization wave spreads through the Purkinje fibers, specialized conducting cells that transmit signals very rapidly. After a short path in the septum, the AV bundle fibers divide into left and right bundle branches. The bundle branch fibers continue downwards to the heart apex where they divide in smaller fibers that spread out among the contractile cells. The process of action potential generation and conduction is depicted in Figure 1.6.

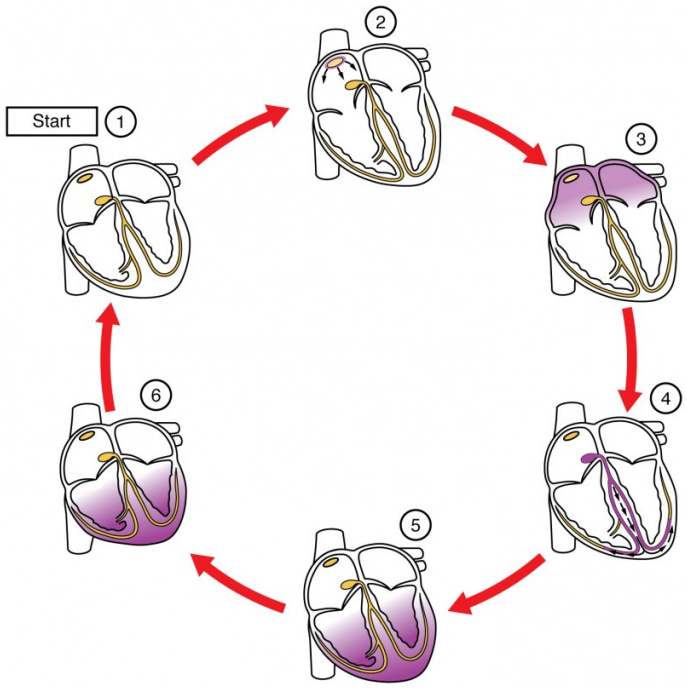

Figure 1.6 – Action potential generation and conduction in the heart [8].

The SA node is the main pacemaker and sets the pace of the heartbeat. Other groups of cells, such as the AV node and the Purkinje fibers, can act as pacemakers under some conditions. However, as their depolarization rate is lower than that of the SA node, they don't usually set the heart rate. This happens because in the heart the pace is set by the fastest pacemaker available. The depolarization rate of the SA node is between 60 and 100 beats per minute, the junctional foci has a firing rate between 40 and 60 bpm, and

the ventricular foci fire action potentials at a rate between 20 and 40 beats per minute. Only in the case when the SA node is damaged and cannot function, one of the other pacemaker (the fastest one available) takes over and the heart rate will match the action potential fire rate of the new pacemaker. In a specific condition known with the name of *complete heart block*, the electrical conduction between the atria and the ventricles node is disrupted and the action potential never reaches the ventricles. In this case, the ventricles are coordinated by their autorhythmic cells which discharge at a rate of 35 bpm. The ventricles will contract at a slower rate with respect to the atria and, if the contractions are too slow to provide an adequate supply of blood, it will be necessary to implant an electrical device, known as pacemaker, that provides impulses which causes the heart to beat at a determined rate.

1.2 Electrocardiography

1.2.1 Electrocardiogram

At the beginning of the XX century a Dutch physician and physiologist, Willem Einthoven, invented the first practical electrocardiogram (ECG or EKG). In 1924 Einthoven was recognized with the Nobel prize in Medicine thanks to his invention. The electrocardiograph is a device able to record the electrical activity of the heart. The cardiological diagnostic exams can be classified in two categories: invasive and non-invasive. Among the non-invasive exams it is worth to cite the following:

- Resting ECG
- Stress ECG test
- Blood exams
- Echocardiography
- Radiology techniques

The main invasive exams are the following:

- Coronary catheterization
- Angiography

Among those, the ECG is the most common and adopted instrumental exam, able to give indirect information about the heart functioning. It is possible to use electrodes placed on the skin of the individual to record the electrical activity because salt solutions, such as the extracellular fluid, are good electrical conductors. The electrical signal is then transmitted to the electrocardiograph by means of conductive cables. The very first electrocardiograph is dated 1887, but the procedure was perfected only at the beginning of 1900 thanks to Einthoven. Einthoven also assigned the letters to the ECG waves and he described the traces of many cardiovascular diseases. He gave the definition of “Einthoven’s triangle”, an imaginary triangle drawn around the heart when electrodes are placed on both arms and on the left leg, as depicted by Figure 1.7. The sides of the triangle are numbered and they correspond to the three bipolar leads, or pair of electrodes, used for the ECG recording. For each lead, an electrode acts as the positive electrode of a lead, while another electrode acts as the negative electrode of the lead. A bipolar lead can be defined in a different way as the electrical potential different between a pair of electrodes. However,

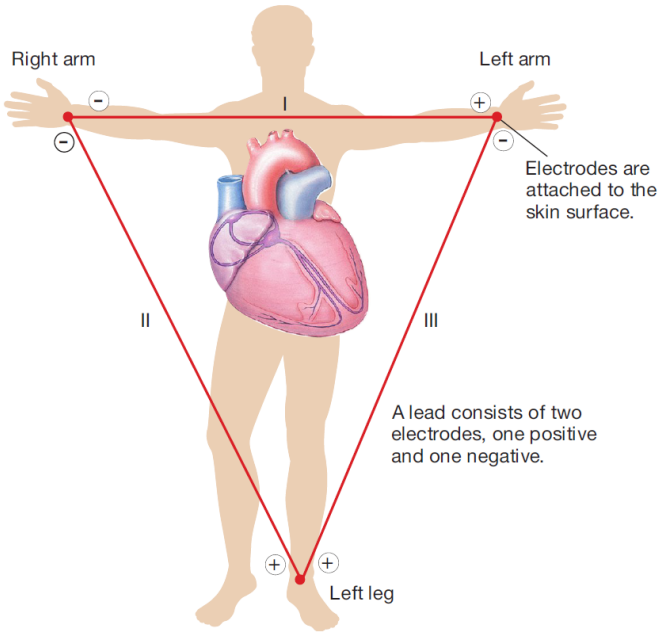

Figure 1.7 – Graphical representation of Eintoven's triangle.

leads can also be derived from the potential difference between a physical electrode and a virtual electrode whose potential reference is defined as the average potential of a group of electrodes. Leads are classified into three types: limb, augmented limb, and precordial. In a typical diagnostic exam, a total of 12 ECG leads are recorded by means of 10 electrodes attached to the patient's body. The 12-lead ECG is composed by three limb leads, three augmented leads, and six precordial leads. Basically each lead allows the system to explore the heart electrical activity from a different angle. The limb and augmented limb leads explore the frontal (or coronal) plane, whereas the precordial leads lie on the transverse (or horizontal) plane. In other words, the ECG makes it possible to explore the depolarization vector (dipole moment) by performing multiple scalar measurements.

Limb leads

The bipolar limb leads are the ones that represent the vertexes of the Einthoven's triangle. The electrodes used to form these signals are located on the limbs, on both arms and on the left leg. Each lead is labeled through a Roman numeral.

- Lead I is the voltage between the left arm (LA) electrode and the right arm (RA) electrode

$$I = LA - RA$$

- Lead II is the voltage between the left leg (LL) electrode and the right arm (RA) electrode

$$II = LL - RA$$

- Lead III is the voltage between the left leg (LL) electrode and the left arm (LA) electrode

$$III = LL - LA$$

Augmented limb leads

The augmented limb leads are derived from the same electrodes used for the bipolar limb leads. They are unipolar leads in the sense that each lead uses a reference potential, the Goldberger's central terminal, as the negative pole. Golberger's central terminal is a combination of inputs from two limb electrodes, with a different combination for each augmented lead.

- Lead augmented vector right (aVR) is the voltage between the right arm electrode and the combination between the left arm and the left leg electrodes

$$aVR = RA - \frac{1}{2}(LA + LL)$$

- Lead augmented vector left (aVL) is the voltage between the left arm electrode and the combination between the right arm and the left leg electrodes

$$aVL = LA - \frac{1}{2}(RA + LL)$$

- Lead augmented vector foot (aVF) is the voltage between the left leg electrode and the combination between the right arm and the left arm electrodes

$$aVF = LL - \frac{1}{2}(RA + LA)$$

Precordial leads

The precordial leads lie on the transverse plane, perpendicular with respect to the other six leads. The six precordial electrodes are used as positive poles for the six corresponding precordial leads: V_1, V_2, V_3, V_4, V_5, V_6. The negative pole is represented by the Wilson's central terminal which acts as a common virtual electrode. The Wilson's central terminal (V_W) is determined as the average potential of the RA, LA, and LL electrodes.

$$V_W = \frac{1}{3}(RA + LA + LL)$$

1.2.2 ECG waves

An ECG trace represents the summed electrical potentials generated by all the cardiac cells. Different components of the signal represents depolarization or repolarization of the atria and the ventricles. Since the depolarization initiates a muscle contraction, the electrical events recorded with the ECG can be associated with the mechanical events of contraction and relaxation. A typical ECG trace can be seen as a (quasi) periodic waveform characterized by two main components: waves and segments. A wave appears as a deflection from the baseline, whereas segments are portion of the signal between two consecutive waves. Intervals can be defined as the combination of waves and segments. As depicted by Figure 1.8, in a normal ECG waveform recorded from lead I, different waves, segments, and intervals can be distinguished:

- **P wave** which corresponds to the depolarization of the atria. It is a small wave with an amplitude between 0.2 mV and 0.4 mV and a variable duration between 60 ms and 120 ms. In this period of time the atria are excited, while the rest of the heart is relaxed.

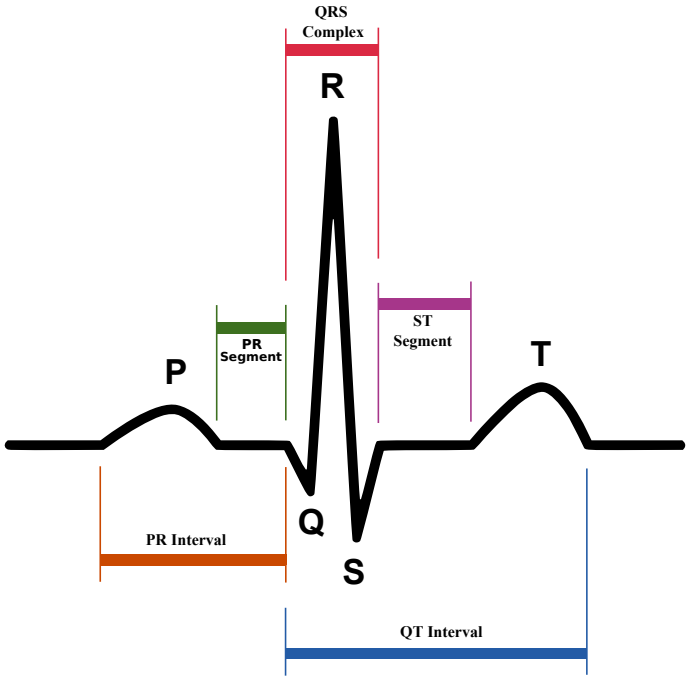

Figure 1.8 – Normal synus rhythm ECG wave [9].

- **QRS complex** which corresponds to the depolarization (activation) of the ventricles and it is composed by three different waves:
  - Q wave, a first small negative deflection which corresponds to the septum depolarization. In this instant, the electrical stimulus is going beyond the bundle of His and its branches.
  - R wave, a positive deflection having a big amplitude with respect to the other waves, which corresponds to the depolarization of the left ventricle apex.
  - S wave, the second negative deflection of the QRS complex, which represents the depolarization of the basal and posterior regions of the left ventricle.

  During the QRS complex the ventricles are exited, while the atria are relaxed. The time duration of the complex is between 60 ms and 90 ms, whereas the amplitude is between 1 mV and 2 mV.

- **T wave** which corresponds to the repolarization of the ventricles. This wave indicates that ventricles are returning in the relaxed state. It has a duration between 180 ms and 200 ms and an amplitude between 0.4 mV and 0.5 mV.

- **PR segment**, the flat line between the end of the P wave to the onset the QRS complex which reflects the slow conduction in the AV node. The PR segments serves as the baseline (called also isoelectric line) of the ECG curve. Any deflection is measured using this segment as reference.

- **ST segment** which is the period between the S wave and the beginning of the T wave. It represents the time interval between the ventricular depolarization and the ventricular repolarization. The ST segment should be an isoelectric line and it must be studied carefully since it is altered by a wide range of conditions. There are two types of alterations: ST segment depressions means that the ST segment is displaced

below the level of the PR segment, whereas ST segment elevation implies that the ST segment is above the level of the PR segment.

- **PR interval** which is the distance from the onset of the P wave to the onset of the QRS complex. This interval is used to assess whether the conduction from the atria to the ventricles is normal.
- **QT interval** which reflects the total duration of the ventricular depolarization and repolarization. It is measured from the onset of the QRS complex to the end of the T wave. The duration of the QT interval is inversely related to the heart rate and at rest it is usually between 350 ms and 440 ms.

The repolarization of the atria is not represented because it is hidden by the ventricles depolarization. Moreover, in certain acquisitions it is possible to observe a small wave which comes after the T wave. It is called the "U wave" and it is thought to represent the repolarization of the Purkinje fibers. However, the exact genesis of the U wave is yet to be discovered. It is important to notice that the mechanical events (contraction and relaxation) have a small time delay with respect to the electrical signals.

1.2.3 ECG interpretation

An electrocardiogram provides valuable information concerning the heart rate, the conduction of the electrical signal, and the condition of the heart tissues. Interpreting some details can be quite challenging and, for this reason, the ECG must be read in a systematic way [10]. Many parameters and dysfunctions can be extracted from the traces and some of them are listed below:

- **Rhythm** - The sinus rhythm, which is the normal rhythm, should have the following characteristics: a frequency between 50 and 100 bpm, each P wave preceding the QRS complex, a positive deflection of the P wave in lead II and a constant PR interval. A heart frequency below 50 bpm can indicate a sinus bradycardia or more serious conditions. On the other hand, a heart rate faster than 100 bpm is called tachycardia. If the rhythm is not regular, there is the presence of an arrhythmia.
- **P wave and PR interval** - P wave must be positive in lead II otherwise the rhythm cannot be sinus rhythm, whereas the PR interval must be between 12 ms and 22 ms in all leads. The PR interval in an indicator of different types of AV blocks .
- **QRS complex** - QRS complex duration, shape, and amplitude is a main indicator of different dysfunctions.
- **ST segment** - The ST segment should be flat and isoelectric, but it may be slightly upsloping in the transition with the T wave. A benign ST segment elevation is very common, particularly in the precordial leads (V2 to V6). ST segment depression is quite uncommon an particularly suspicious in the chest leads.
- **T wave** - The T wave should be concordant with the QRS complex and positive in most leads. When analyzing chest leads, the amplitude should be higher in lead II. In precordial leads the maximum amplitude should be reached in V2-V3. An inverted T wave is accepted in lead V1 and III, whereas it may indicates and ischemia (post or ongoing) if a T wave inversion happens on other leads.

Additionally, it is fundamental to compare the ECG with previous recordings on the same subject. All changes are of interest and may indicate pathology.

1.2.4 Electrocardiograph

The electrocardiograph is an instrument able to acquire and record ECG traces. Electrocardiographs, or ECG devices, can range from wearable or portable handheld units with a cost lower than 200 $, to clinical instruments that cost many thousands of dollars [11]. A generic block diagram of a diagnostic electrocardiograph can be seen in Figure 1.9.

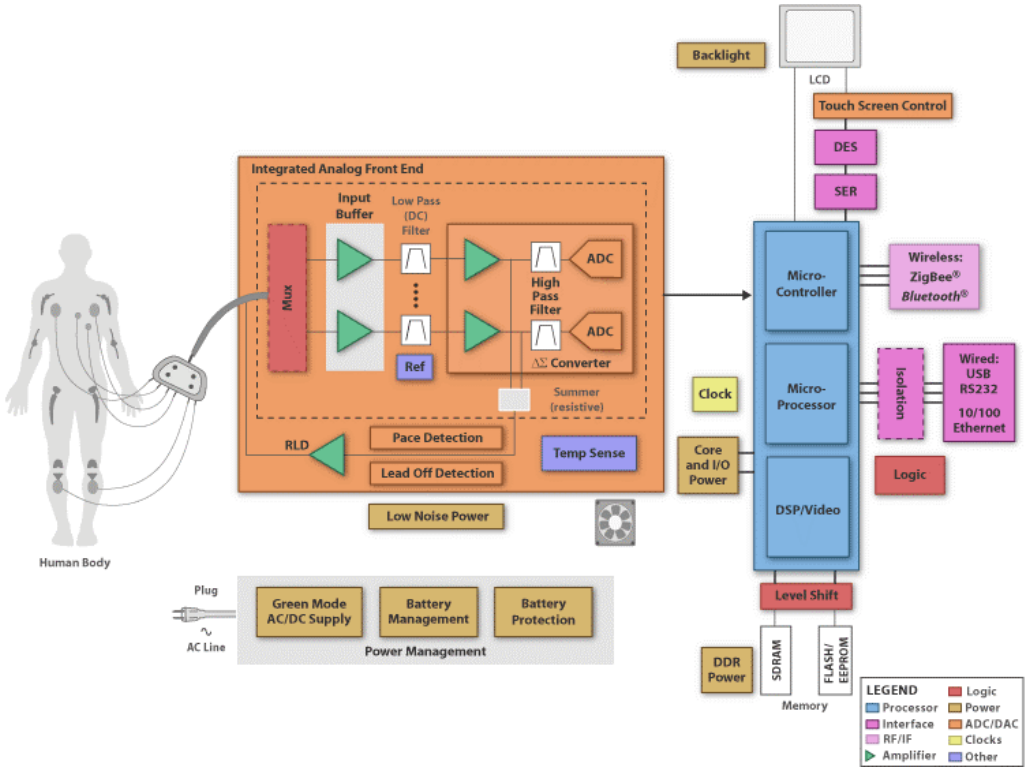

Figure 1.9 – Block diagram of a diagnostic electrocardiograph.

Even though the performance and the design details can vary a lot depending on the final application, the basics of the ECG measurement are the same for all the devices. All ECG pick up the signals through electrodes places on specific locations on the individual's body. According to the application, an ECG device can be designed to record from 1 to 12 leads (referred to as channels as well). In addition to bioelectric signals, some devices are able to detect two artificial signals:

- **pace** signal which comes from implanted pacemakers. The pace signal has a relatively short duration, typically from tens of microseconds to some milliseconds, with an amplitude between few millivolts to nearly a volt. Often, the electrocardiograph must be capable of detecting the pace signal while preventing it from corrupting the signals coming from the heart

- **lead-off** signal, used to detect situations when an electrode is making a poor contact with the subject's skin. To accomplish this, many ECG devices generates a signal to measure the impedance between the electrode and the body and alert whenever this becomes too high. Some ECG are also able to use the same principle of measurement in order to detect the respiration rate. The lead-off measurement may be carried out using DC or AC signals.

Electrodes

The mechanism of electric conductivity inside the body involves ions as charge carriers [12]. Thus, the process of picking up bioelectric signals involves the transduction of ionic currents into electric currents required by electrical instrumentation. This function is carried out by electrodes made of electrical conductors in contact with the aqueous ionic fluids of the body. At the interface between an electrode and an ionic solution redox (reduction-oxidation) reactions have to occur for a charge to be transferred between the electrode and the solution. The interaction between a metal in contact with a solution of its ions produces a local change in the concentration of ions near the metal surface. This causes the charge neutrality not to be conserved in this region and the electrolyte surrounding the metal is at a different potential with respect to the rest of the solution. Therefore, a potential difference known as half-cell potential exists between the metal and the bulk of the electrode. Different potentials occur for different materials and the half-cell potential is important when using electrodes for DC or low frequency measurements. The half cell potential for different materials is depicted in Table 1.1.

Metal and reaction	Half cell potential [V]
$Al \rightarrow Al^{3+} + 3e^{-}$	-1.706
$Ni \rightarrow Ni^{2+} + 2e^{-}$	-0.230
$H_2 \rightarrow 2H^{+} + 2e^{-}$	0.000 (by def.)
$Ag + Cl^{-} \rightarrow AgCl + e^{-}$	+0.233
$Ag \rightarrow Ag^{+} + e^{-}$	+0.799
$Au \rightarrow Au^{+} + e^{-}$	+1.680

Table 1.1 – Half cell potentials for different materials and reactions.

However, this potential can be altered when current is passing through the electrode which causes an effect known as polarization, which consists in an alteration of the charge distribution in the solution in contact with the electrode. Non-polarized electrodes allow the current to pass freely across the electrode-electrolyte interface without changing this charge distribution. The silver-silver chloride electrode has characteristic similar to a perfectly non-polarizable electrode and, for this reason, it is widely used in biomedical applications. Additionally, Ag/AgCl electrodes exhibit less electrical noise than the polarizable counterparts making them suitable for the measurement of very low voltage signals.

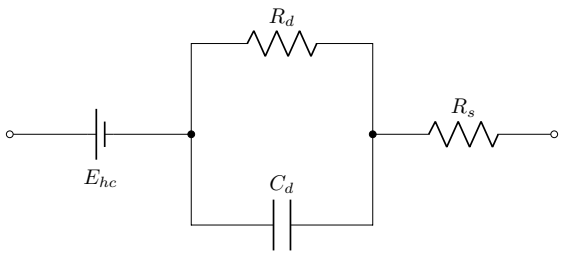

Figure 1.10 – Equivalent circuit model of an electrode.

The electrical behavior of an electrode is generally non linear and under the assumption

of low voltages and currents can be described by means of the equivalent circuit depicted in Figure 1.10, in which:

- R_d and C_d represents the electrode-electrolyte impedance
- R_s models the electrical resistance of the electrode and the wires connected to it
- E_{hc} is the half-cell potential

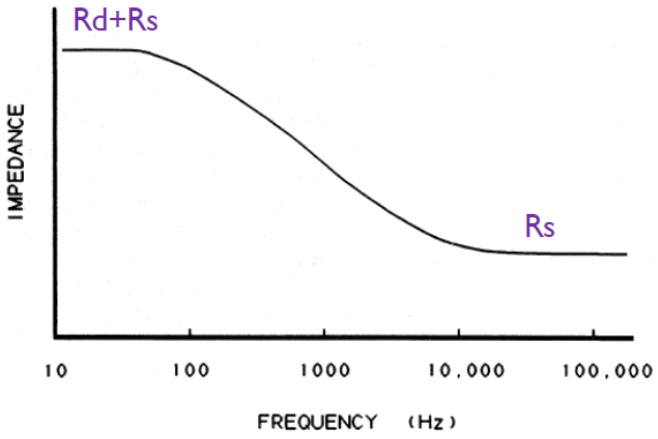

Figure 1.11 – Electrode impedance characteristic.

The electrical parameters of the electrode's model can be extracted by measuring the impedance at high and low frequencies, as shown in Figure 1.11. Different types of skin electrodes are available for the ECG measurement and some of them are the following:

- Disposable electrode - It is the typical electrode most used in clinical measurements and it is characterized by the lowest per-unit cost. It consists of a silver plated snap button in contact with a small silver-silver chloride disk making contact with a sponge impregnated with high viscosity electrolytic gel. The whole structure is kept against the skin by means of an insulating and adhesive disk.
- Suction electrode - Sometimes it is used in precordial leads and they are kept in position thanks to the rubber bulb which is pressed and then released when the electrode is places on the skin. Its main advantage is the ease of use and the ability to make a measurement and move it to another point to repeat the measurement.
- Flexible electrode - It is specifically used for neonates monitoring. It is basically a metal plate electrode in which the thickness of the metal is less than a micrometer. The metal film is supported by a polyester or polyimide substrate. This kind of electrode is x-ray transparent since the metal layer is very thin. Electrodes does not need to be removed during x-rays thus avoiding substantial skin irritation in infants.

ECG analog front-end architectures

The first useful step for the design of an analog front end is to understand the characteristics of the signal that has to be processed by the system. The ECG front-end must be able to deal with a weak signal ranging from 0.5 to 5.0 mV, combined with a DC component with an amplitude up to ±300 mV due to the electrode-skin contact, and common mode components

up to 1.5 V. A standard clinical ECG application has a bandwidth of 0.05 Hz to 150 Hz. For monitoring purposes, the bandwidth can range from 0.5 Hz to 50 Hz, whereas it can reach 1 kHz for pacemaker detection. The amplitude and the ECG signal in combination with its required resolution, determine the dynamic range requirement of the front-end. The frequency components of the signal and the final application for the device, set the bandwidth requirement of the front-end. The skin-electrode interface gives a DC offset that must be taken into account in such a way that the signal chain does not saturate. There are two possible solutions of managing this offset: eliminate it completely or preserve it. In addition, ECG signals can be corrupted by several sources of disturbances [13] such as:

- Power-line interference with a frequency of 50-60 Hz and harmonics picked up from the power mains
- Variable contact between the electrodes and the skin causing baseline drift
- Motion artifacts that cause an impedance change in the electrode-skin interface
- Muscle contraction which generates electromyogram-typ signals (EMG) which are mixed with the ECG signals
- Respiration which causes a baseline drift
- Electromagnetic interference from other electronic devices picked up by the wires acting as antennas
- Noise coupled from other electronic devices

For an accurate recording all these sources must be considered and filtered out. These disturbances can manifest themselves as either a normal-mode signal or a common-mode signal. Common-mode interference can be mitigated in three possible ways:

- Increasing the isolation of the front-end electronics ground from the earth ground as much as possible
- Increasing the common-mode rejection of the front-end circuitry

Features	Device type					
	Monitor	Diagnostic	Telemetry	Holter	Defibrillator	Consumer
RF immunity	U	U	S	S	S	N
Min. frequency [Hz]	0.05	0.05	0.1	0.1	0.5	0.5
Max. frequency [Hz]	500	500	50	150	40	40
ADC sample rate [kHz]	1-100	1-100	1	1	0.25	0.25
ADC resolution [bits]	12-20	12-20	12-20	12-20	12	10-12
Right leg drive	A	A	S	S	N	S
Pace detection	A	A	U	U	U	S
Lead-off detection	A	A	U	U	A	S
Respiration	U	S	S	S	S	N
Defib. compatible	A	U	A	U	A	S

A=always, U=usually, S=sometimes, N=never

Table 1.2 – Elecrocardiographs' features depending on the appplication.

- Driving the patient body with a counter-phase common-mode signal. This solution is best known as right leg drive (RLD) [14].

One of the main specifications that determine the performance of an ECG analog front-end is the input referred noise. Typically, medical instrumentation standards impose (e.g. IEC60601-2-51,27) that this value should be lower than $30\,\mu V_{RMS}$. Additionally, many ECG devices are required to tolerate and recover rapidly from a defibrillation event. Table 1.2 summarizes the main features of an analog front-end depending on the application. Moreover, in the following paragraphs two possible architectures will be outlined [15].

AC-coupled analog front-end A first block in the signal chain is intended for patient safety and isolation. The lead selection circuitry makes it possible to determine the electrodes combinations required for each different lead. The ECG electrodes are a high impedance signal sources, therefore instrumentation amplifiers (IA) characterized by high input impedance (more than $10\,M\Omega$) and high CMRR (greater than 100 dB) are used. Before the signal is fed to the ADC an amplification is required in order to exploit its dynamic range. Assuming a typical ADC full-scale voltage of 2.5 V and a maximum amplitude of ECG signals of 5 mV, the total gain should be of 500. The gain is distributed in such a way that the DC component of the ECG signal does not saturate the acquisition chain. In particular, the instrumentation amplifier is set to have a small gain (a typical value should be 5). Thus, a high-pass filter (HPF) with a cut frequency of 0.05 Hz is added to rid the signal of DC component. The signal is then amplified using another amplifier with a high gain value (e.g. 100). This amplifier should be characterized by a low noise value, so it does not dominate the noise of the system. The gain stage is followed by an optional high-pass filter, a multiplexer, and a low-resolution ADC (16 bit). Typically the ADC is a successive approximation register (SAR) type ADC.

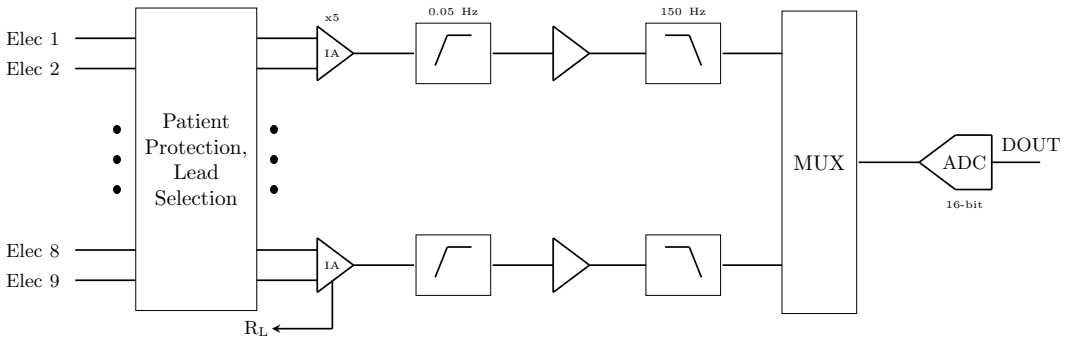

Figure 1.12 – Block diagram of the AC-coupled ECG AFE.

DC-coupled analog front-end The second architecture preserves the DC component of the ECG signal. In this variant exploits a gain stage built upon the same instrumentation amplifier seen for the AD-coupled solution. On the other hand, there is a significant reduction in hardware, which implies both lower power consumption and lower cost. At least two blocks (i.e. the high pass filter and the gain stage) are eliminated. This kind of architecture requires a high-resolution (24 bit) low-noise ADC in order to meet the requirements for a correct representation of the ECG signal. Generally, Dalta-Sigma ($\Delta\Sigma$) ADCs are used for this solution. Filters for the removal of the DC component are typically implemented in a digital way.

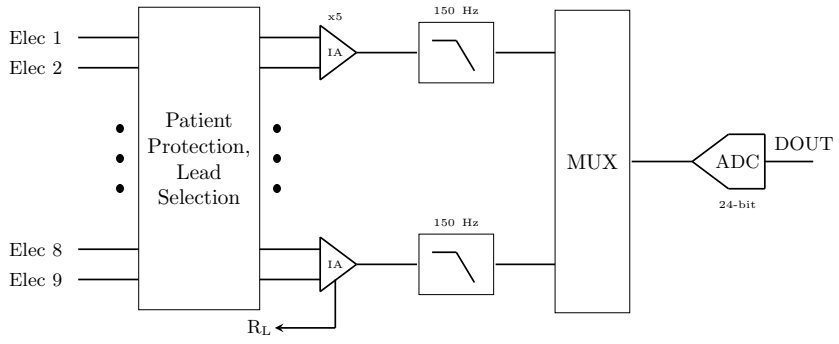

Figure 1.13 – Block diagram of the DC-coupled ECG AFE.

1.3 Photoplethysmography

Photoplethysmography, better known as PPG, is a low-cost and non-invasive electro-optical technique that exploits a light source, usually represented by LEDs, and a photodetector (PD) placed on the skin in order to measure the volumetric variations of blood circulation [16][17]. This is possible because the amount of optical absorption or reflection depends on the quantity of blood that is present in the optical path covered by the PPG sensor [18]. This measurement can provide valuable information concerning the cardiovascular system. The popularity of PPG as a heart rate monitoring method has recently increased, mainly thanks to the simplicity of its operation, the wearing comfort ability, and its cost effectiveness [19].

1.3.1 History of PPG

The origin of the PPG technique can be placed before the first half of the Twentieth century, when two research groups (Militor and Kniazuk of the Merck Institute of Therapeutic Research, New Jersey, and Hanzlik et al. of Stanford University School of Medicine) introduced similar instruments used to measure the blood volume variations in the rabbit ear after venous occlusion and prescription of vasoactive drugs. In the following years, the researcher Alrick Hertzman, from the School of Medicine of St. Louis, published a paper (1937) that contributed significantly to establish the PPG technique. In this article, a description of the reflection mode system was provided, aiming to measure blood volume changes in the fingers. The year after the paper, Hertzman tried to validate the PPG technique by checking the measurements made with that approach and those obtained by mechanical plethysmography. Almost in the same period, he and another researcher, Dillon, splitted the AC and DC components with separate electronic amplifiers and monitored vasomotor activity. Hertzman also understood that potential sources of error can be reduced with good contact between the sensor and the skin, but without excessive pressure that can lead to blanching. For this reason, more elaborated positioning devices have been developed. In more recent decades, thanks to the advancements in opto-electronics and clinical instrumentation, photoplethysmography emerged significantly. Moreover, these changes led to a considerable improvement in size, sensitivity, reliability, and reproducibility of PPG probe design. The major clinical application of PPG technology derives from the pulse oximeter, a non-invasive method for monitoring patients arterial oxygen saturation.

1.3.2 Principle of operation

As aforementioned, a photoplethysmography system is made of a photodetector and a light source, usually LEDs. Two possible configurations [20][21] are available for measuring physiological parameter with the PPG technique (Figure 1.14):

- **Transmissive mode** - the light source and the photodetector are placed on opposite sides of the tissue but directly on it. It allows to obtain a good signal, but the measurement sites are limited, since the position has to guarantee that the transmitted light can be detected. For this reason, the most suitable points are fingertip, earlobe, nasal septum, cheek and tongue. The first two options are the preferred for monitoring, although the perfusion level is low and they are susceptible to environmental conditions; the last three can be used only during anesthesia procedure.
- **Reflective mode** - the light source and the sensor can be placed directly on the same side of the tissue. It does not have problems related to the positioning sites, but it is affected by motion artifacts and pressure disturbances, such as the contact force between the PPG sensor and the measurement point that may deform the arterial geometry by compression.

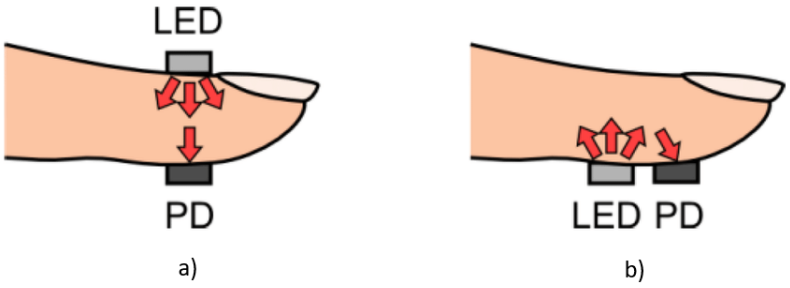

Figure 1.14 – PPG possible configurations: transmissive (a) and reflective (b).

According to the level of depth that has to be reached, a specific wavelength of the light source is chosen. Green and yellow sources have wavelengths of 565 and 590 nm respectively and they are usually adopted in reflective PPG sensors. Red or near infrared light sources, having a wavelength much higher than the other colors (680 - 810 nm), are exploited mostly in transmissive applications. Infrared light is the most used one since it has the deepest level of penetration into the tissues and it is able to reflect the blood pulse from deep tissues. Red and infrared light can penetrate about 2.5 mm, whereas green light penetrates less than 1 mm into tissue [22]. However, several green light based photoplethysmography devices are commercially available, since green has much greater absorbitivity for both oxyhaemoglobin and deoxyhaemoglobin compared to infrared light. This leads to a change in reflected green light that is higher than the infrared one, resulting in a better signal-to-noise ratio for the green light source when blood pulses through the skin.

1.3.3 PPG waveform

The photoplethysmographic waveform consists of two different components: a pulsatile current (AC) and a direct current (DC) [23]. The AC component is synchronized with the heart and it is related to the arterial pulsation, therefore it varies with the same frequency

of the pulse. For this reason, it can be used for the estimation of the heart rate and blood perfusion. The DC component is quasi-constant and refers to the consistency of the tissue in addition to the pulsatile blood. It cannot be considered completely constant because there are slow variations due respiration, thermoregulation and sympathetic nervous system activity. In Figure 1.15 both the waveform components are shown.

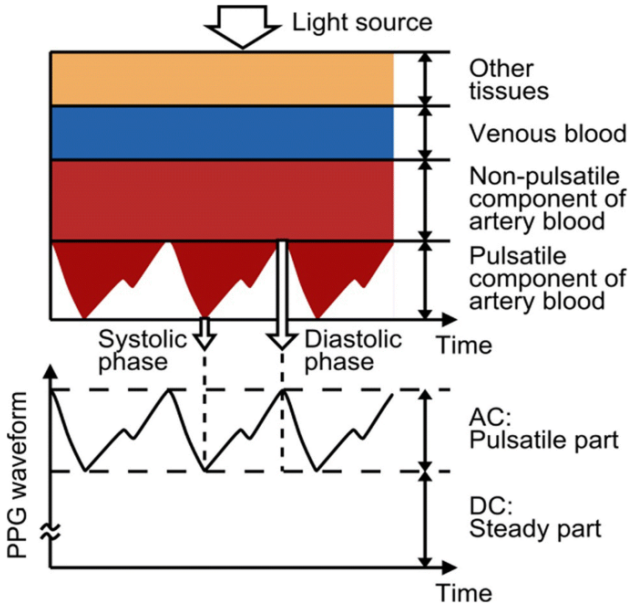

Figure 1.15 – PPG signal waveform and components.

1.3.4 Factors affecting signal quality

A PPG signal typically contains not only the backscattered light coming from the tissue, but also artifacts that derive from ambient light and poor contact with the skin. The quality of the sensor recording is affected by numerous factors such as the subject's skin structure, skin pigments and event the skin temperature. In order to mitigate the negative effects and, at the same time, keep the power consumption low, advanced PPG circuits integrate specialized signal processing and sampling schemes. One of the main tricky objectives in designing wearable devices consists in addressing the contamination of the signal that derives from the ambient light, which continuously changes. Moreover, indoor lights usually possess a flicker that tracks the powerline frequency, obscuring in this way information included in the AC component of a PPG signal. Another factor that has a relevant impact on the sensor recording is represented by the intermittently poor contact between the tissue and the photodetector. This can lead to motion artifacts that make it difficult to measure some physiological parameters during the subject's movement, especially on wearable devices where the action cannot be limited. Additionally, to these concerns whit PPG, the detectable signal magnitude is affected by the melanin concentration of the skin or skin pigments. Melanin, through its structure, attenuates the incident light. It is located in the epidermal layer, where there is no blood supply, so the target for a PPG device is always sub-epidermal. To overcome a weak signal due to dark pigmentation, several possible solutions can be adopted, such as a stronger light source, as well as the selection of a different light wavelength, like near infrared, less affected by melanin absorption [24].

1.3.5 Clinical applications of PPG technique

PPG can be adopted in many different clinical settings, including monitoring of physiological parameters (heart rate, pressure, blood oxygen saturation etc.), vascular assessment (vessels conditions and diseases related to them) and autonomic functions (variability of blood pressure and heart rate, neurological assessment etc.). The heart rate is an important physiological parameter monitored both inside the hospital and in ambulatory environments. As explained before, the AC component of the PPG signal is synchronous with the cardiac activity and therefore it can be used to estimate the heart rate. In pulse oximetry systems, this information is usually obtained with the SpO_2 level (blood oxygen saturation). This information can be determined by pointing red and near infrared light on the skin. The amplitudes of the AC signals related to these wavelengths are sensitive to variations in SpO_2 because of the differences in the light absorption of oxyhaemoglobin and carboxyhaemoglobin at these wavelengths. Then, computing their amplitude ratio and considering PPG DC components, SpO_2 can be estimated. Both the reflection and transmission modes can be exploited to measure this parameter. However, there are some limitations: readings may be affected by dyshaemoglobinaemias that can lead to a drop of the accuracy at low saturation levels. Moreover, a problem related to the confidence degree exists, because the accuracy can be reduced in presence of significant motion artifacts or cardiac arrhythmia. As for blood pressure measurement, it is a significant parameter that needs to be considered in different situations in order to assess some clinical conditions, such as the tracking of the beat-to-beat blood pressure, the autonomic function and vascular diseases. In the literature some approaches that estimate blood pressure exploiting non-invasive PPG-based systems were investigated.

Chapter 2

Wearable system for ECG measurement

This chapter describes the development of a wearable platform for ECG measurement. The system was designed with the aim to provide a miniaturized device able to record the traces of multiple leads. In fact, most of the commercial consumer devices measure only one lead, thus providing incomplete information about the cardiac electrical activity. The hardware and firmware development will be described along with the performance achieved by the platform in terms of power consumption and input referred noise. The system is completed by a mobile app that allows to easily perform measurements. At the end of the current chapter, a comparison between the system proposed in this work and several state-of-the-art solutions is provided.

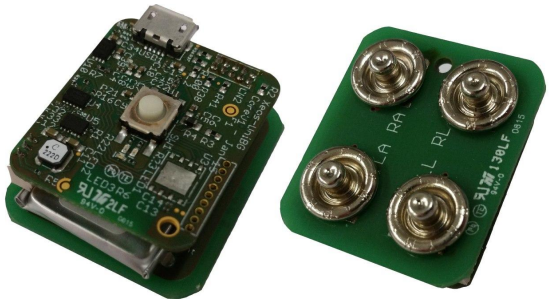

Figure 2.1 – Photograph of the ECG wearable platform.

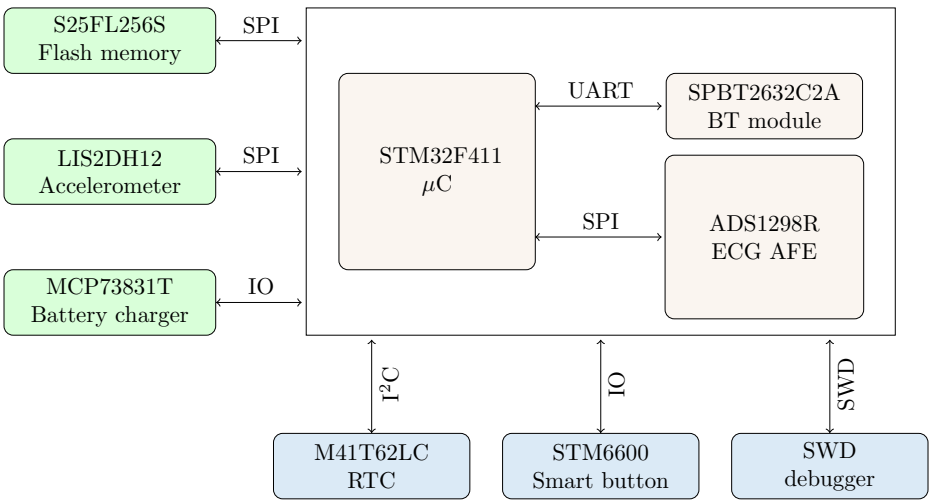

Figure 2.2 – Block diagram of the wearable sensor system for biopotential measurements.

2.1 Hardware

The electronic system presented in this work is the result of a design aiming to provide as many desirable features as possible in a reasonable form factor, in such a way that integration within a wearable system can be easily achieved. As it can be seen by the photograph depicted in Figure 2.1, the system is composed of two different boards: the higher one integrates the main electronics, whereas the lower one provides an interconnection with the ECG cables. The battery is located in between the two boards; the overall form factor achieved is 30 x 25 x 25 mm and the system weights 26 g (case included). Figure 2.2 shows the block diagram of the platform and the main building components of the electronic system are the following:

- **STM32F411VEH6** microcontroller [25] based on the high-performance Arm® Cortex® M4 32-bit RISC core operating at a frequency up to 100 MHz. The processing core features a FPU and implements a full set of digital signal processing (DSP) instructions and a memory protection unit (MPU) which enhances application security. The microcontroller incorporates high-speed embedded memories (512 kB of flash memory and 128 kB of SRAM) and an extensive range of I/Os and peripherals connected to two APB buses and two AHB buses. The STM32F411VEH6 device combines the fairly high processing capabilities to a low power consumption in a miniaturized UFBGA100 package with dimensions of 7 x 7 mm (L x W).

- **TPS62740** buck converter [26] which allows to scale down to the 3.3 V operating voltage. The device is particularly suited for light load since it guarantees up to 90 % efficiency at 10 µA output current. The typical quiescent current of the converter is 360 nA and it supports output currents up to 300 mA. The device features an auxiliary rail that can be used to power subsystems that can be selectively turned off during low power states. The buck converter is available in a small 12 pins 2 x 3 mm WSON package.

- **MCP73831T** linear charge management controller [27] which supervise the charging process of the single cell 155 mAh Li-poly battery (the model was chosen to fit in between the two PCBs). The charge current is set to 50 mA through the specific resistor and the charge is carried out by means of a standard micro-USB 5 V power supply connected to the dedicated port. The integrated circuit is available in a 8 pin 2 x 3 mm DFN package.

- **STM6600** smart push button on/off controller [28]. If the supply voltage is above a threshold, the enable output which allows to power up the system is asserted by a press of the button. An interrupt is triggered by pressing the push-button during normal operation or if an undervoltage condition is detected. With a long-push of the button it is possible to reset the system by disconnecting the power. The controller also offers a debounce feature and it is available in a TDFN12 2 x 3 mm package.

- **ADS1298R** ECG analog front end [29] with integrated delta-sigma ($\Delta\Sigma$) analog-to-digital converters (ADCs) with built-in programmable gain amplifiers (PGAs) and onboard oscillator. The device features will be described deeply in the dedicated subsection. The front end is available in a 8 x 8 mm down-scaled BGA64 package. The required 3 V analog voltage is supplied by means of the **TLV705** Low-Dropout Regulator (LDO) available in a miniaturized DSBGA4 0.77 x 0.77 mm package.

- **LIS2DH12** low-power 3D three-axis accelerometer [30] with a digital SPI interface output. The device features configurable full scales of $\pm 2/\pm 4/\pm 8/\pm 16$ g and selectable output data rates from 1 Hz to 5.3 kHz. It is possible to set interrupt generators for free-fall and motion detection. The IC is available in a 2 x 2 mm VLGA12 package. In this research, the accelerometer was used as a wake up source from low power state and to measure the user's activity. In future developments it will be helpful as it can be exploited in combination with the ECG to estimate energy expenditure [31].
- Epcos **B57861S104F40** NTC thermistor [32] for the measurement of the body temperature at skin level. The sensor is located in the lower board.
- Panasonic **ERTJ1VS104FA** NTC thermistor [33] for ambient temperature measurement. The sensors is placed on the higher board.
- **M41T62** Real Time Clock (RTC) [34] with embedded 32 kHz oscillator. It is available in a small LCC8 1.5 x 3.2 mm package.
- **SPBT2632C2A** class 2 Bluetooth module [35] which allows to communicate up to 10 m at a rate of 560 kbps with Serial Port Profile (SPP) service active. The module is supplied by the auxiliary output of the step-down converter, so in the lowest power consuming states it can be selectively switched off.
- **S25FL256S** NOR flash memory [36] with a capacity of 256 Mbit. It is available in a WSON8 package sized 6 x 8 mm.

The system features an exposed connector which allows to upload the firmware and perform the debug operations by means of the external debugger ST-Link V2 or compatible devices through the offered SWD (Serial Wire Debug) interface. A push button is used to perform some basic operations like startup and power-off. The electronic system is completed by a green and a blue LED that allow to discriminate the operating mode of the wearable platform. Table 2.1 depicts some features of the main components, with a particular focus on the power consumption. Two different interface boards used to interconnect the system with the electrodes were developed. One was used to perform measurements using the standard disposable gel electrodes and features a micro-USB connector suitable for a custom developed ECG cable. The second interface board exposes female button clips and was used to perform measurements with dry textile-based electrodes. The device was enclosed in a 3D printed plastic case which protects the electronics.

Part number	Description	Main features	Current consumption
STM32F411VE	MCU	3x USARTs 4x SPIs 3x I^2Cs 1x SDIO 1x USB 2.0 12 bit ADC 10 timers 512 kB flash memory 128 kB SRAM	128 µA/MHz
TPS62740	Buck converter	Selectable output voltage and output currents up to 300 mA	Up to 96 % efficiency
MCP73831T	Battery charger	Programmable charge current from 15 to 500 mA	1.5 mA charging 1 µA shutdown
STM6600	Smart button	Smart push-button on-off controller	6 µA
ADS1298R	ECG AFE	24 bit ADCs Programmable gain SPI interface	3.25 mA High res. mode
LIS2DH12	Accelerometer	±2 g/±4 g/±8 g/±16 g full scales SPI/I^2C serial interfaces	20 µA @ 100 Hz High res. mode
M41T62	RTC	I^2C serial interface	375 nA
SPBT2632C2A	BT module	UART serial interface SPP service AT2 command set Integrated antenna	11.2 mA Connected, no traffic
S25FL256S	Flash memory	256 Mbit capacity SPI serial interface	100 mA (peak)

Table 2.1 – Main features of the components included in the wearable system for biopotential measurements.

2.1.1 ADS1298R Analog Front End

The ADS1298R analog front-end used for ECG measurements deserves a separate in-depth analysis. As depicted by the functional block diagram in Figure 2.3, the integrated circuit incorporates simultaneous sampling, 24 bit, delta-sigma ($\Delta\Sigma$) ADCs with built-in programmable gain amplifiers, internal reference and onboard oscillator. The ADS1298R incorporates all the features commonly required in medical instrumentation for electrocardiogram applications and enables the development of down-scaled devices. Even if the chip integrates ECG specific circuitry, it is suitable also for other kinds of biopotential measurements such as electromyography (EMG) or electroencephalography (EEG). The

ADS1298R operates at output data rates from 250 Hz to 32 kHz allowing the pace detection by means of specific procedures. The right leg drive (RLD) subcircuit allows to select any combination of the input channels to generate the corresponding signal and lead-off detection can be performed through the internal circuitry. Moreover, the ADS1298R include an integrated respiration impedance measurement function which is useful to detect the respiration rate and sleep apnea. In the following sections, the features leveraged in the development of the wearable platform are described.

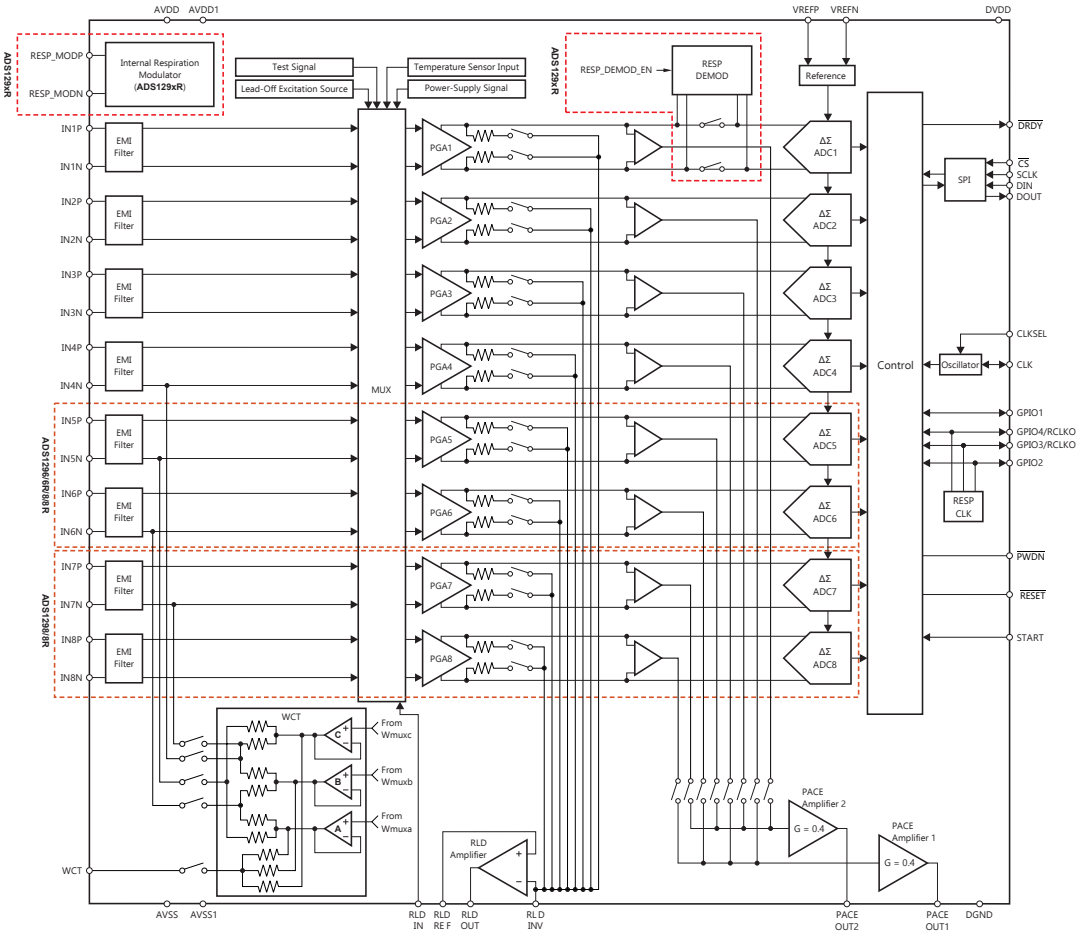

Figure 2.3 – ADS1298R functional block diagram.

Power-up sequencing and conversion

All digital and analog input signals of the AFE must be kept low until the power supplies have stabilized, as shown in Figure 2.4. When the voltages reaches their final value, it is possible to supply master clock signal to the `CLK` pin. After waiting for a time t_{POR} or after `VCAP1` voltage is greater than 1.1 V, whichever time is longer, a reset pulse can be sent. It can be transmitted using either the $\overline{\texttt{RESET}}$ pin or `RESET` command to initialize the digital portion of the chip. After releasing the $\overline{\texttt{RESET}}$ pin, the configuration registers can be programmed. The `START` command enables the samples conversion according to the saved configuration. This command can be transmitted at any time; if the conversions are already in progress, there will be no effects. The conversion process can be stopped by means of the `STOP` command. `RDATAC` command allows to download the acquired samples when

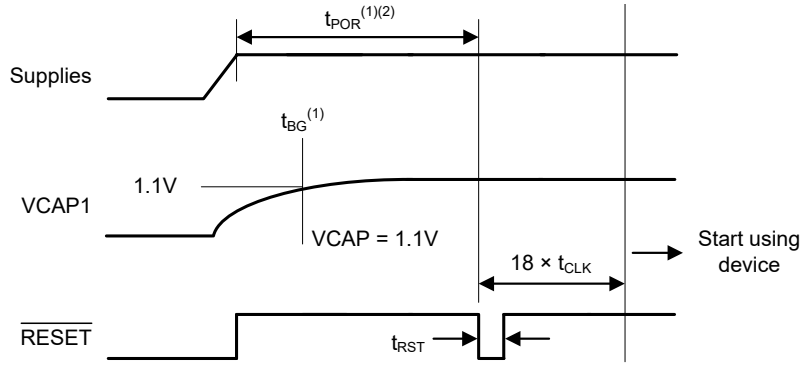

Figure 2.4 – ADS1298R power-up timing diagram.

all the ADS1298R channels ended the data conversion; this event is signaled through the $\overline{\texttt{DRDY}}$ signal. The data download procedure can be triggered by an interrupt conveniently configured on the host microcontroller. Continuous data conversion is the default mode, but it is possible to configure the analog front end to perform a single readout. The read operation can overlap the occurrence of the next $\overline{\texttt{DRDY}}$ event without data corruption. Data readback is preceded by a status word containing the values for `LOFF_STATP`, `LOFF_STATN` and part of `GPIO` registers. Therefore, the number of bits of the data output is equal to 24 status bits + 24 bits per channel x 8 channels = 216 bits. The data format for each channel is represented in two's complement and MSb first. The LSb has a weight of $V_{REF}/2^{23} - 1$ and for the developed system $V_{REF} = 2.4V$. The commands which determine the operations of the ADS1298R are listed in Table 2.2.

Command	Description	1st Byte	2nd Byte
System commands			
`WAKEUP`	Wake up from standby mode	`00000010 (0x02)`	
`STANDBY`	Enter standby mode	`00000100 (0x04)`	
`RESET`	Reset the device	`00000110 (0x06)`	
`START`	Start/restart (synchronize) conversions	`00001000 (0x08)`	
`STOP`	Stop conversions	`00001010 (0x0A)`	
Data read commands			
`RDATAC`	Enable read data in continuous mode	`00010000 (0x10)`	
`SDATAC`	Stop read data in continuous mode	`00010001 (0x11)`	
`RDATA`	Read data by command	`00010010 (0x12)`	
Register read commands			
`RREG`	Read `nnnnn` registers starting at addess `rrrrr`	`001rrrrr`	`000nnnnn`
`WREG`	Write `nnnnn` registers starting at addess `rrrrr`	`010rrrrr`	`000nnnnn`

Table 2.2 – ADS1298R commands list.

Input channels

The ADS1298R input stage allows a flexible configuration of each input channel as can be seen by the block diagram in Figure 2.5. It is possible to selectively power-down channels, choose the signal to be measured, and set the desired gain.

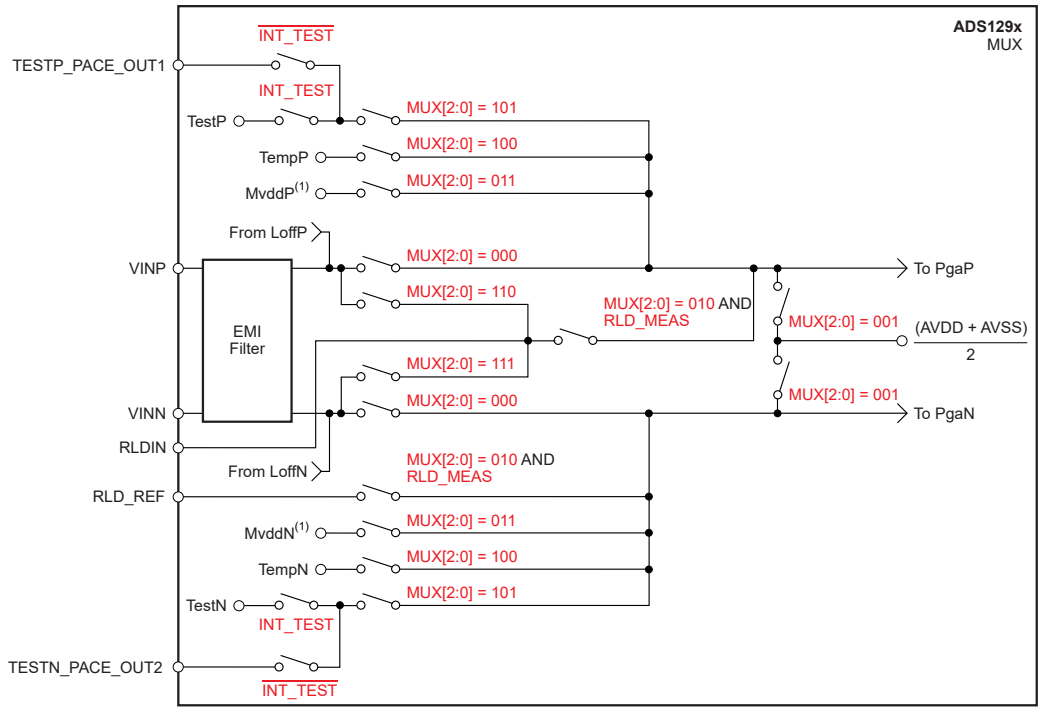

Figure 2.5 – ADS1298R input multiplexer structure for one channel.

The configuration is established by the values set in `CHnSET` registers (`n` spans form 1 to 8 and identifies the register associated with a specific channel). The gain field (bits 6:4) determines the PGA gain setting configurable from 1 to 12 in the following steps: 1, 2, 3, 4, 6, 8, 12. The input channel selection can be performed by writing the multiplexer field (bits 2:0). `TEST_PACE_OUT1`, `TEST_PACE_OUT2` and `RLD_IN` are common signals to all the eight blocks, whereas `VINP` and `VINN` are separate for each channel and they are directly connected to the input pins of the analog front-end. Each input can be shorted in order to perform offset or noise measurements. It is suggested that, if a channel is powered down, the input should be shorted as well. During standard operation, the default setting is "normal electrode input".

Right Leg Drive (RLD)

As described in the previous chapter, the right leg drive (RLD) circuit allows to reduce the common-mode interference in an ECG system. The RLD circuit senses the common-mode voltage of a selected set of electrodes and creates a negative feedback loop by driving the body with an inverted common-mode signal. As depicted in Figure 2.6, the ADS1298R integrates multiplexers that allow to select the set of signals used for the feedback. The reference voltage for the RLD circuitry is generated internally and it is equal to ([AVDD + AVSS] / 2).

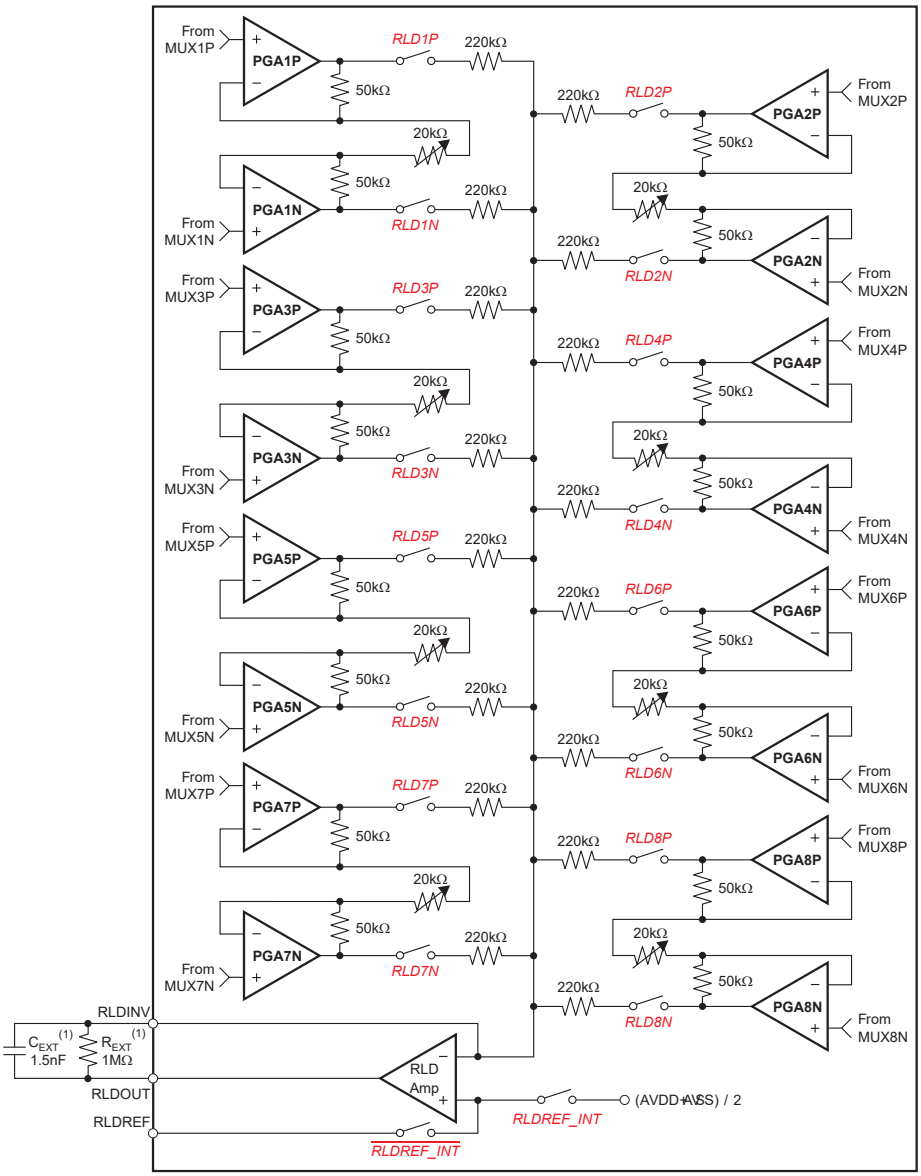

Figure 2.6 – ADS1298R right leg drive channel selection.

Wilson Central Terminal

When measuring the unipolar chest leads, the Wilson Central Terminal (WCT) is defined as the average voltage of right arm, left arm and left leg electrodes. This voltage is used as the negative reference voltage for the measurement of precordial leads. Figure 2.7 depicts the block diagram of the circuitry that allows to generate the WCT voltage. Three multiplexers allow to route any one of the eight available signals (from `IN1P` to `IN4N`) to each of the buffers used to generate the average. Each of the three amplifiers can be powered down and the average voltage required is provided at the `WCT` pin. It has to be noted that WCT amplifiers have limited drive strength, and thus, they should be buffered if used to drive low-impedance loads. The typical application consists in the connection of WCT signal to the negative inputs of the ADS1298R channels used for the measurement of chest leads.

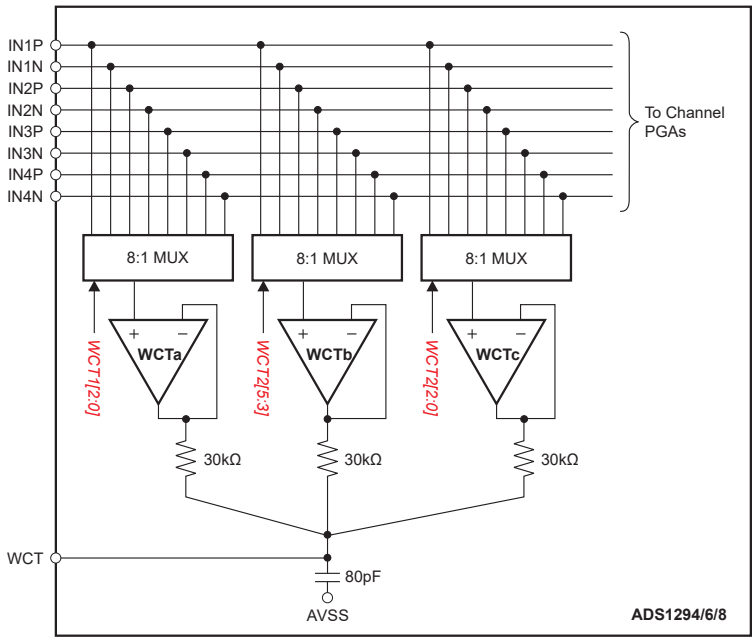

Figure 2.7 – Wilson central terminal voltage selection.

Augmented leads

In a typical implementation of a 12-lead ECG with eight channels, the augmented leads are calculated in a digital way. Nevertheless, in certain applications, it may be required that all the leads are derived in the analog domain. The ADS1298R provides the option to generate the Goldberger Central Terminal (GCT) signals required for the measurement. The appropriate averages can then be routed to channels 5, 6 and 7. In this implementation more than eight channels are used to acquire the standard 12 leads ECG and two ADS1298R must be daisy chained.

Respiration measurement

The ADS1298R allows the measurement of the respiration rate based on the principle of impedance pneumography. The principle is to measure the change of impedance of the thoracic cavity during breathing. The internal modulation block is controlled by the `RESP_MOD_EN` bit whereas the demodulation block is enabled by the `RESP_DEMOD_EN` bit. The modulation signal is a square wave of magnitude $VREFP - AVSS$ and the outputs are available at the `RESP_MODP` and `RESP_MODN` pins of the chip. The modulation frequency is either 64 kHz or 32 kHz and, when the respiration option is enabled, channel 1 of the AFE is used to acquire the respiratory impedance. The right arm and left arm electrodes are typically used for this measurement. The circuit allows to perform respiration and ECG measurements at the same time. Figure 2.8 shows the block diagram of the described internal respiration circuitry.

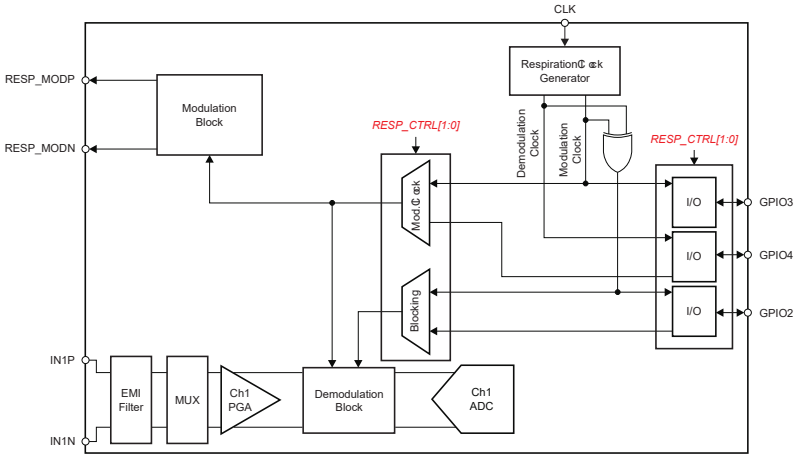

Figure 2.8 – Block diagram of the internal respiration circuitry.

2.2 Firmware

2.2.1 Firmware development

The firmware of the wearable ECG system was developed using the HAL (Hardware Abstraction Layer) APIs distributed by STMicroelectronics [37]. The HAL drivers are built around a generic architecture and allow to develop upper layers, like the application or middlewares, improving the code reusability and portability to other devices. The HAL APIs are split in two categories: generic APIs which provide functions common to all the devices of the STM32 family and specific features for a given group of devices or part numbers. The main features of the HAL drivers are the following:

- Three types of programming models supported: polling, interrupt and DMA.
- Multiple instances of the same peripherals (SPI1, SPI2 etc.) allowing concurrent API calls.
- User callbacks already implements (initialization/deinitialization, peripheral interrupt events, errors).
- Concurrency management for shared resources by means of object locking mechanisms.
- Timeout implemented for all blocking processes.

The HAL drivers are combined with STM32CubeMX, a graphical tool that allows to generate the C initialization code to set up the defined operating mode [38]. Through the interface it is possible to configure the microcontroller pinout, the clock tree and the specific configuration for peripherals and middlewares. Potential conflicts or invalid settings caused by wrong parameters are highlighted by means of warning or error icons. Figure 2.9 shows the pinout view in STM32CubeMX, whereas Figure 2.10 depicts the clock tree which displays the clock distribution to the various microcontroller peripherals. At the end of the configuration process it is possible to proceed with the generation of the C initialization code. STM32CubeMX takes care of the translation of the chosen settings into related routines. The Integrated Development Environment (IDE) used for the firmware production was Atollic Truestudio for STM32 (version 9.3.0).

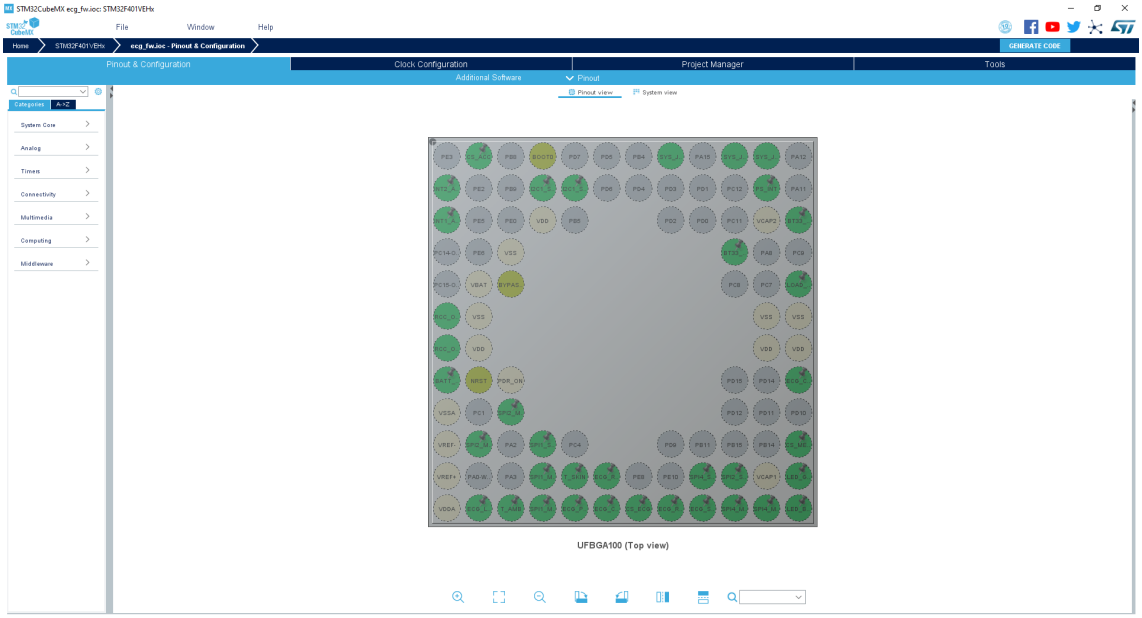

Figure 2.9 – Pinout configuration in STM32CubeMX.

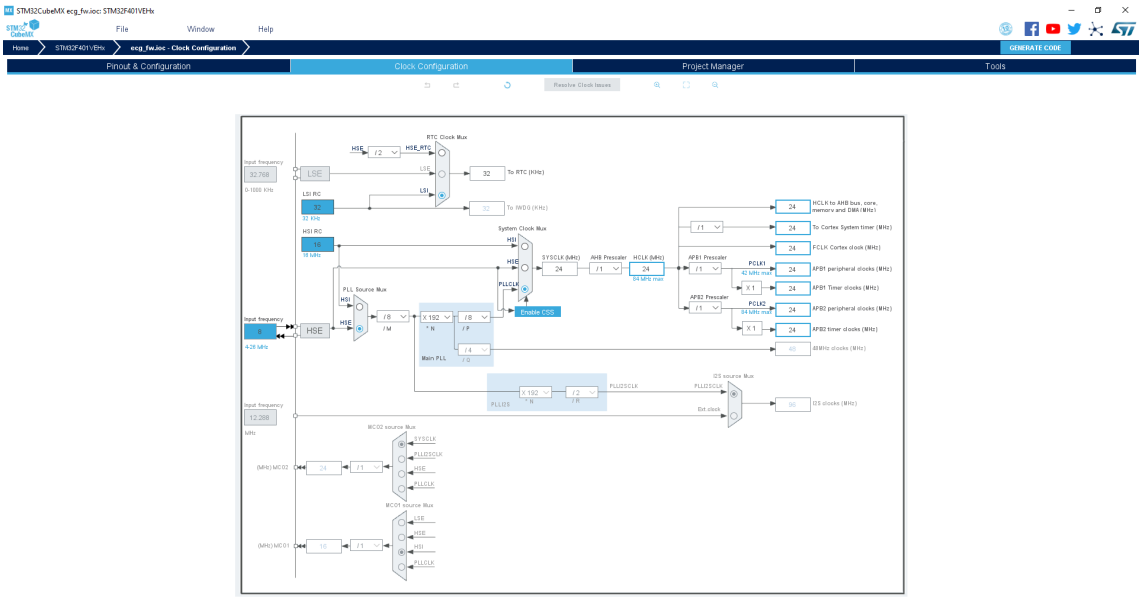

Figure 2.10 – Clock configuration in STM32CubeMX.

2.2.2 Bootloader and memory map

The bootloader is the first code to be executed after power up and reset, and runs before the main application firmware starts. It performs different hardware and software checks (e.g. it verifies through a cyclic redundancy check - CRC - if the application firmware is not corrupted before loading it) and allows to communicate by means of the Bluetooth link in order to update the MCU firmware. The bootloader is located at the first memory address executed after reset. Once the bootloader determines that the bootloadable image (i.e. the application firmware) is valid, the booloader will turn over the control to the main application. The user can force the system to stay in bootloader mode through the

CMD_RESTART command or by performing a long push button action during startup. In bootloader mode the blue and the green leds blink at a frequency of 0.5 Hz. In this state, it is possible to update the application firmware by means of a specific software. If the new application is downloaded and installed successfully, the CRC is updated. Before the development of the bootloader, it is important to define the flash memory map in order to establish the sectors allocated to bootloader, application firmware and configuration variables. Figure 2.11 shows the memory map planned and the sectors of the STM32F411 microcontroller.

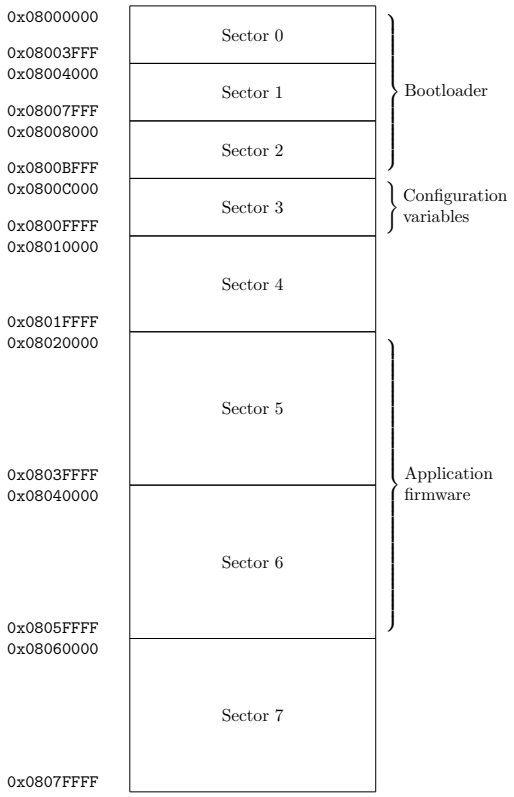

Figure 2.11 – ECG system main memory map.

2.2.3 Application firmware

A Finite State Machine (FSM), depicted in Figure 2.12, was used to formalize the behavior of the application firmware. At a given time, the system is in a specific state and different functionalities are implemented in each state; the change from one state to another is called transition and it happens in response to some inputs. The implemented states are described below.

OFF In the *off* state the system can be only switched on by pressing the button. With a long push button action, the system starts in bootloader mode and an over the air (OTA) firmware update can be performed.

INIT The *init* state identifies the platform during the initialization in which the following procedures are performed:

- Clocks configuration. The main system clock is initially set to 24 MHz used for the states in which data collection is performed (*stream*, *log* and *low power log* states).
- Configuration of interrupt priorities for the main process and the data collection job.
- Real time clock (RTC) initialization.
- Configuration of the `LIS2DH12` accelerometer according to default settings. In such configuration the output data rate is set to 100 Hz and all the axes are enabled with a full scale of ±8 g.
- The auxiliary output of the `TPS62740` step-down converter is enabled in order to supply the Bluetooth module.
- The ECG Analog Front-End is initialized using the settings stored in the configuration memory space. If no valid configuration is found, the default one envisions the measurement of the limb leads ECG, a sampling frequency of 500 Hz and the respiration impedance measurement enabled.
- Initialization of the `S25FL256S` NOR flash memory used to store data acquired during the *log* mode.
- Check in order to verify that each peripheral is communicating correctly.

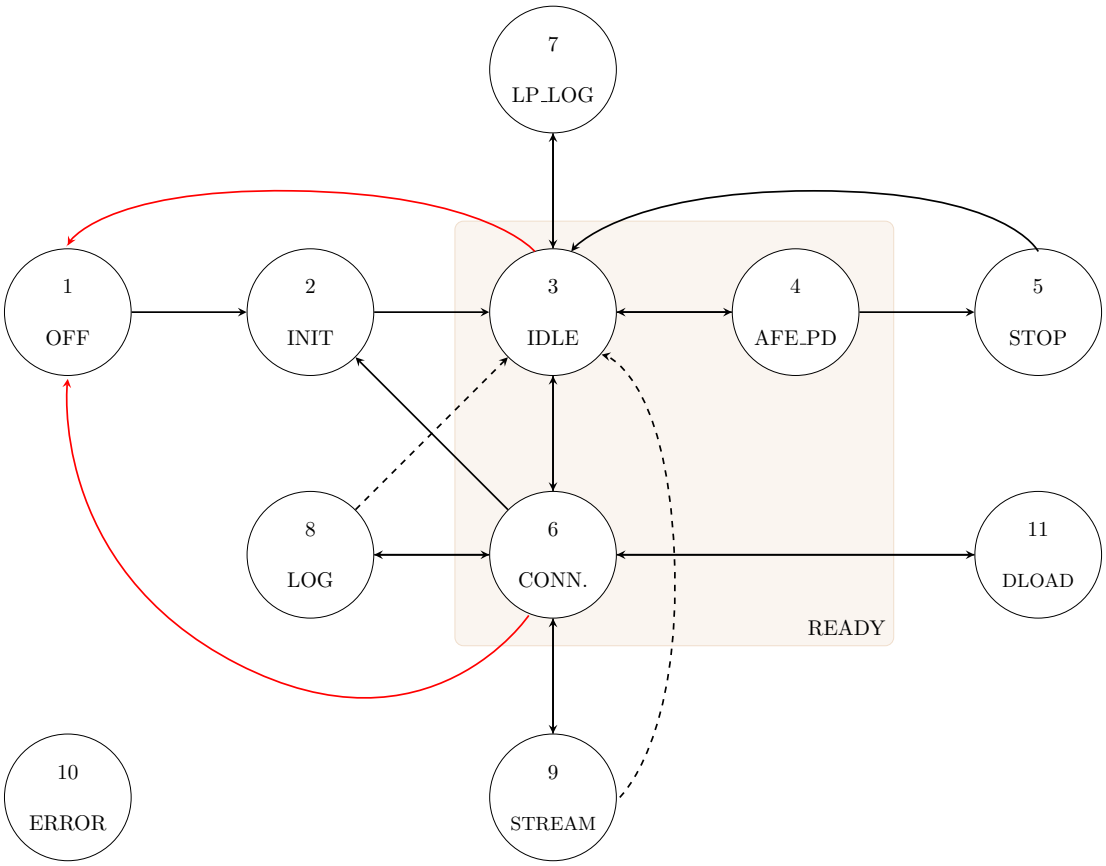

Figure 2.12 – Finite State Machine of the implemented firmware.

The green led remains on during the *init* state. If the initialization process ends with a positive outcome, the system goes in the *idle* state.

READY The *ready* group is made up of *idle*, *afe powered down* and *connected* states. When the system is in one of these states, the main clock is set to a frequency of 8 MHz and the PLL is switched off in order to lower the power consumption. The blue led blinks for 200 ms each 2 s and the BT module remains in deep sleep mode awaiting for an incoming connection. When it is established, the platform goes in the *connected* state. Otherwise, if no connection is performed within 10 s, the ADS1298R is put in standby mode (*afe powered down* state).

STOP After 170 s in which the platform is in the *afe_pd* state without incoming Bluetooth connections, the system goes in *stop* mode. In this state, the power consumption is lowered at its minimum. The Cortex-M4 core is stopped and the clocks are switched off (the PLL, the HSI and the HSE are disabled) while SRAM and register content are kept. During this state, all non required I/O pins are configured in analog mode to minimize energy consumption.

LP_LOG The *low power log* state is reached with a short press of the push button if it isn't connected to any devices through the Bluetooth link. An acquisition session is started using the default configuration set by means of the `CMD_LOG_SETUP` command. The Bluetooth module is powered off to minimize the power consumption and, for this reason, no incoming connection is accepted. The end of the acquisition is performed by pressing again the push button.

LOG The *log* state can be reached in two possible ways: by pressing the push button from the *connected* state or by sending the command `CMD_START_LOG`. The system verifies whether the memory is not full or busy and starts the acquisition, otherwise the transition is not performed and a specific error message is reported.

STREAM A new streaming session is started by sending the `CMD_STREAM` command. The system transmits periodically the selected ECG and bioimpedance signals, along with the acceleration data, at a desired frequency. Each time that a message is transmitted and the blue LED blinks for a small amount of time. The acquisition is stopped through the `CMD_STOP_SESSION` command or if the Bluetooth connection is lost. The samples acquired during the *stream* state are stored in a buffer and transmitted in bursts of messages with a format that will be described in the communication protocol.

DLOAD In the *download* state it is possible to get a previous log file saved in the onboard memory. The file number to be downloaded is specified through a specific parameter in the `CMD_READ_FILE` command and, if the file exists, the system begins the transmission of the content. The *download* state is identified by a fast blink of the green LED. When the transmission is completed or if errors occur during the download, the system returns automatically to the *connected* state. Errors are detected by means of an acknowledgment mechanism in which the client device must confirm the reception and the correct CRC of a bunch of packets within a timeout.

ERROR The *error* state is reached when an unrecoverable error happens. When the system is in this state, stream and log are inhibited. For this reason the user should proceed with the device restart using the specific command or by performing a long push of the button.

2.2.4 Communication protocol

The designed system complies with a bidirectional communication protocol which can be used via Virtual COM Port offered by the available Bluetooth module. When the system completes the startup, client devices supporting Bluetooth SPP (Serial Port Profile) are allowed to connect with the platform. This protocol which defines the rules and the format of the exchanged messages is based on the Type Length Value (TLV) format depicted in Figure 2.13. This convention establishes that each packet contains one byte indicating the command, one byte which represents the number of bytes in the value (e.g. the length of a string) and the value, if present (e.g. the string). The most significant bit of the type field allows to specify the access method: read (MSb set to 1) or write (MSb set to 0).

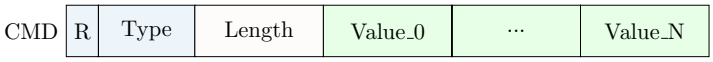

Figure 2.13 – Message in the TLV command format.

Each TLV packet receives an acknowledgment (ACK), either positive (success) or negative (error), carrying information about the outcome in the same TLV format. As summarized in Figure 2.14, the ACK response contains the `ACK_CODE` (`0x00`) which identifies that the message is actually an ACK, the value length and the actual value. The length of the value field is at least equal to 2, as it carries information about which message the ACK refers to and the error code. In case the command sent previously needs some information back, the bytes following the error code byte contain the information.

Figure 2.14 – ACK message in the TLV command format.

In order to avoid collisions, a header and a trailer are added at the beginning and at the end of the message respectively. The header is "?!", whereas the trailer is "!?". The commands are used to control the state of the system and to exchange data. Commands defined in the protocol for the ECG wearable system are summarized in Table 2.3. The syntax and the semantics of each message is then described in the following paragraphs.

Code	Command	Description	Access
0x01	CMD_SHUTDOWN	Shutdown the system	W
0x02	CMD_STATE	Get/set the state of the system	R/W
0x03	CMD_RESTART	Restart the system	W
0x04	CMD_BATTERY	Get the battery state of charge	R
0x05	CMD_TEMPERATURE	Get the measured ambient and skin temperature	R
0x06	CMD_DATE	Get/set the date	R/W
0x07	CMD_STORE_PARAMS	Force the system to store configuration parameters (used only for debug purposes)	W
0x08	CMD_START_LOG	Start a log session	W
0x09	CMD_ERASE_MEMORY	Erase the content of the log memory	W
0x0A	CMD_MEMORY_BUSY	Get the log memory state (busy or available)	R
0x0B	CMD_GET_LOG_FILES	Get the number of log files store on the onboard memory	R
0x0C	CMD_READ_FILE	Begin the download of a specific log file	R
0x0D	CMD_GET_MEMORY	Get the percentage of free memory	R
0x0E	CMD_STREAM	Start a streaming session	W
0x0F	CMD_STOP_SESSION	Stop the current session (stream or log)	W
0x10	CMD_ACC_FS	Get/set the accelerometer full scale	R/W
0x11	CMD_ECG_CONFIG	Read/write a register of the ADS1298R	R/W
0x12	CMD_LOG_CONFIG	Get/set the default configuration of a log session (used to initiate a low power log session)	R/W
0x13	CMD_SETUP	Get the main settings of the wearable system: accelerometer full scale and content of ADS1298R registers	R/W

Table 2.3 – Commands list.

CMD_SHUTDOWN

The system can be shut down by issuing the command 0x01 in write mode. The system will return an ACK_SUCCESS or ACK_ERROR. In case of success, after 2 seconds after the reception of the command, the system will be shut down and any Bluetooth connection will be lost.

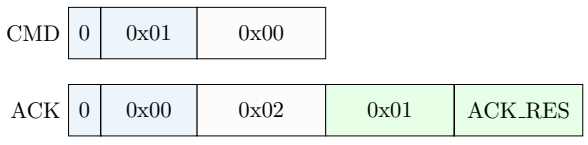

Figure 2.15 – Shutdown command format.

CMD_STATE

The state of the system can be get or set by means of the command ID `0x02`. To get the state of the system, the command `0x82` must be issued with `0x00` as length and no payload. In case of `ACK_SUCCESS`, the payload length will be 3 bytes. The third byte carries information about the state of the system. In case of `ACK_ERROR`, the payload length is 2 bytes.

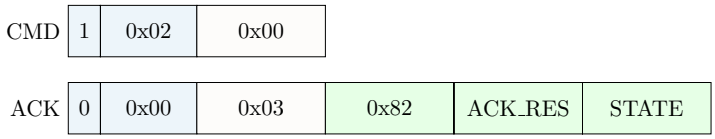

Figure 2.16 – State command (read) format.

To set the state of the system, the command `0x02` must be issued with `0x01` as length and with the code of the state as payload. Typically this command is used only for debug purposes as it can result in an error when a forbidden transition is performed.

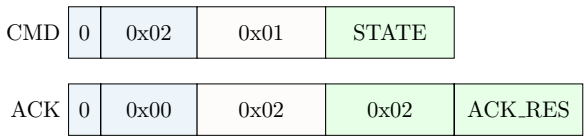

Figure 2.17 – State command (write) format.

The list of the codes associated with the possible states is depicted in Table 2.4.

Code	State
`0x01`	Startup
`0x02`	Ready (connected)
`0x03`	Stop
`0x04`	Log
`0x05`	Stream
`0x06`	Readout
`0xFF`	Error

Table 2.4 – State codes of the system.

CMD_RESTART

The system can be restarted by means of the command code `0x03`. The system will return an `ACK_SUCCESS` or `ACK_ERROR`. In case of success, after 2 seconds from the reception of the command, the system is restarted and the Bluetooth connection will be lost.

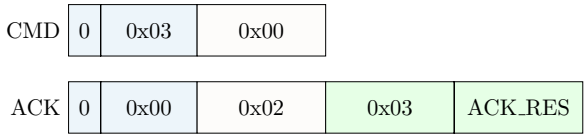

Figure 2.18 – Restart command format.

A restart in bootloader mode can be forced by means of the same command with a payload length of `0x01` and a payload of `0x01`. For a standard reset it can be used this alternative syntax, but the payload must be `0x00`.

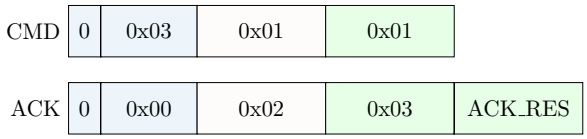

Figure 2.19 – Restart in bootloader mode command format.

CMD_BATTERY

The battery state of charge can be retrieved through the command code `0x04`. The system will return an `ACK_SUCCESS` or `ACK_ERROR`. In case of success, the payload length will be 3 bytes. The third byte carries information about the state of charge of the battery reported in percentage.

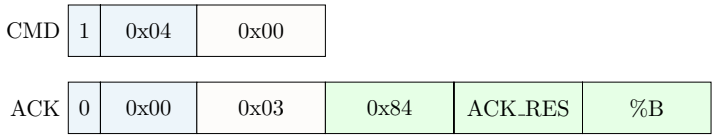

Figure 2.20 – Battery command format.

CMD_TEMPERATURE

The ambient and skin temperature can be retrieved through the command code `0x05`. The system will return an `ACK_SUCCESS` or `ACK_ERROR`. In case of success, the payload length will be 4 bytes. The third and fourth bytes represent the acquired environmental temperature, whereas the fifth and the sixth are the skin temperature.

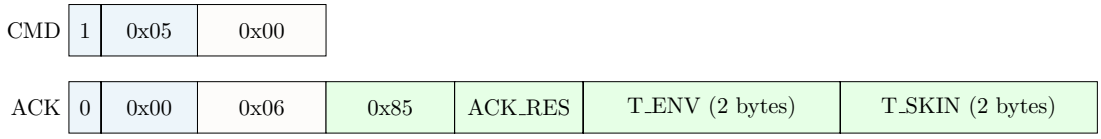

Figure 2.21 – Temperature command format.

Each temperature output measured using the onboard thermistors is split in two fields: 8 bits for the integer value (represented in 2's complement) and 4 bits for the fraction (MSb first).

CMD_DATE

The epoch can be get or set through the command code `0x06`. To set the date a command `0x06` must be issued with payload length of `0x04` and with payload the Unix epoch represented with a 32 bit signed integer. The system will return an `ACK_SUCCESS` or `ACK_ERROR`.

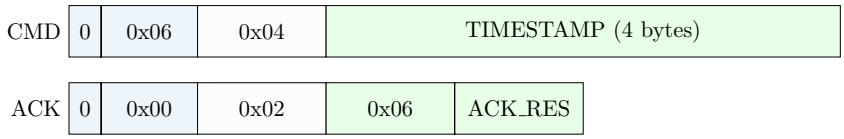

Figure 2.22 – Date command (write) format.

To get the date a command `0x86` must be issued with `0x00` as payload length. The system will return an `ACK_SUCCESS` or `ACK_ERROR`. In case of success, the payload length will be `0x06` bytes and the payload will be the Unix timestamp represented with a 32 bit signed integer.

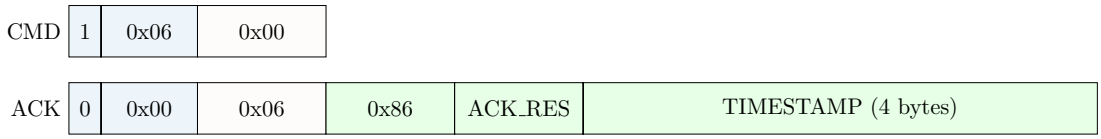

Figure 2.23 – Date command (read) format.

CMD_STORE_PARAMS

To store the system parameters on the MCU flash memory, a command 0x07 must be issued with `0x00` as payload length. The system will return an `ACK_SUCCESS` or `ACK_ERROR`.

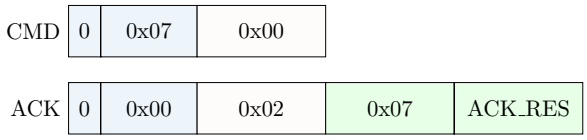

Figure 2.24 – Store params command format.

CMD_START_LOG

A log session can be started by means of the command ID `0x08`. To start the session, the command must be issued with length `0x05` and the following payload.

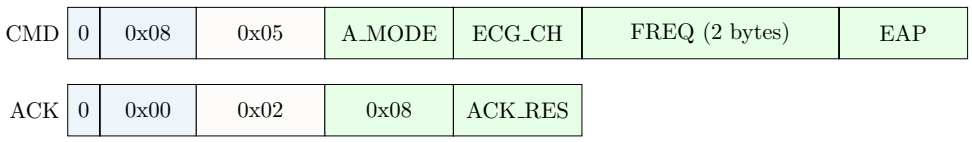

Figure 2.25 – Start log command format.

- `A_MODE` (1 byte). This byte allows to select whether the ECG and/or the accelerations are logged.
  - `0x01`: ECG only
  - `0x02`: accelerometer only
  - `0x03`: ECG and accelerometer
- `ECH_CH` (1 byte). By means of this byte it is possible to select the ECG channels to be acquired. By setting a specific bit to 1, the corresponding channel is enabled. The MSb represents the state of channel 1, whereas LSb represents the state of channel 8, as depicted below. Any combination is allowed, but a maximum number of 4 channel can be acquired. If the value of `A_MODE` is equal to `0x02`, this byte produces no effects on the configuration.
- `FREQ` (2 bytes). The nominal frequency of the acquisition (this value should be a divider of 1000).
- `EAP` (1 byte). Value of the prescaler used to determine the acceleration sampling frequency. The accelerometer values are sampled at a frequency equals to the ratio between `FREQ` and `EAP`.

  $$f_{acc} = \frac{f_{ECG}}{EAP}$$

  This value is relevant only when `ACQ_MODE` is set to 0x03 (ECG + accelerometer) and it must be chosen from the allowed values listed in Table 2.5 according to the number of ECG channels enabled for the acquisition.

# ECG	EAP
1	1, 2, 4, 5
2	1, 2, 5
3	4
4	3

Table 2.5 – Allowed values for `EAP`.

The system will return an `ACK_SUCCESS` message if the log starts successfully. Otherwise, it will return an `ACK_ERROR` if the memory is full or busy because of an erase task in progress.

CMD_ERASE_MEMORY

The log memory can be erased by means of the command code `0x09`. The system will return an `ACK_SUCCESS` or `ACK_ERROR`. In case of success the log memory will be erased.

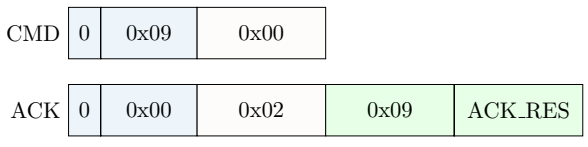

Figure 2.26 – Erase memory command format.

CMD_MEMORY_BUSY

The actual state of the memory can be retrieved by means of the command code `0x0A`. The system will return an `ACK_SUCCESS` or `ACK_ERROR`. In case of success the payload length will be `0x03` and the payload will be the state of the memory (`0x01` busy, `0x00` available).

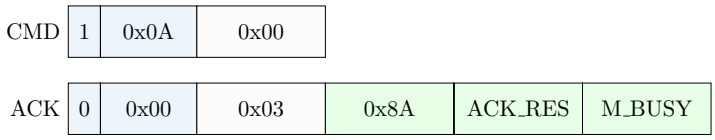

Figure 2.27 – Memory busy command format.

CMD_GET_LOG_FILES

The number of acquisition logged on the onboard memory can be retrieved by means of the command code `0x0B` having `0x00` as payload length. The system will return an `ACK_SUCCESS` or `ACK_ERROR`. In case of success the payload length will be `0x04` and the payload will return the number of files logged (2 bytes).

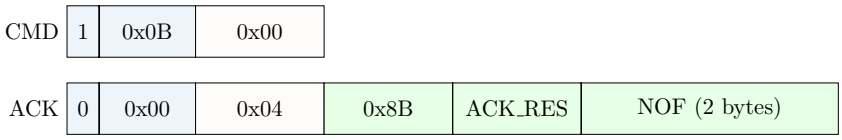

Figure 2.28 – Get lof files command format.

CMD_READ_FILE

A logged file can be read out by means of the command code `0x0C`. The payload length must be `0x02` and the payload will be the index of the file to be read (2 bytes). The system will return an `ACK_SUCCESS` or `ACK_ERROR`. In case of success the payload length will be `0x06` and the payload will be the length of the file to be read. After the `ACK_SUCCESS` message, the system will transmit the required file. The file is made up by an header page containing useful information concerning the specific acquisition and the following pages have a format which is the same that will be described for the *stream* messages.

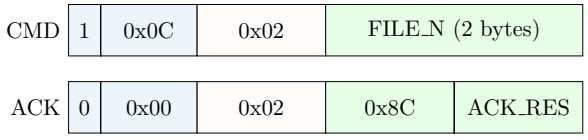

Figure 2.29 – Read file command format.

CMD_GET_MEMORY

The percentage of available memory can by retrieved by means of the command code `0x0D`. The system will return an `ACK_SUCCESS` or `ACK_ERROR`. In case of success the payload length will be `0x03` and the payload will be the available memory.

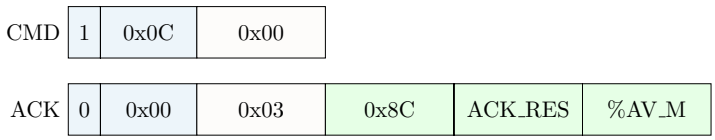

Figure 2.30 – Get memory command format.

CMD_STREAM

The data streaming can be started by means of the command ID `0x0E`. To start the session, the command must be issued with length `0x05` and the same payload described for the command `CMD_START_LOG`.

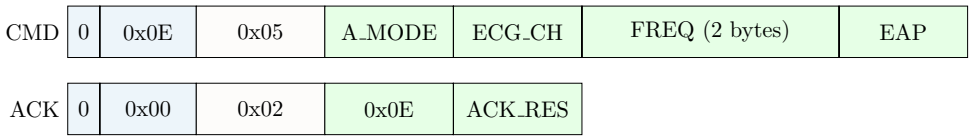

Figure 2.31 – Stream command format.

CMD_STOP_SESSION

A streaming or log session can be stopped by means of the command ID `0x0F`. The system will return an `ACK_SUCCESS` and it will go in the *connected* state.

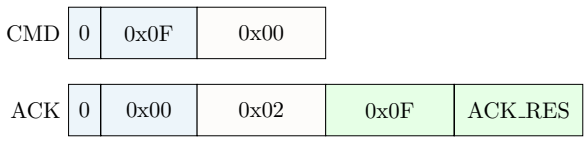

Figure 2.32 – Stop session command format.

CMD_ACC_FS

The accelerometer full scale can be changed issuing the command ID `0x10`. The payload length must be `0x01` and the payload is the full scale according to Table 2.6.

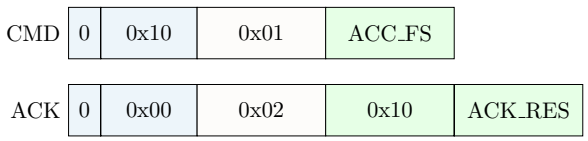

Figure 2.33 – Accelerometer full scale command (write) format.

Value	Full scale
0x00	±2 g
0x10	±4 g
0x20	±8 g
0x30	±16 g

Table 2.6 – Accelerometer full scale settings.

In a similar way, the full scale setting can be obtained with the command ID 0x90.

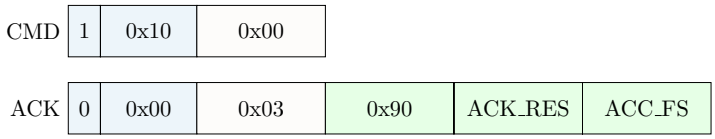

Figure 2.34 – Accelerometer full scale command (read) format.

CMD_ECG_CONFIG

To set the value of a specific register of the ADS1298R, a command 0x11 must be issued with payload length of 0x02 and with payload the address of the register to be written and the value to be set. The system will return an ACK_SUCCES or ACK_ERROR.

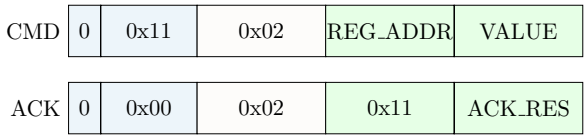

Figure 2.35 – ECG config command (write) format.

To get the value of a specific register, a command 0x91 must be issued with 0x01 as payload length and with payload the register address. The system will return an ACK_SUCCES or ACK_ERROR. In case of success, the payload length will be 4 bytes and the payload will be the address of the register and the read value.

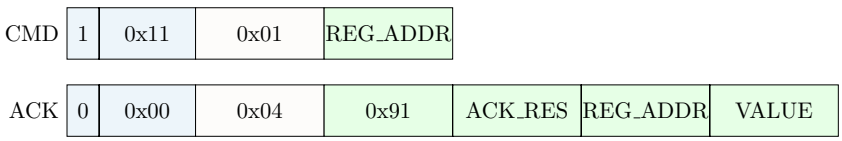

Figure 2.36 – ECG config command (read) format.

CMD_LOG_CONFIG

The default log mode can be configured through the command ID 0x12. This mode is the one which is considered when a user starts a log by pressing the onboard button. To configure the parameters, the command must be issued with length 0x05 and the same payload described for the command CMD_START_LOG.

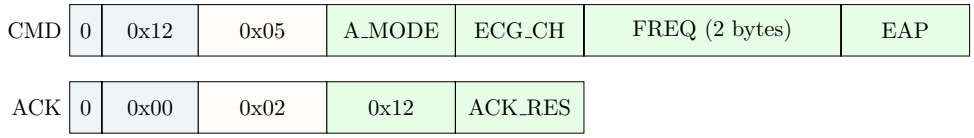

Figure 2.37 – Log config command (write) format.

To retrieve the default log configuration, the command ID `0x92` can be issued. The system will return an `ACK_SUCCESS` and the payload will have the same format described for the command `CMD_START_LOG`.

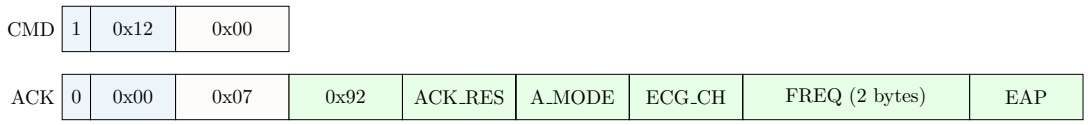

Figure 2.38 – Log config command (read) format.

CMD_SETUP

The command ID `0x93` allows to obtain relevant information about the configuration of the ADS1298R and the accelerometer full scale. When the command is issued, the system returns an ACK with a payload made of 30 bytes. Two bytes specify the acknowledged command and the outcome, one byte the accelerometer full-scale and the others represent the content of all the configuration registers of the ADS1298R ECG analog front-end.

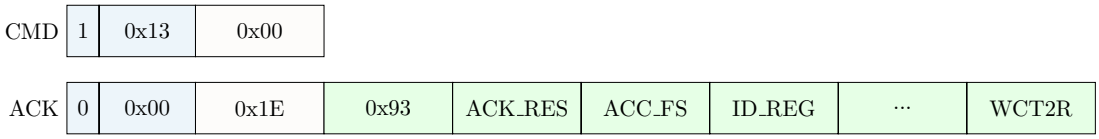

Figure 2.39 – Setup command format.

Data messages format

During the *stream* state the system transmits the acquired samples using a specific message format, as depicted by Figure 2.40.

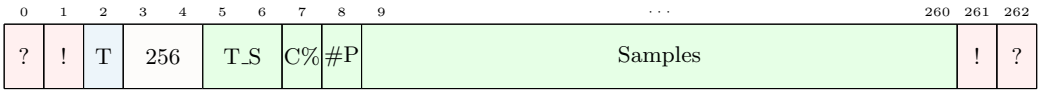

Figure 2.40 – Data message format used to transmit the acquired samples during a streaming session or when a log file got downloaded.

The message complies with the TLV format, except for the Length field which is 2 bytes long. The total size of the message including the delimiters is 263 bytes. The Type field is valued `0x07` (which correspond to the code of `CMD_STREAM` command) and the payload length is equal to 256 bytes. The first four bytes of the payload represents respectively the skin temperature (2 bytes), the state of charge and the progressive number of packet

transmitted. The next 252 bytes are used to store the acquired samples. According to the chosen configuration, acquired data are appended to the message at the first memory location available. ECG samples are in ascending order with respect to the channel number, whereas an accelerometer sample is interposed each `EAP` (the parameter described in the `CMD_STREAM`) ECG samples. This kind of storage policy ensures that the payload is exploited over its full length. The same mechanism was used for the packets transmitted during a log file *readout* which is similar to a stream session. In this way the data decoding in the receiver side is performed in the same way regardless of the two distinct states.

2.3 Android application

The wearable system is completed by a specifically designed Android application. Through this mobile software, any user is able to perform measurements without having a deep knowledge of the sensor system. On the other hand, an expert user can see further information concerning the configuration of the analog front-end. The application communicates with the wearable platform using the Bluetooth link and the protocol described before. Samples are presented in real-time to the user and they can be exported in a log file for further data analysis.

2.3.1 Android

Android is a mobile operating system based on a modified version of the Linux kernel. It originated from Android Inc., a small firm founded in 2003 by Andy Rubin, Rich Miner, Nick Sears and Chris White, with the aim of developing mobile-based software able to provide to the user a deeper ability to customize the device according to its needs. In 2005 Google acquired Android Inc. in order to supply to the market a reference solution for smartphones. After its unveil occurred in 2007, Android was released with an open source license, so each developer is able to download and edit the entire source code. This has allowed variants of Android to be developed on a range of other electronic devices, such as digital cameras, entertainment systems and game consoles. Since 2008, Android has seen numerous updates which have incrementally improved the operating system, adding new features and fixing bugs of previous releases. Each major release is identified by a number called "API level" and named in alphabetical order after a dessert or sweet treat. Every version comes with its own SDK (software development kit) which includes all the latest features. Android was chosen by several subjects of the mobile industry to rival the competition of Apple and its iPhone. This contributed to the success of the operating system: since 2011 Android is the most adopted OS and at the end of 2019 had a market share of 74 %. Android runs on a variety of devices of different screen sizes and densities. This means that it is able to handle applications that run on small mobile devices, as well as applications that are executed on large screens. This feature gave to Android a great advantage, but, on the other hand, this means that developers should make the effort of optimizing their software for different screen sizes. Android system provides a consistent development environment across devices and handles most of the work required to adjust each user interface (UI) to the screen on which it is displayed. Android has a wide set of features supported natively and some of them are listed below.

- **Mobile connectivity** - A wide range of network standards are supported including GSM/EDGE, UMTS, HSPA, LTE, 5G, WiMAX.

- **Short range wireless** - Bluetooth is supported for a wide variety of profiles and use cases. Other major short range wireless protocols available in Android are Wi-Fi, NFC and IrDA.
- **Messaging** - Besides the classical SMS and MMS, Google Cloud Messaging (GCM) is a service that allow developers to send short messages to their users without needing a proprietary solution.
- **Storage** - SQLite, a lightweight relational database, is used for data storage purposes.
- **Web browser** - It is Based on the open-source Blink layout engine, coupled with Chromium's V8 Javascript engine supporting HTML5 and CSS3.
- **Multitasking** - Users can jump from an application to one another and multiple tasks can run simultaneously.
- **System apps** - Android comes with a set of core apps for calendars, clock, contacts and more. The system apps provide also capabilities that developers can access from their own app.

The open-source nature of Android encouraged a large community of developers and enthusiasts that deliver new features through applications, develop updates for older devices and create alternative versions of the original operating system. Often the developed software brings updates faster than official manufacturer channels with a comparable level of quality.

2.3.2 Platform architecture

Android operating system is a software stack made by several components which can be divided into six sections and five main layers, as show in the architecture diagram depicted in Figure 2.41. This means that each layer can exploit services offered by underlying layers and offer services to upper layers. The base layer relies on the Linux kernel for functionalities such as memory management and threading. The hardware abstraction layer (HAL) provides standard interfaces that expose hardware capabilities of the device to the Java API framework. Each library module implements the drivers for a specific component, such as the audio or the Bluetooth module. From the version 5.0 of Android (API level 21) each app runs its own instance of the Android Runtime (ART). ART is specifically designed to run multiple virtual machines with a low memory impact and some of the main features are the following:

- Ahead-of-time (AOT) and just-in-time (JIT) compilation.
- Optimized garbage collection.
- Advanced debugging features.

Prior to Android 5.0, Dalvik was the Android runtime. If an application runs on ART, then it should be able to work on Dalvik, but the reverse may not be true. The entire set of features offered by Android OS are available through APIs written in Java language. These are the building blocks used by developers to design their own app. Some of the major features of the Java API framework include the following:

- A ViewSystem used to design the app UI. It includes lists, text boxes, buttons and many other graphical elements.

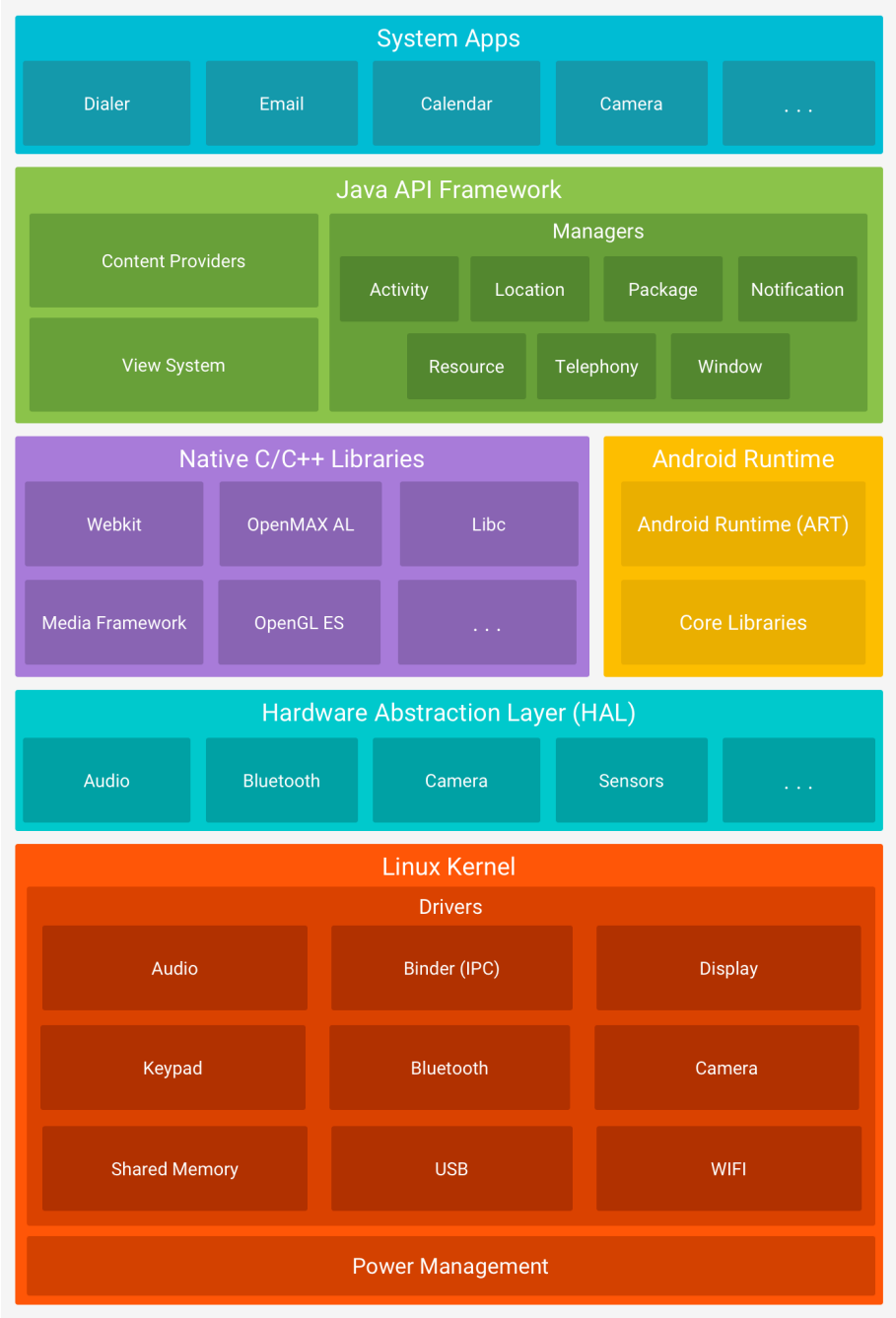

Figure 2.41 – Android operating system software stack.

- A notification manager which enables all applications to display custom messages in the status bar.

- Content providers that allow to access data from other apps, such as the contact app, or to share their own data.

Many system components are built from native libraries written in C and C++. Developers can also write their applications using the Android NDK which exploits a direct interface with the core libraries.

2.3.3 Android main components

The Android SDK tools compile the source code, the data and resource files into an APK, an Android package, which is an archive file with an `.apk` extension. The APK file contains everything that is required by the application to be installed on a device [39]. Some of the fundamental building blocks and concepts are the following:

- Activity
- Intent and IntentFilter
- Fragment

Activity The activity is a crucial component of an Android application and the way activities are launched is a fundamental part of the platform's application model [40]. An activity provides the window in which the app draws the user interface. Generally, an activity implements one screen in an app and the application can consist of multiple activities. Each activity has its own lifecycle and it can host one or more fragments.

Intent and Intent Filter The Android architecture is optimized and allows to exploit the available resources in a better way. To achieve this goal, the Intent mechanism has been developed. An Intent is a messaging object which requests an action from another app component. There exists two types of intents:

- **Explicit intents** specify which application will satisfy the intent. Typically it is used to start a known component in the same app.
- **Implicit intents** do not call a specific component, but they declare the general action to be performed. A component from another app will be able to handle the intent.

When an implicit intent is used, the Android system finds the appropriate component to be launched by comparing the intent to the intent filter declared in the manifest file of applications installed on the device. If the intent matches an intent filer, the system starts that component. If multiple intent filter are compatible, the systems allows to pick which one to use. Summarizing, the intent filter is a mechanism that declares the capabilities on an app which can be used by another applications.

Fragment The idea of fragment was introduced in Android 3.0, the first release supporting tablets and larger screens [41]. A fragment represents a portion of a user interface and multiple fragments can be assembled in a single activity. A fragment always depends on an activity and its lifecycle if affected by the activity's lifecycle. However, fragments can be added or removed when the activity is running. Moreover, they can be assembled in different ways depending on the screen size of the device that is running the application.

2.3.4 Activity lifecycle

During the navigation through, out of, and back to an application, the activity instances transition in different states in their lifecycle [42]. The Activity class provides callbacks that allow to capture the state change. Within these callback methods, the developer can declare the activity behavior in response to a specific event. A good implementation of the activity lifecycle should ensure that the application avoids:

- Crashing if the user switches to another app.
- Consuming a lot of system resources when it is not used.
- Losing the progress when the user leave the application and return to it at a later time.
- Crashing or losing the progress when the screen changes the orientation.

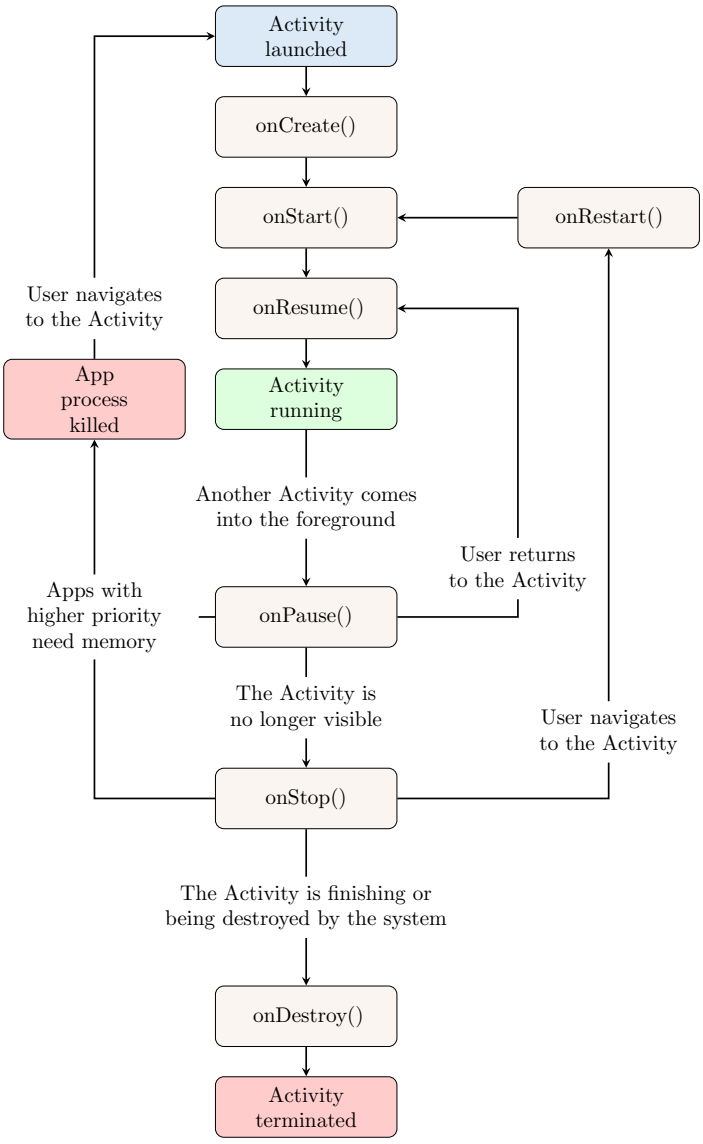

Figure 2.42 – Diagram of the Android activity lifecycle.

An illustration of the activity lifecycle is shown in Figure 2.42. Depending on the complexity of the activity, not necessarily all the callback methods have to be implemented. When the activity is launched, the `onCreate()` method is called and the basic initialization logic that happens only once for the entire life of the activity should be implemented here. The `onStart()` call makes the activity visible to the user and it is where the app initializes the code that maintains the user interface (UI). The `onResume()` method is launched when

the activity comes into foreground. This is the state in which the user is able to interact and the app stays in this state until something takes focus away from the app (in this case the `onPause()` method is called). The `onStop()` callback is launched when the activity is no longer visible to the user, for example when another activity is started and covers the entire screen. This method is called when the activity is about to be terminated. The `onDestroy()` is called before the activity is terminated either in consequence of `finish()` being called or when the system is destroying the activity due to a configuration change (for example the device screen rotation).

2.3.5 Fragment lifecycle

Each fragment has its own lifecycle and it can be added or removed in an activity when it is in execution. A fragment must always be hosted in an activity and the fragment's lifecycle is directly affected by the host activity's lifecycle.

The same concept of callback method observed in the activity class is available for fragments. Typically the following methods should always be implemented:

- `onCreate()` - Essential components of the fragment that must be retained when it is paused or stopped must be initialized in this section.
- `onCreateView()` - This callback is launched when the fragment has to initialize the user interface.
- `onPause()` - It is called when the user is leaving the fragment, so every changes should be committed.

The lifecycle of a fragment ends with two callbacks methods: `onDestroy()` and `onDetach()`. These methods remove the fragment from the host activity and free the used resources. If the host activity goes into pause or stop state, all the fragments attached to it follow the same flow. The reverse it's not true: a fragment can be removed from or added to an activity which is in the active state. A complete diagram of the fragments' lifecycle is depicted in Figure 2.43.

2.3.6 Bluetooth in Android

The Android platform includes support for the Bluetooth network stack which allows to exchange data with other wireless devices [43]. The application framework provides access to the Bluetooth functionality through the Android Bluetooth APIs. These APIs provide a means to connect to other devices and enable point-to-point and multi-point wireless communication. The main features offered by the Bluetooth APIs in Android are the following:

- Scan for other Bluetooth devices
- Query the local Bluetooth adapter for already paired wireless devices
- Establish RFCOMM channels
- Connect to other devices by means of service discovery
- Transmit and receive data to and from other devices
- Manage multiple connections

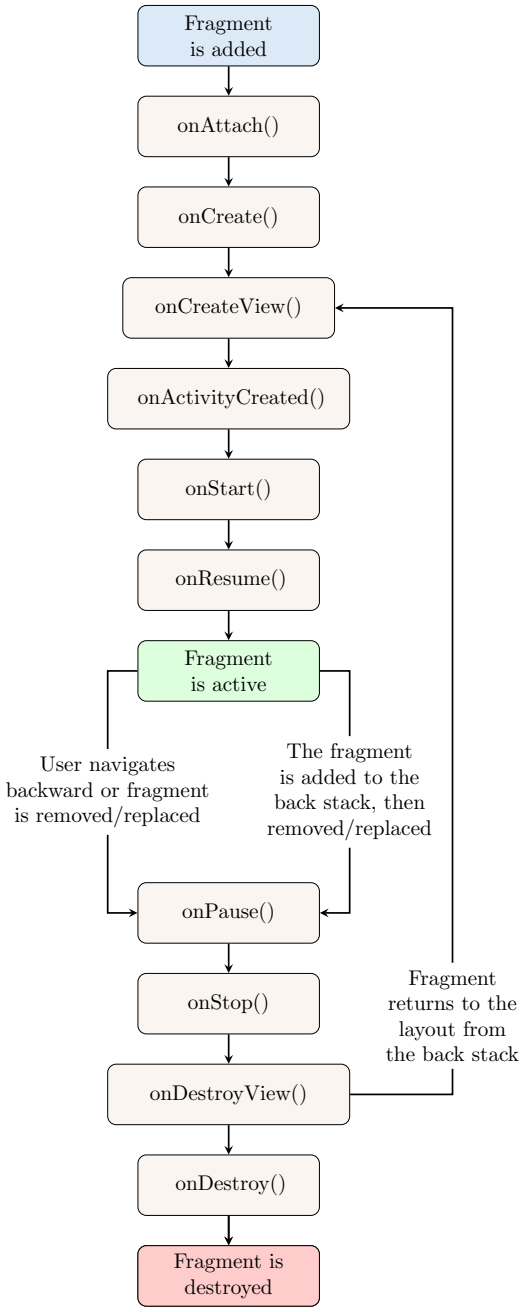

Figure 2.43 – Diagram of the Android fragment lifecycle.

In order to exchange data between *Classic Bluetooth* enabled devices, a channel of communication must be formed using a pairing process. One device, a discoverable device, makes itself available for incoming connection request, while another device finds the discoverable device using a service discovery process. After the pairing request acceptance performed by the discoverable device, the two systems complete the bonding process with the exchange of security keys. The devices store these keys for later use and they are enabled to communicate each other. When the session is complete, the device that initiated the request can release the communication channel. However the two devices remain bonded, so they can connect automatically and start a new session as long as they are in

range and neither device removed the bond.

Two permissions are mandatory and must be declared in the manifest file of the application which want to use the Bluetooth features. The first one is `BLUETOOTH` and it is required in order to perform any communication, such as connection requests and transferring data. The other permission is `ACCESS_FINE_LOCATION` and it is needed because the scan process can be used to gather information about the location of the user. This information may come directly from beacons used in specific locations or from user's own devices. If the application is designed to run a device discovery, the `BLUETOOTH_ADMIN` permission must be declared in addition to the others. Starting from Android 3.0, the Bluetooth APIs include support for Bluetooth profiles, wireless interface specification for the communication between devices. In particular, the Serial Port Profile (SPP), used for the communication with the wearable ECG platform, defines how to set up virtual serial ports and connect two Bluetooth enabled devices. In this connection the Android device acts as a client, whereas the ECG platform is the server and accepts incoming connections. First the *BluetoothDevice* object must be used in order to acquire a *BluetoothSocket* and initiate the connection. The basic procedure is as follows:

1. Get the *BluetoothDevice* object from the list of paired devices or through a Bluetooth discovery.

2. Using the *BluetoothDevice*, obtain a *BluetoothSocket* using the *createRfcommSocketToServiceRecord(UUID)* method. For the Serial Port Profile a standard UUID is defined.

3. Perform the connection using the *connect()* method and, if the remote device accepts the connection, the communication channel is opened. The *connect()* call is a blocking call, so it should be implemented in a separate thread with respect to the UI.

After the remote device is successfully connected, it has a connected *BluetoothSocket*. The *InputStream* and the *OutputStream* can be obtained from the socket and they handle the data transmission.

2.3.7 Application architecture

Android Studio is the IDE used for the development of the ECG Android application. It is based on JetBrains IntelliJ IDEA and it integrates the Android SDK. The application was designed using the model-view-presenter (MVP) architectural pattern in which there are three different entities:

- **Model** - it is responsible of handling data and the communication.

- **View** - it represents the UI, so it is responsible of displaying data and it notifies the Presenter about user actions.

- **Presenter** - it retrieves data from the Model and it pass them to the view. The Presenter also decides the reactions to input notifications from the View. For this reason it contains the larger part of the application logic.

MVP is a derivation of the model-view-controller (MVC) architectural pattern, but in the MVP View is more separated from Model. In Figures 2.44, 2.45, and 2.46 class diagrams of the developed application are shown.

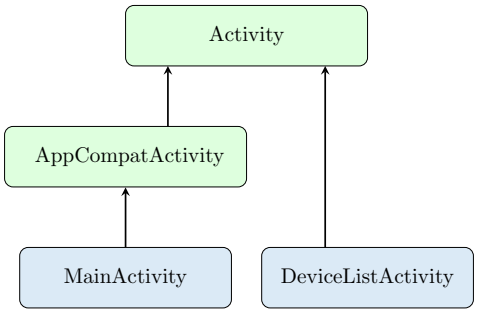

Figure 2.44 – Activities class diagram.

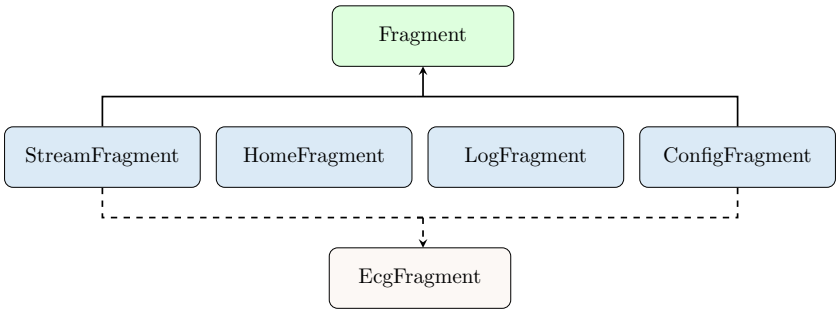

Figure 2.45 – Fragments class diagram.

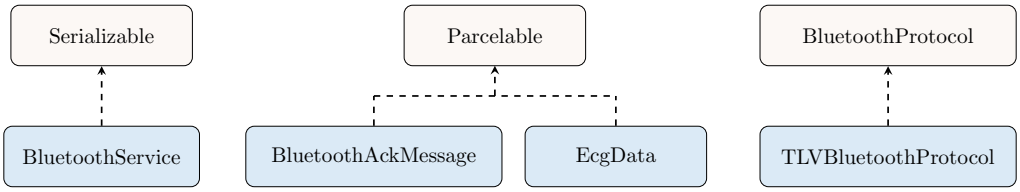

Figure 2.46 – Class diagram of generic classes.

2.3.8 User guide

The developed Android application that allows to communicate with the wearable ECG system is composed of different screens which can be reached through a navigation drawer. The user interface is compliant with the guidelines defined by the material design team at Google. If the user clicks the menu icon in the action bar or swipes the finger from the left edge of the activity, the navigation drawer appears as depicted by Figure 2.47.

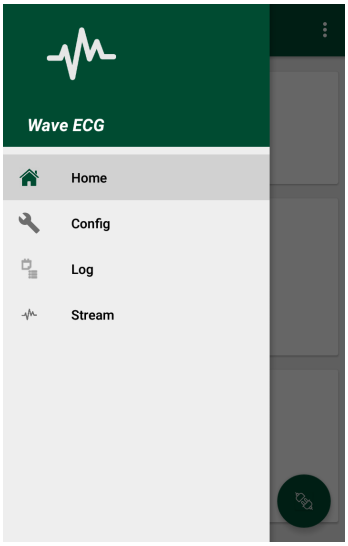

Figure 2.47 – App's navigation drawer.

The available categories are the following:

- **Home** view is a dashboard of the ECG system. When the Android device is connected to it, main configuration parameters, such as the active channels and the battery state of charge, are shown. From this section the user can synchronize the date and the time of the ECG platform.

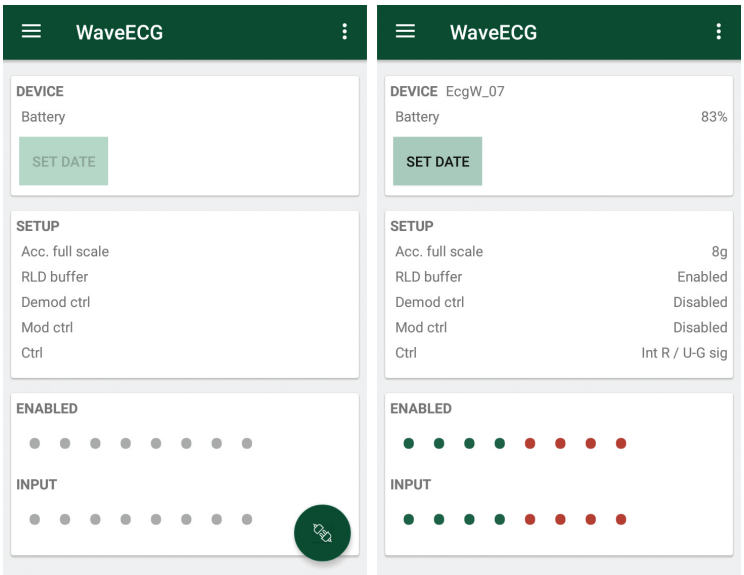

Figure 2.48 – Home section view. The left screen depits the view when the phone is not connected to the ECG system, whereas the right screen shows the configuration when the device is connected to the platform.

- **Configuration** section allows to set the parameters used to start a new streaming or log session. In fact, as depicted by Figure 2.49, by means of a friendly interface the user can select all the parameters required by the communication protocol to initiate an acquisition. When the Android device is not connected to a remote ECG system, all the options are locked and parameters can't be modified until a connection is established.

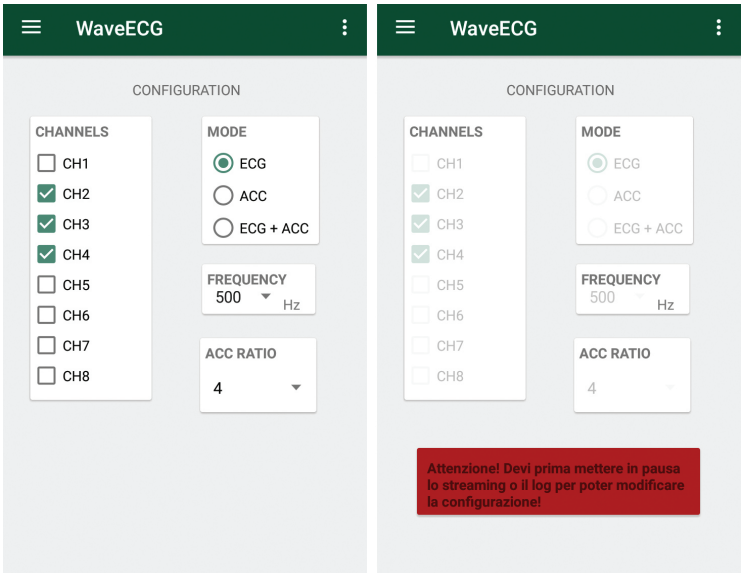

Figure 2.49 – Configuration section view.

- **Log** tab in which the percentage of occupied memory and the number of stored files are displayed. From this section, it is possible to erase the memory, to start and to stop a log session.

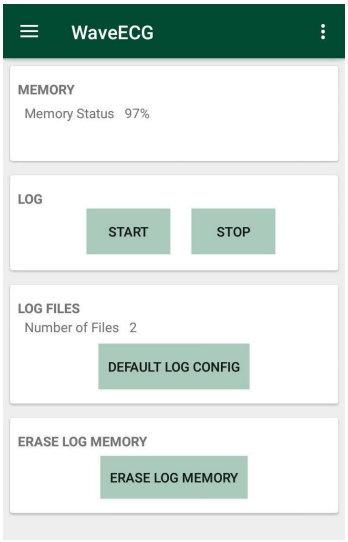

Figure 2.50 – Log section view.

- **Streaming** section in which streaming acquisitions can be controlled and the received data are plotted. According to the actual configuration, the user is able to see the representation of enabled ECG channels and accelerations. At the end of an acquisition, it is possible to save the samples of the current acquisition in a log file that will also contain the streaming configuration.

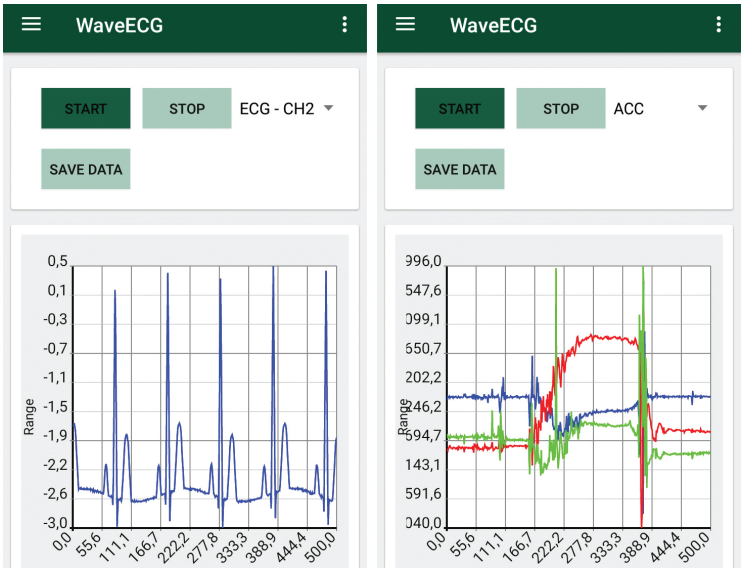

Figure 2.51 – Streaming section view. In the left screen an ECG trace is displayed, whereas in the right screen a plot of the accelerations is shown.

2.4 Characterization and measurements

2.4.1 Power consumption

The power consumption of the developed ECG wearable system was measured in order to assess its autonomy. The platform's current drawn depends on the system state therefore measurements were performed for the main states defined in the firmware.

State	Current	Power	Autonomy
Off	4.221 µA	16.040 µW	–
Stop	129.315 µA	491.397 µW	1198 h
Idle	3.618 mA	13.748 mW	42.8 h
Connected	14.429 mA	54.830 mW	10.7 h
Log	19.998 mA	75.992 mW	7.7 h
LP log	8.954 mA	34.025 mW	17.3 h
Stream	20.842 mA	79.200 mW	7.4 h

Table 2.7 – Average power consumption of the wearable ECG system in different operating states.

The system was supplied with a constant voltage of 3.8 V by means of a Keysight E3631A power supply and the current measurements were performed using an Agilent 34461A digital multimeter. The multimeter was set with an aperture of 0.02 PLC (power line cycles) to capture fast transients and 100000 samples were averaged for each state. In order to have a better statistical significance, the power consumption was measured for 4 different systems and Table 2.7 reports the mean value observed on the platforms. The autonomy for each state does not take into account possible state transitions due to timeouts, external events or user commands and it is computed considering the battery capacity of 155 mAh.

For specific applications which require long term monitoring, batteries with higher capacity can be fitted. The battery life in the off state is not reported because the current drawn is comparable with the self-discharge rate of the battery.

2.4.2 Input-referred noise

The noise performance is particularly relevant when measuring low-amplitude biopotential signals. The noise of the ADS1298R analog front-end depends on the data rate and PGA settings. The RMS and peak-to-peak noise was calculated using a minimum of 1000 consecutive readings measured at a frequency of 500 Hz, thus corresponding to 1 minute long acquisitions. The inputs of the ADS1298R were internally shorted by setting the specific registers and the characterization was reiterated for each channel and PGA gain. Tables 2.8 and 2.9 show the measured RMS and peak-to-peak input-referred noise.

Input-referred RMS noise [μV_{RMS}]							
PGA Gain	**1**	**2**	**3**	**4**	**6**	**8**	**12**
Channel 1	1.61	3.71	0.80	0.77	0.69	0.62	0.61
Channel 2	2.16	1.18	0.88	0.74	0.66	0.59	0.57
Channel 3	2.12	1.22	0.99	0.75	0.67	0.62	0.56
Channel 4	2.08	1.34	1.13	0.75	0.71	0.68	0.71
Channel 5	2.26	1.22	0.91	0.84	0.76	0.66	0.60
Channel 6	2.13	1.32	1.07	0.90	0.93	0.83	0.63
Channel 7	2.12	1.20	0.92	0.95	0.68	0.75	0.76
Channel 8	2.10	1.17	0.93	0.73	0.65	0.56	0.55
Average	2.07	1.55	0.95	0.80	0.72	0.66	0.62

Table 2.8 – Measured input-referred noise expressed in μV_{RMS} of the ECG analog front-end.

Input-referred peak-to-peak noise [μV_{pp}]							
PGA Gain	**1**	**2**	**3**	**4**	**6**	**8**	**12**
Channel 1	10.01	21.41	4.77	4.29	3.15	4.15	3.19
Channel 2	14.31	6.72	6.49	4.65	4.10	3.65	2.88
Channel 3	15.45	6.87	5.15	5.44	3.96	3.50	3.08
Channel 4	11.73	8.58	5.63	4.58	3.72	3.83	3.12
Channel 5	12.30	7.15	5.53	5.15	4.39	4.15	3.43
Channel 6	13.45	39.05	5.46	4.86	3.53	3.18	3.31
Channel 7	13.45	7.44	5.34	4.72	3.77	3.25	3.34
Channel 8	12.87	7.87	5.05	4.94	3.67	3.72	2.69
Average	12.95	13.18	5.42	4.83	3.78	3.68	3.13

Table 2.9 – Measured input-referred noise expressed in μV_{pp} of the ECG analog front-end.

In a second configuration, noise was measured by physically shorting ECG cables in

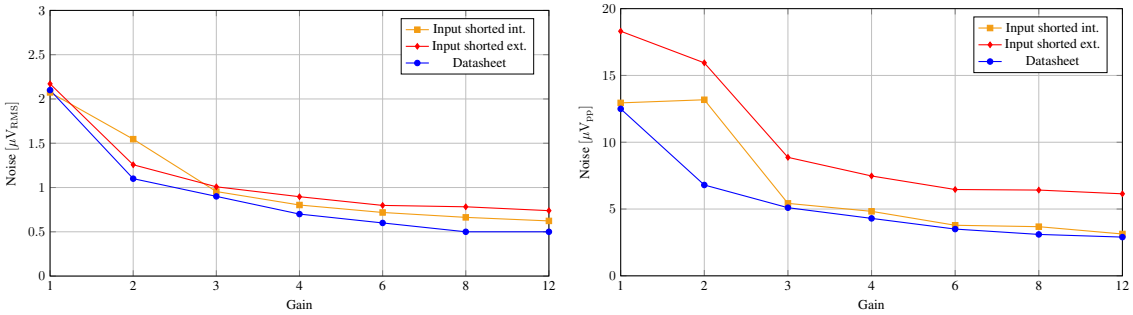

(a) Input-referred RMS noise

(b) Input-referred peak-to-peak noise

Figure 2.53 – Measured noise values of the ECG wearable system.

order to consider disturbances picked up by PCB traces, board-to-board connectors and wires. The plots depicted in Figure 2.53 summarizes the results and make a comparison with the ADS1298R noise values obtained from its datasheet. It is possible to conclude that measured values are compatible to what declared in the analog front-end datasheet. Using any of possible PGA settings, the noise is much less than $30\,\mu V_{\mathrm{RMS}}$ which is the typical specification for ECG medical instrumentation (IEC60601-2-51,27).

2.4.3 Measurements with patient simulator

Preliminary measurements on the wearable ECG systems have been carried out using a patient simulator, a device able to replicate human vital signs. The model used for these measurement is the Rigel 333, a multi-parameter simulator designed to generate patient signals of ECG (up to 12 leads), arrhythmia, invasive blood pressure, respiration and temperature. The device also simulates square, sine, triangle and pulse waveforms. The menu is operated by means of specific buttons and the functions are displayed on a LCD display. The patient simulator is powered by a 9 V battery and the main parameters configurable are displayed in Table 2.10.

ECG	
Performance waveforms	sine, square, triangle, pulse
Frequency (perf.)	0.1 Hz - 100 Hz
Amplitude (perf.)	0.1 mV - 5 mV
Leads	12, referred to RL
Rate (ECG)	30 bpm - 350 bpm
Amplitude (ECG)	0.1 mV - 5 mV
Arrhythmias	more than 20 types
Respiration	
Rate	15, 30, 60, 120 bpm
Baseline impedance	100, 250, 500, 750 Ω
Impedance variation	0.1, 0.5, 1, 1.5 Ω
Apnea	Yes

Table 2.10 – Main features of Rigel 333 patient simulator.

The patient simulator was connected with the wearable system using the snap but-

ton/banana adapters provided with the Rigel 333 device [44]. It has to be noticed that lead I and lead III are respectively 0.6 and 0.4 times the amplitude of lead II.

Amplitude [mV]	Meas. amplitude [µV]		
	Lead I	Lead II	Lead III
0.1	63.26	102.62	41.22
0.2	121.46	199.96	80.92
0.5	294.99	493.50	198.75
1	598.34	1002.12	403.29
2	1193.86	1999.45	804.72
3	1790.04	2999.66	1207.59
4	2385.51	3997.60	1609.00
5	2982.16	4997.44	2011.12

Table 2.11 – Measured amplitudes of the triangle waveform generated by the Rigel 333 patient simulator.

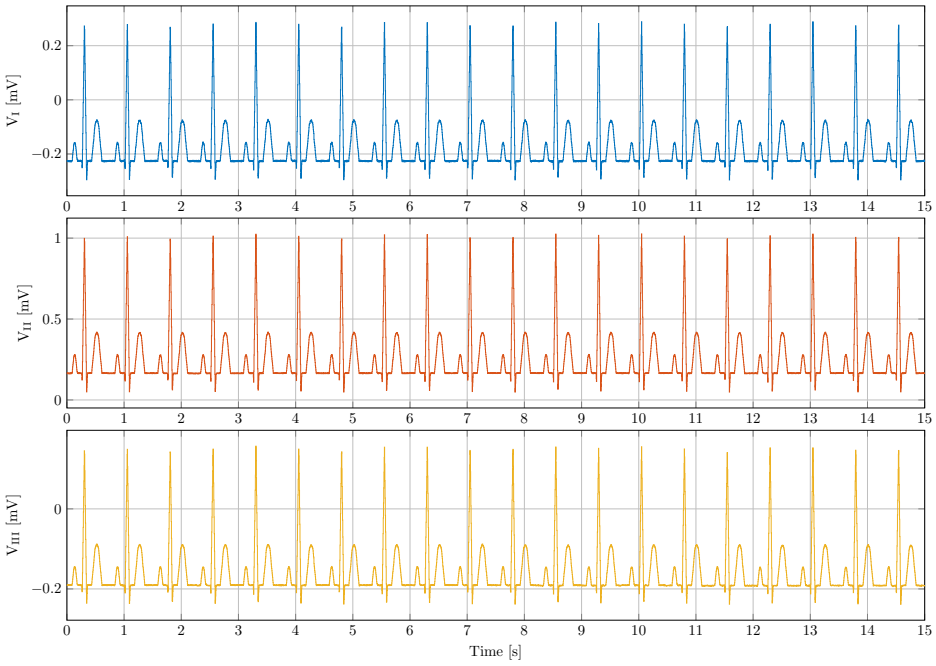

Figure 2.54 – ECG traces generated by the patient simulator and acquired at a frequency of 500 Hz using the wearable system.

Preliminary measurements were carried out by measuring the limb leads of the patient simulator set to generate sine, square and triangle performance waveforms. For each lead, the mean amplitude of the signal acquired by the wearable system was computed. Table 2.11 summarizes the results obtained with a triangle waveform for all the allowed amplitudes of the patient simulator. In a similar way the patient simulator was set to

output a normal sinus rhythm with a rate of 80 bpm and the three bipolar leads were measured. Figure 2.54 depicts the acquired ECG signal with an amplitude (referred to Lead II) of 1 mV. As it can be noticed, all the relevant waves are correctly represented and their respective amplitudes and duration can be easily calculated.

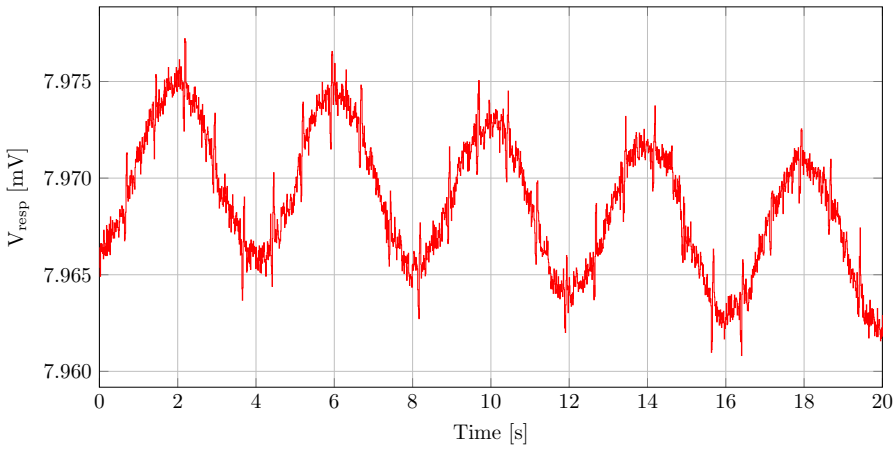

Figure 2.55 – Respiratory impedance signal generated by the patient simulator and acquired using the wearable system.

An additional set of measurements was performed to measure the respiratory impedance generated by the patient simulator. As depicted by Table 2.10 different settings are available for the baseline impedance and the impedance variation. Figure 2.55 depicts the measurement of the respiration trace with a baseline impedance of 500 Ω, an impedance variation of 1 Ω and a breath rate of 15 bpm.

2.4.4 Measurements with gel electrodes

Disposable ECG Ag/AgCl gel electrodes are the standard in hospital exams and they consist in a foam substrate with a thin silver-plated disk covered by electrolyte gel. The substrate uses an adhesive to provide a stable mechanical contact with the skin. Measurements have been carried out using disposable ECG electrodes connected to the platform to assess the performance of the device with medical grade electrodes. Several measurements were performed in order to validate the correct operation of the system and the capability to acquire a good quality signal in different circumstances. The following figures depict some representative measurements performed using the wearable ECG system:

- At rest with the right leg drive (RLD) buffer disabled.
- At rest with the right leg drive (RLD) buffer enabled.
- During a light physical exercise (RLD buffer enabled). The exercise was performed in supine position and the volunteer was asked to perform the following tasks: deep breathing, hands raising, abdominal crunches.
- During a slow pace walk (RLD buffer enabled).

It is possible to observe that the RLD buffer allows to acquire clearer traces since common mode interferences, mainly 50 Hz pickup and harmonics from the power mains, are attenuated. Moreover, during motion the recorded waveforms have sufficient quality to distinguish all the specific waves of an electrocardiogram.

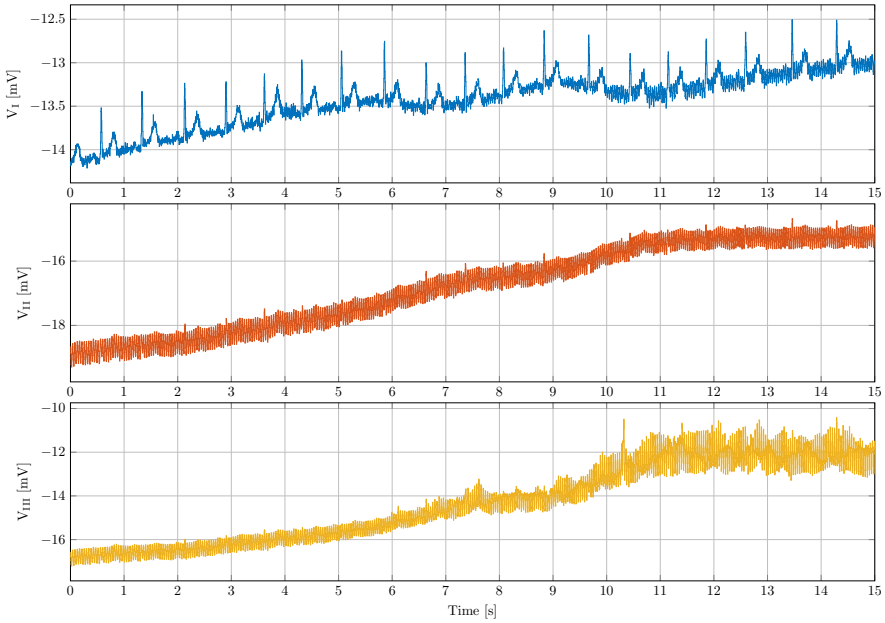

Figure 2.56 – ECG traces acquired in rest condition with the RLD buffer disabled.

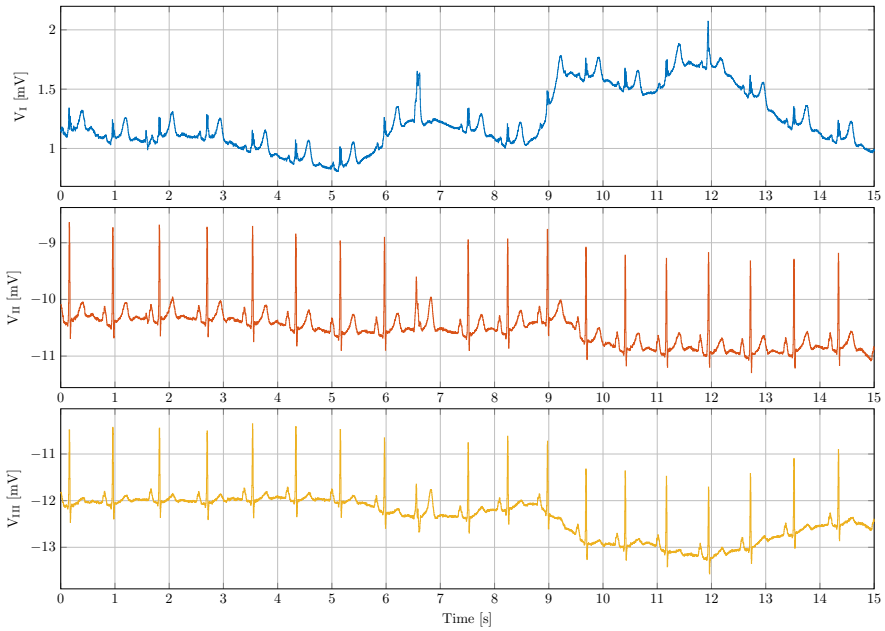

Figure 2.57 – ECG traces acquired in rest condition with the RLD buffer enabled.

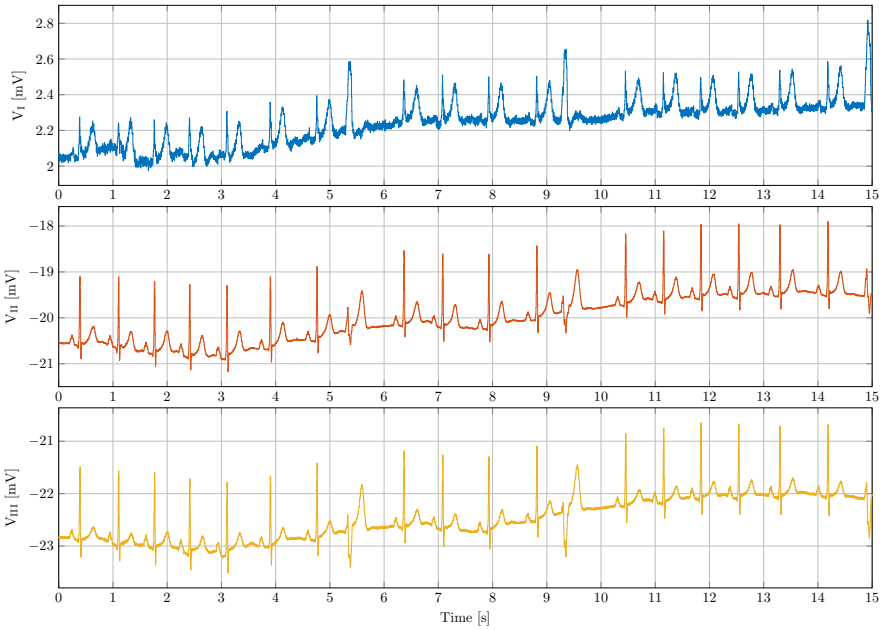

Figure 2.58 – ECG traces acquired during a light physical exercise with the RLD buffer enabled.

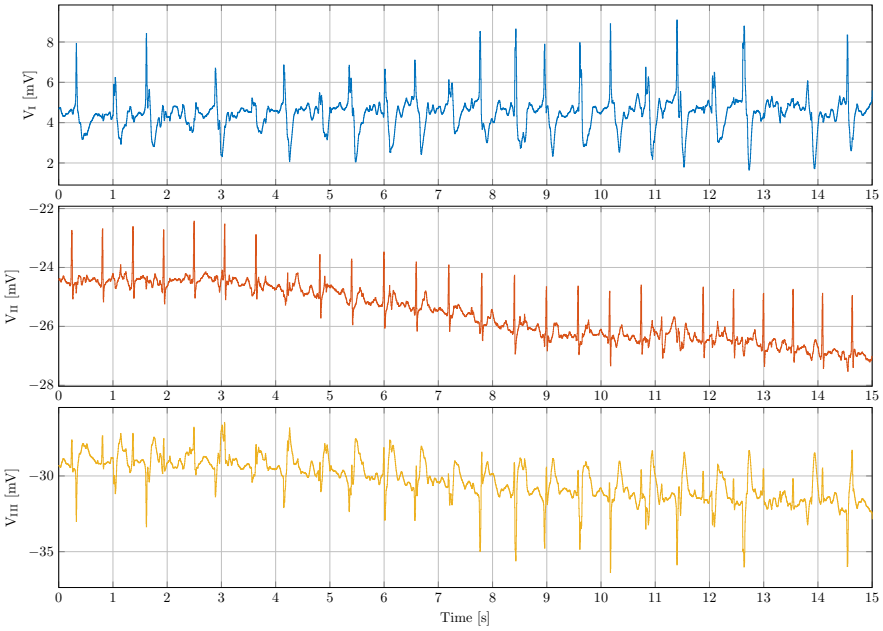

Figure 2.59 – ECG traces acquired during a slow pace walk with the RLD buffer enabled.

2.4.5 Measurements with smart textiles

To demonstrate the feasibility of a fully wearable system based on the proposed hardware, graphite treated textiles have been used as electrodes to carry the ECG signals from the body. One of the main advantages of these textiles is that they feature a low electrical resistivity and almost any kind of substrate can be treated by applying a thin layer of graphite paste, making them suitable for garments and wearable applications. In the framework of a wider project aimed to prove the usability of such materials for the development of wearable electronics, several kinds of textiles treated differently were characterized by evaluating the surface resistance. Among these, the one featuring the lowest surface resistance was used for the development of ECG electrodes. Strips of conductive paste were laid down on a technical t-shirt and a button female connector has been crimped at one end of each strip, in such a way to provide an extraction point and a connection to the electronic system, whereas a wider area has been tailored at the other end of the strip to improve the electrical contact with the body skin. The total resistance, measured between the two ends of the strip, is equal to 120 Ω. Two electrodes are located on the upper chest whereas the other two are situated on the abdomen in order to make possible the measurement of the three leads ECG and to drive the right leg electrode. Figure 2.60 shows the final prototype of t-shirt, whereas Figure 2.61 depicts the measured ECG traces using the smart textile based electrodes in which all the waves are clearly represented. It is important to notice that no filtering techniques were applied to the recorded signals.

Figure 2.60 – Prototype of the t-shirt with conductive traces.

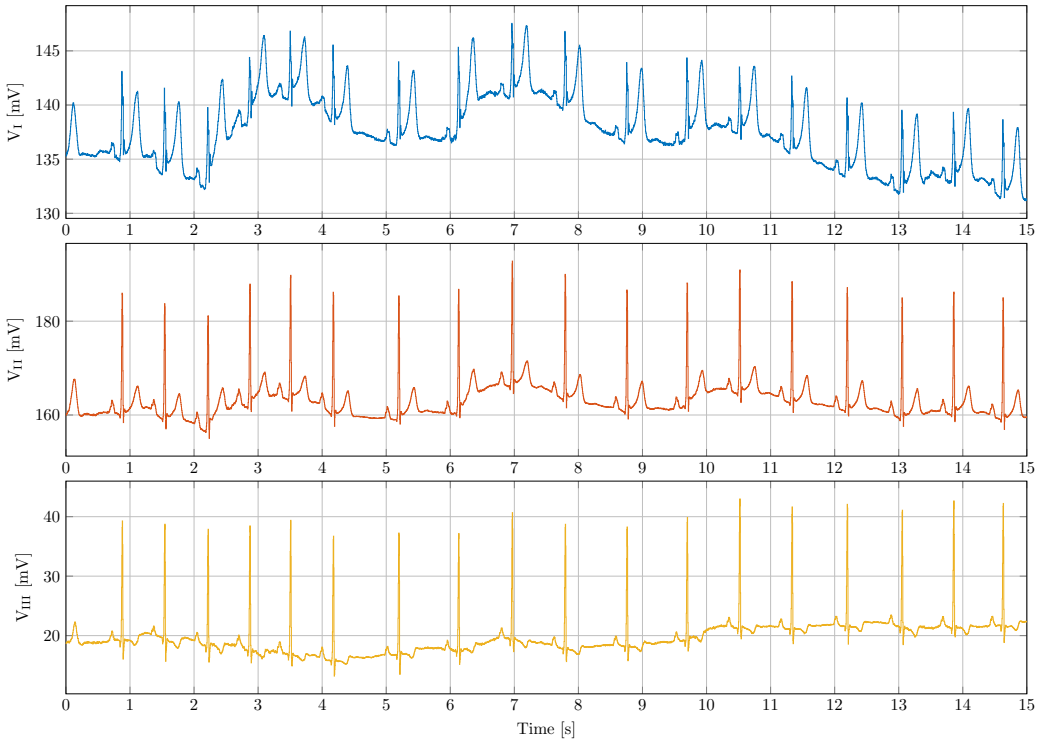

Figure 2.61 – ECG traces acquired using the prototype of t-shirt based on smart-textiles.

2.5 State-of-the-art

In this section several wearable systems for ECG measurement are analyzed in order to perform a comparison between the presented device and the state-of-the-art solutions. A wide variety of systems were considered, and both commercial and research devices were included. This kind of platform are becoming more and more relevant in different field of application: from telemedicine to fitness tracking. They have to meet several requirements in terms of miniaturization, for an easy to use and non-invasive solution, power consumption, for a higher longevity of the system without the need of being frequently recharged, and embedded processing, to increase the Signal-to-Noise ratio and reduce the overhead on the end user visualization and analysis side.

2.5.1 Delano et. al.

A low-power wearable ECG was developed by Delano et. al. in 2013 [45]. The system was designed to perform long-term data acquisitions and to maximize both comfort and ECG signal quality. The devices consists of a central PCB that contains one electrode and most of the electronics. Two additional satellite PCBs house the remaining electrodes and buffer circuits to complete the system. The ECG traces are recorded on a removable micro SD card and the autonomy can reach one week of continuous operation. The monitor was compared with a commercially available device and results showed that the QRS sensitivities are comparable. Figure 2.62 shows a photograph of the presented cardiac monitor worn at the chest.

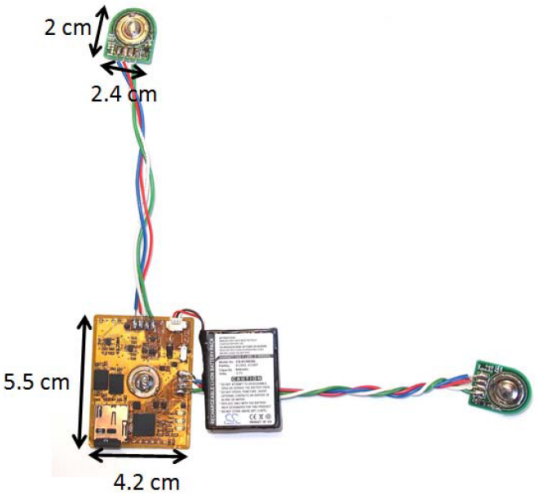

Figure 2.62 – Photograph of the ECG device presented by Delano et. al.

2.5.2 Wang et. al.

The device presented by Wang et. al (2010) [46] is a ECG acquisition module with three-lead recording capability. A king of dry foam electrode which can adapt to the skin surface and guarantees small relative motion of the skin to electrode was used to acquire ECG signals. The electrodes were embedded in a vest designed to collect the ECG form the human body continuously during daily activities. The collected traces are transmitted via Bluetooth to a smartphone and then forwarded to a remote server. The healthcare server analyzes the traces and triggers alerts if anomalies are detected. The system, whose block diagram is depicted in Figure 2.63, has an autonomy of 33 hours.

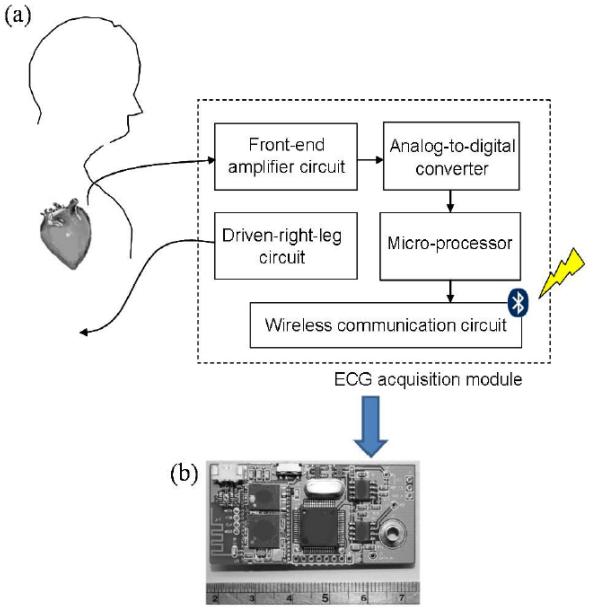

Figure 2.63 – Photograph and block diagram of the ECG device presented by Wang et. al.

2.5.3 Lee et. al.

The system designed by Lee et. al. (2014) [47] is a ECG sensing device with a wireless module that can be mounted on a custom t-shirt. The sensor node includes a microcontroller and an analog-to-digital converter which digitizes and process the measured ECG and accelerometer signals. The processed data are encapsulated into packets and transmitted by means of a Zigbee module to the relay nodes. The bio-shirts for male and female are designed with two conductive fabric electrodes sewed onto the shirt to obtain the ECG signal from the individual's chest. A custom protocol was developed in order to build a fast link exchange scheme. The proposed protocol minimized the abrupt path breakage and packet loss caused by movements of the mobile node. Figure 2.64 shows a photograph of the system mounted on the prototype of the describe t-shirt.

Figure 2.64 – Photograph of the ECG device mounted on male and female shirts presented by Lee et. al.

2.5.4 Gjoreski et. al.

The device presented by Gjoreski et. al. in 2014 [48] is a body sensor network consisting of an ECG sensor and two wearable accelerometers. Figure 2.65 depicts the architecture of the system. The ECG node is constituted by two self-adhesive electrodes, an analog front-end, a microcontroller and a Bluetooth v 4.0 radio. The analog front-end is designed to remove unwanted disturbances and to amplify the ECG signal, whereas the digitization is carried out by the MCU integrated ADC. The accelerometers were integrated in order to recognize the activity performed by the user.

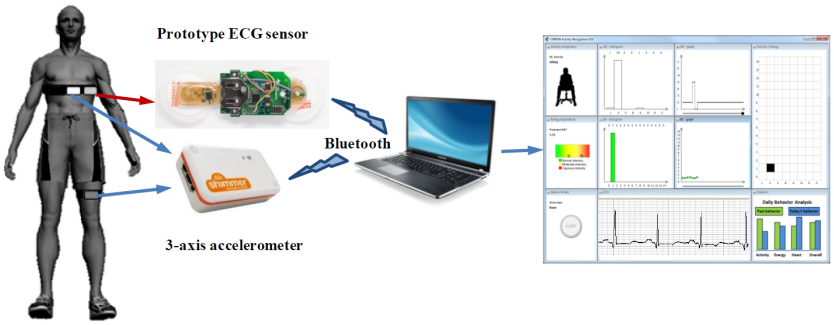

Figure 2.65 – System design of the ECG system presented by Gjoreski et. al.

2.5.5 Valchinov et. al.

In 2014 Valchinov et. al. [49] presented a wireless ECG system using dry-contact electrodes. The system is composed of two main parts: an analog front-end that senses and amplifies the cardiac biopotential and a digital part that samples and transmits data to a remote device for storage and processing. The system is completed by a pair of coin sized dry-contact electrodes manufactured on a standard printed circuit board. The main wireless unit contains a microcontroller and a 2.4 GHz radio. The nRF51422 system-on-chip (SoC) embeds a transceiver which supports both ANT and Bluetooth Low Energy protocols. The system is powered by a lithium polymer battery which provides about 24 hours of continuous monitoring. Preliminary test measurements were performed with the proposed ECG system using a compression vest to ensure optimal electrodes fixation to the body by providing firm thoracic elastic enclosure. Results showed that the proposed system is suited for mobile monitoring applications for health and sports.

2.5.6 Spanò et. al.

The solution presented by Spanò et. al. (2016) [50] is an ECG remote monitoring system dedicated to non-technical users in need of long-term health monitoring in residential environment integrated in an Internet-of-Things (IoT) infrastructure. The proposed platform has three main parts: the sensor, the IoT server, and the user interfaces for data visualization and management. Lightweight wearable ECG sensors collect data and sent them in real time via a wireless connection to a gateway connected to the Internet. The IoT server converts the raw payload into a "universal" format making the data visualization and processing separated from measurement and data collection. The entire system is configurable through a web interface from any device connected to the Internet. The wearable ECG sensor consists of a battery-powered chestbelt enabling the measurement and streaming transmission of ECG signals during daily routines. The belt is equipped by two dry electrodes. The circuitry extracts, filters, amplifies, and digitizes the ECG signal which is then acquired by the microcontroller and transmitted using a Zigbee radio. The prototype of the system is shown in Figure 2.66.

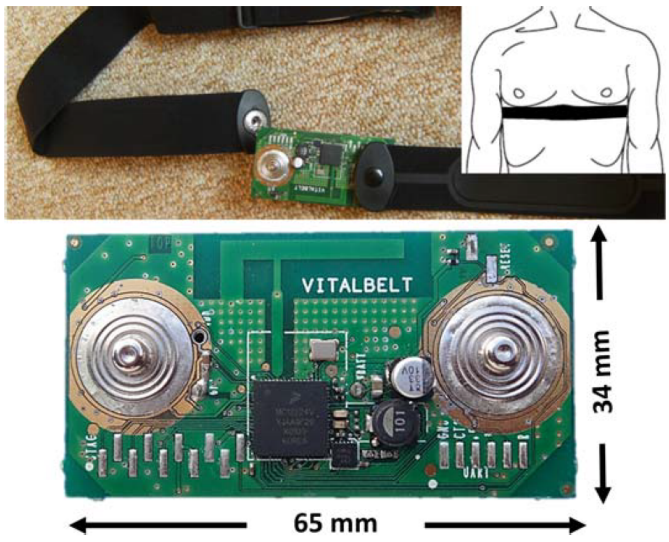

Figure 2.66 – ECG system developed by Spanò et. al.

2.5.7 Preejith et. al.

The device presented in 2016 by Preejith et. al. [51] is a low-power ECG platform for continuous and minimally invasive monitoring. The developed platform includes a wearable ECG patch with wireless connectivity and a gateway device for data visualization. The patch node integrates a feature extraction and rhythm analysis algorithm. Additionally, the device is able to store raw data locally for offline analysis. The devices can operate in two different modes: continuous monitoring and real time visualization. By default, continuous monitoring mode is enabled and the signals are acquired and processed using the proprietary algorithms in order to extract relevant features. On the other hand, real time visualization mode allows to display the real-time data acquired by the system. Figure 2.67 shows a photograph of the developed hardware.

Figure 2.67 – ECG system developed by Preejith et. al.

2.5.8 Zephyr BioHarness 3

BioHarness 3.0 (Figure 2.68) [52] is a small device which allows to acquire and transmit several parameters useful for the individual's monitoring. It is proposed for different application fields ranging from sport to fitness and from medicine to defense. It is possible to mount the main unit on a specifically developed garment which integrates dry electrodes and wires. The device is powered by a lithium-ions rechargeable battery that allows to achieve 24 hours of continuous transmission or 35 hours in log mode.

Figure 2.68 – Photograph of the Zephyr BioHarness 3.0 device.

2.5.9 Alivetec Alive

Alive Bluetooth Heart and Activity Monitor (Figure 2.69) [53] is a telemedicine device which can be used to monitor patients affected by cardiac diseases, but it is easily adaptable in other contexts such as rehabilitation or physical performance assessment. Thanks to the integrated Bluetooth transceiver is is possible to transmit and visualize the acquired signals on a smartphone. The device is completed by a mobile application that allows to display the real-time ECG traces. The system is powered by a rechargeable battery which guarantees up to 48 hours of continuous operation. Moreover, the ECG signal can be recorded on an external micro SD memory card.

Figure 2.69 – Photograph of the Alivetec Alive Bluetooth heart and activity monitor.

2.5.10 State-of-the-art comparison

The system proposed in this work has been compared to wearable state-of-the-art solutions presented in literature and commercially available in terms of number of leads, additional sensing capabilities, RLD circuit, dimensions, AFE noise, wireless capabilities and power consumption. Results are summarized in Table 2.12. As it can be noticed, the proposed system is among the few featuring more than 1 lead ECG and respiration detection, as well as body skin temperature measurement and the RLD capability. The current consumption in streaming mode, during which the entire raw measurements of the 3 leads and the bioimpedance sampled at 500 Hz are transmitted through the Bluetooth link, is about 30 mA, setting the battery life of the system to about 7 hours of continuous operation. However, the power consumption can be lowered significantly by enabling the low power log mode that allows to achieve an autonomy of 17 hours , and a higher capacity battery can be used in order to increase time between charges. All these features have been achieved in a form factor which is comparable to or lower than state-of-the-art solutions, making the proposed system an attractive solution for wearable multi-lead ECG applications.

	Leads count	Resp.	Body temp.	RLD circuit	Area W x L [mm^2]	Height [mm]	Resolution [bit]	Sample rate [Hz]	Input noise [nV$_{RMS}$]	Wireless conn.	Current drawn [mA]	Battery capacity [mAh]	Autonomy [h]
[45]	1	No	No	Yes	55 x 42	6.9	12	250	3600	No	2.72	600	220
[46]	1	No	No	Yes	40 x 25	0.6	12	512	n.d.	BT	31	1100	33
[47]	1	No	No	No	58 x 22	n.d.	14	100	n.d.	Zigbee	41.8	500	10
[48]	3	Yes	No	No	n.d	n.d.	10	125	n.d.	BT	n.d	180	n.d.
[49]	1	No	No	Yes	n.d	n.d.	10	500	n.d.	BLE	11	280	24
[50]	1	No	No	No	65 x 34	17	24	320	48	Zigbee	4.07	650	160
[51]	1	Yes	No	Yes	130 x 50	11	12	750	n.d.	BLE	9	390	96
[52]	3	Yes	Yes	No	28 (diam.)	7	12	250	n.d.	BT	n.d.	n.d.	18
[53]	1	No	No	No	90 x 40	16	8	300	n.d.	BT	n.d.	n.d.	48
This work	3 (11)	Yes	Yes	Yes	30 x 25	10	24	500	620	BT	8.95	155	17

Table 2.12 – Performance comparison between the presented ECG wearable system and the state-of-the-art solutions.

Chapter 3

Wearable in-ear PPG system

This chapter illustrates a wearable system able to acquire, store and transmit PPG signals in a small form factor compatible with ear canal level measurements. The platform is completed by a software that allows to command its operation. Different measurements were performed in order to characterize the system and determine the best configuration leading to a trade off between power consumption and signal quality. Moreover, an investigation of the best body measurement location has been carried out and two different algorithms have been developed: the former is a lightweight procedure for heart rate (HR) estimation suitable for embedded implementation, whereas the latter features a motion mitigation adaptive filter to compensate the effect of motion artifacts (MAs). It is worth to note that the system is particularly suited to be used during motion and it is easily integrable in earbuds or headphones. Finally, an assessment of the system presented in this work was performed by comparing its main features with the state-of-the-art devices.

3.1 Hardware

The system was designed to be composed of two distinct systems on board. The main board integrates the electronics needed for managing system operation, data acquisition, storage and transmission, whereas the probe board integrates the PPG sensor, a 3D MEMS (Micro Electro-Mechanical Systems) accelerometer and a Low-Dropout Regulator to power the low-voltage digital circuitry at 1.8 V. This board is designed to be comfortably located in the ear canal thanks to its form factor of 10 x 5 x 3.4 mm (L x W x H).

3.1.1 First motherboard prototype

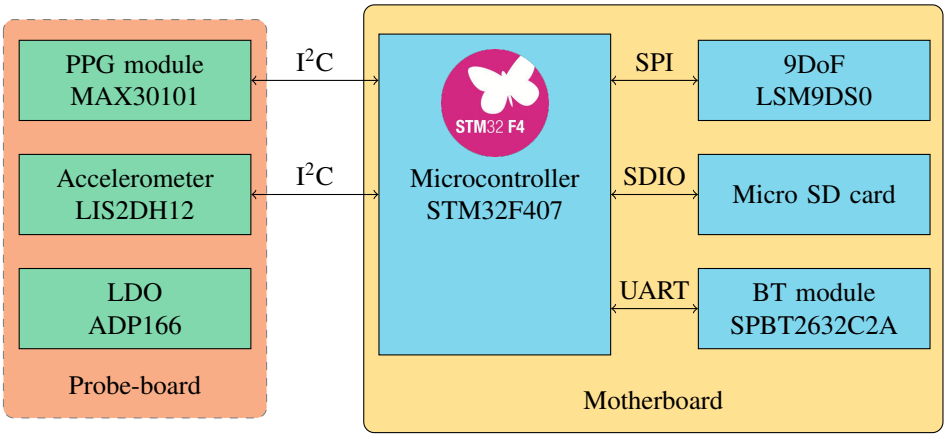

Figure 3.1 – Block diagram of the wearable sensor system for PPG measurements (first prototype).

A first prototype was built using a *neMEMSi Xtreme*, a hardware platform developed in the Microeletronics laboratory of the University of Bergamo in collaboration with 221e Srl. The system is a general purpose inertial platform based on MEMS sensors that integrates computational capabilities and a Bluetooth 3.0 wireless module. Thanks to the integrated sensors, the system can be used as a low-power AHRS (Attitude and Heading Reference System). The motherboard, whose block diagram is shown in Figure 3.1, is made up by the following main blocks:

- **STM32F407IEH6** microcontroller [54] manufactured by STMicroelectronics and based on the high-performance ARM® Cortex® M4 32-bit RISC core operating at a frequency up to 168 MHz. The Cortex® core features a Floating Point Unit (FPU) single precision and implements a set of DSP instructions. The microcontroller embeds 512 kB of flash memory and 192 kB of random access memory and an extensive range of enhanced I/Os and peripherals connected to two APB buses, three AHB buses and a 32-bit multi-AHB bus matrix. The STM32F407IEH6 microcontroller is available in a scaled UFBGA176 10 x 10 mm package.

- Three **TPS79933** Low-dropout regulators [55] used to power the sensors, the Bluetooth radio and the microcontroller. The operating voltage of *neMEMSi Xtreme* is equal to 3.3 V and the supply is made available through a dedicated connector which allows to power to the probe board.

- **L6924D** charger [56] dedicated to single-cell Li-Ion/Polymer battery packs. It works in linear mode and allows to charge the battery with a constant current/constant voltage (CC/CV) profile. It integrates all the power elements in a small 3 x 3 mm VFQFPN16 package.

- **LSM9DS0** system-in-package [57] featuring a 3D accelerometer, a 3D gyroscope and a 3D magnetic sensor. It allows to set the full scale of each specific sensor and it communicates with the host microcontroller through a SPI interface. The LSM9DS0 is available in 4 x 4 mm LGA24 package.

- **M41T62** Real Time Clock (RTC) [34] with embedded 32 kHz oscillator in a small LCC8 1.5 x 3.2 mm package.

- **SPBT2632C2A** class 2 Bluetooth module [35] which allows to communicate up to 10 m at a rate of 560 kbps with Serial Port Profile (SPP) service active.

- **Micro SD** card slot supported by the SDIO (Secure Digital Input Output) interface offered by the microcontroller in two different modes: 1 or 4 bits wide bus. The maximum communication speed is achieved with the maximum clock frequency of 48 MHz.

The electronic system features a connector which allows to upload the binary code and perform the debug operations by means of the external ST-Link V2 debugger through the SWD interface. A micro-switch is used to power on and switch off the system, whereas two buttons make it possible to reset the system or to start an acquisition session. Moreover, thee LEDs (blue, green and orange) can be switched on to discriminate the state of the system. A specific connector provides an interface to the probe board for the power supply and the serial communication signals. *neMEMSi Xtreme* has an overall form factor of 54 x 25 x 6 mm and Table 3.1 depicts some features of the main components.

Part number	Description	Main features	Current consumption
STM32F407IE	MCU	4x USARTs 3x SPIs 3x I^2Cs 1x SDIO 1x USB 2.0 3x 12 bit ADCs 14 timers 512 kB flash memory 192 kB SRAM	238 µA/MHz
TPS79933	LDO	200 mA max. current 100 mV dropout 35 μV_{RMS} out noise	40 µA quiescent current
L6924D	Battery charger	Programmable charge currents up to 1 A	1.8 mA charging 60 µA shutdown
LSM9DS0	Inertial module	3D accelerometer 3D gyroscope 3D magnetometer SPI/I^2C serial interfaces	350 µA acc + magn 6.1 mA gyro
M41T62	RTC	I^2C serial interface	375 nA
SPBT2632C2A	BT module	UART serial interface SPP service AT2 command set Integrated antenna	11.2 mA Connected, no traffic

Table 3.1 – Main features of the components included in the first motherboard prototype for PPG measurements.

3.1.2 Final motherboard

After the demonstration of the correct operation of the first prototype, the final motherboard was developed in order to optimize the power consumption, the form factor and the wearing comfort for the user. Besides the specific implementation, it has to be noticed that the motherboard was designed for general purpose applications and for this reason additional sensors were integrated without jeopardizing the dimensions. The motherboard is composed, as shown by Figure 3.2, by the following building blocks:

- **STM32L475RG** ultra-low-power microcontroller [58] manufactured by STMicroelectronics and based on the high performance ARM® Cortex® core operating at a frequency up to 80 MHz. The processing core features a Floating Point Unit single precision, it implements a full set of DSP instructions and a memory protection unit which enhances application security. The microcontroller embeds 1 MB of flash memory, 128 kB of SRAM, and extensive support for I/Os and peripherals connected to two APB buses, two AHB buses and a 32-bit multi-AHB bus matrix. The device is available in a 10 x 10 mm LQFP64 package. The **ABS06-1-T** SMD crystal was connected to the microcontroller to obtain a more accurate and precise time-base. It

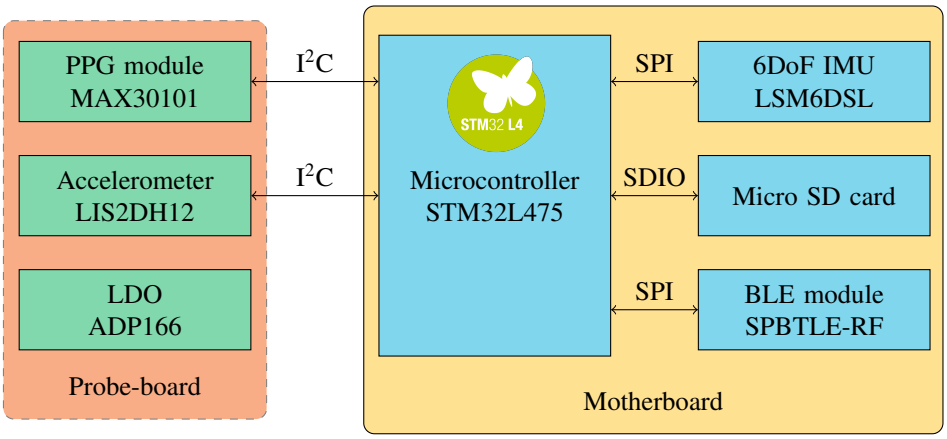

Figure 3.2 – Block diagram of the wearable sensor system for PPG measurements (final version).

generates a clock signal of 32.768 kHz with a frequency tolerance of ±10 ppm (parts per million).

- **TPS62740** step-down converter [26] which allows to scale down to the 3 V operating voltage. The device is particularly suited for light loads since it guaranteed up to 90 % efficiency at 10 µA output current. The typical quiescent current of the converter is 360 nA and it supports output currents up to 300 mA. The device features an auxiliary rail that can be used to power subcircuits which can be selectively turned off during low power states. The buck converter is available in a small 12 pin 2 x 3 mm WSON package.

- **MCP73831T** linear charge management controller [27] which supervises the charging process of the single cell 210 mAh Li-poly battery. The charge current is set to 50 mA. The IC is available in a small TSOP5 package.

- **MAX17048** fuel gauge [59] for lithium-ion batteries which uses a modeling algorithm to track the battery state-of-charge (SoC) continuously over varying charge and discharge conditions. The SoC and battery voltage can be read out by the microcontroller through an I²C compatible serial interface. The IC automatically detects when the battery enters a low current state and enables a low power 3 µA hibernate mode, while still providing accurate tracking of the state of charge. The MAX17048 is available in a small 2 x 2 mm TDFN8 package.

- **LSM6DSL** system-in-package [60] featuring a 3D digital accelerometer and a 3D digital gyroscope with full scale ranges of ±2 / ±4 / ±8 / ±16 g and ±125 / ±250 / ±500 / ±1000 / ±2000 dps respectively. The IC communicates with the host microcontroller by means of a SPI interface and it is available in a plastic 5 x 3 mm LGA14 package.

- **HTS221** sensor for relativity humidity and temperature [61]. It includes a sensing element and a mixed signal ASIC to provide the measurement to the host microcontroller through a dedicated I²C interface. The temperature accuracy of the device is equal to 0.5 °C, whereas it humidity accuracy is 3.5 % rH. The IC is available in a miniaturized 6 pin 2 x 2 mm LGA package.

- **LPS22HH** piezoresistive absolute pressure sensor [62] functioning as a digital output barometer with a 260 to 1260 hPa absolute pressure range and an accuracy of 0.5 hPa. The IC communicates with an I^2C interface and it is integrated in a 10 pin 2 x 2 mm LGA package.
- **SPBTLE-RF** Bluetooth® low energy master/slave processor module [63] compliant with Bluetooth v4.1. The Bluetooth low energy stack and protocols are embedded into the SPBTLE-RF module, whereas the external host microcontroller is connected to the radio module through a standard SPI interface. A chip antenna is integrated in the module and the overall form factor is equal to 13.5 x 11.5 mm.
- **Micro SD** card slot allowing the usage of an external memory to store raw signals for long term monitoring. Data can be accessed either by removing the SD card or through the USB connection.
- Two 10-pin **connectors** that make it possible to perform debug operations by connection a ST-Link V2 compatible debugger and to extend the sensing and communication capabilities by providing a socket for potential expansion boards. In fact, the system's power supply, as well as the most common communication interfaces can be exploited through this connector by any auxiliary module.

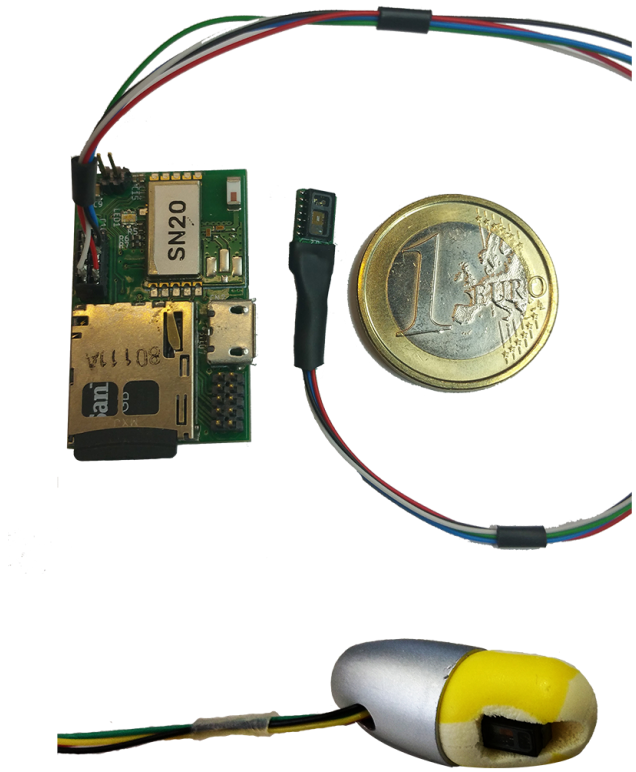

Figure 3.3 – Photographs of the motherboard interconnected with the PPG probe (top). Prototype of regular earbud housing the probe-board (bottom).

Moreover, the motherboard integrates a RGB LED that allows to discriminate the system state and to perform basic debugging operations. The form factor achieved by the motherboard is 32 x 20 x 4.2 mm. The main features of the described components are summarized in Table 3.2, whereas Figure 3.3 shows two photographs of the system.

Part number	Description	Main features	Current consumption
STM32F411RG	MCU	6x USARTs 3x SPIs 3x I^2Cs 1x SDIO 1x USB 2.0 2x 12 bit ADC 16 timers 1 MB flash memory 128 kB SRAM	100 µA/MHz
TPS62740	Buck converter	Selectable output voltage and output currents up to 300 mA	Up to 96 % efficiency
MCP73831T	Battery charger	Programmable charge current from 15 to 500 mA	1.5 mA charging 1 µA shutdown
MCP73831T	Fuel gauge	±7.5 mV precision Configurable alerts I^2C interface	23 µA active 3 µA hybernate
LSM6DSL	6 DoF IMU	3D accelerometer 3D gyroscope Configurable full scales SPI/I^2C serial interfaces	0.45 mA @ 208 Hz Normal mode
HTS221	Humidity and temp. sensor	±3.5 % rH humidity accuracy ±0.5 °C temperature accuracy SPI/I^2C serial interfaces	2 µA @ 1 Hz
LPS22HH	Barometer	0.5 hPa pressure accuracy SPI/I^2C serial interfaces	23 µA active 3 µA hybernate
SPBTLE-RF	BLE module	SPI serial interface BT v4.1 compliant Embedded BLE stack Integrated antenna	250 µA Peripheral adv. (80 ms)

Table 3.2 – Main features of the components included in the final version of the mother-board for PPG measurements.

3.1.3 Probe board

The probe board was designed to be the true sensing unit used for photoplethysmographic acquisitions. Its main requirement was the form factor which was restricted by the ear canal size. The included components are the following:

Part number	Description	Main features
MAX30101	PPG module	Size: 5.6 x 3.3 x 1.55 mm Shutdown current: 0.7 µA PPG supply voltage: 1.7 - 2.0 V LEDs supply voltage: 3 - 5.25 V I^2C serial interface 3 LEDs: red, IR, and green
LIS2DH12	Accelerometer	Size: 2 x 2 x 1 mm Supply voltage: 1.7 - 3.6 V Current consumption: 20 µA @ 100 Hz ±2 g/±4 g/±8 g/±16 g full scales 2 programmable interrupts 6D/4D orientation detection
ADP166	LDO	Size: 0.965 x 0.965 x 0.595 mm Input voltage: 2.2 - 5.5 V Quiescent current: 890 nA Dropout voltage: 120 mV Maximum current: 150 mA Output noise: 9 μV_{RMS}

Table 3.3 – Main features of the components included in the probe-board.

- **LIS2DH12** low-power three-axis linear accelerometer [30] with selectable full scales of ±2 / ±4 / ±8 / ±16 g and sampling frequencies from 1 Hz to 5.3 kHz. The accelerometer is integral with the probe board, therefore motion artifacts degrading the PPG signals can be measured and possibly compensated. The LIS2DH12 is available in a miniaturized 2 x 2 mm LGA12 package.

- **ADP166** low-dropout regulator [64] selected for its very low quiescent current of 590 nA with no loads. The regulator was integrated to supply with the required voltage the digital circuitry of the pulse oximeter module. The fixed 1.8 V output voltage part number was selected and only one input capacitor and one output capacitor of 1 µF each are required for its stable operation. The ADP166 is available in a down-scaled 0.965 x 0.965 mm WLCSP4 package.

- **MAX30101** integrated module for reflective photoplethysmography measurements [65]. It includes internal light sources, photodetectors, optical elements, and low-noise electronics with ambient light rejection. The MAX30101 operates on a single supply of 1.8 V and a separate supply for the internal LEDs. The communication is achieved by means of an I^2C serial interface. The module has a shutdown mode with 0.7 µA standby current to remain constantly powered. The MAX30101 is available in a 5.6 x 3.3 x 1.55 mm 14 pin optical module.

The probe board features a form factor of 10 x 5 x 3.4 mm (L x W x H) and Table 3.3 summarizes the main parameters of its components.

MAX30101 module

The MAX30101, by Maxim Integrated, is a reflective photoplethysmography sensor which can be used as pulse oximeter sensor or heart rate monitor. It includes LEDs having three different wavelengths: red, infrared, and green. Moreover, the MAX30101 integrates in the same package photodetectors, optical elements, and low-noise electronics. The module is particularly suited for wearable applications as it can be integrated in miniaturized systems. The MAX30101 requires a single 1.8 V power supply and a separate power supply for the internal LEDs which is provided by the motherboard and it corresponds to the motherboard's operating voltage. The communication with the host microcontroller is achieved by means of an I^2C serial communication.

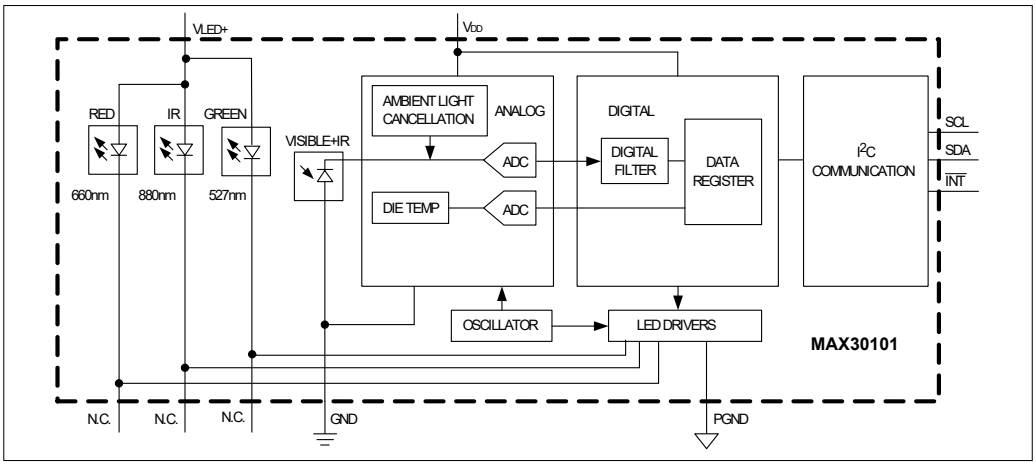

Figure 3.4 – Block diagram of the MAX30101 reflective PPG module.

In Figure 3.4 the block diagram of the MAX30101 module is shown. The main elements are the following.

- SpO_2 subsystem: it contains an internal track and hold circuit to cancel the ambient light, a delta-sigma ADC with a resolution of 18 bit, and a proprietary discrete time filter.
- Temperature sensor: on-chip sensor for calibrating the temperature dependence of the SpO_2 subsystem. The device data is relatively insensitive to the wavelength of the IR LED, whereas the red LED's wavelength is critical for the correct interpretation of data. The temperature sensor has a resolution of 0.0625 °C and it is used to correct data from the error associated with ambient temperature changes.
- LED drivers: each driver is used to modulate led pulses for SpO_2 and HR measurements for a specific LED. The LED current can be programmed from 0 to 50 mA, whereas the LED pulse width can be programmed from 69 µs to 411 µs to optimize accuracy and power consumption depending on the use case.

The MAX30101 has similar features of a device of the same family (MAX30102) adopted in an initial phase of the prototype development. The main difference consists of the integrated LEDs: the MAX30101 includes also a green LED in addition to the red and infrared LEDs of the MAX30102 [66]. The MAX30102 sensor can replace the MAX30101 module when the green LED is not required. Figure 3.5 shows the recommended startup sequence for the MAX30101. It is suggested to power the V_{DD} supply first and then

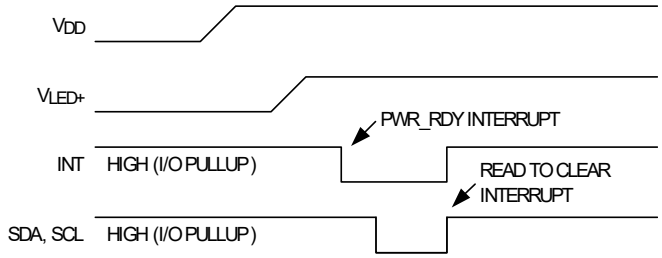

Figure 3.5 – Power-up sequence of the MAX30101 PPG module.

the LED supplies. The interrupt and I^2C pins can be pulled up even when the device is powered-down. After the power is established, an interrupt occurs to alert the system that the PPG module is ready for operation. The interrupt is cleared by reading the specific status register.

3.2 Firmware

3.2.1 Application firmware

The firmware for the wearable PPG system was developed using the same approach described in the previous chapter at Section 2.2.1. The finite state machine in Figure 3.6 formalizes the behavior of the developed firmware.

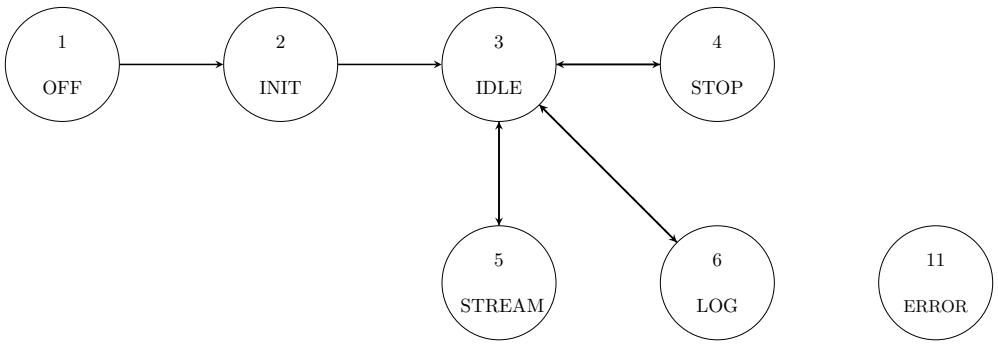

Figure 3.6 – Finite State Machine of the implemented firmware.

It is important to notice that the application firmware is completely interoperable with the MAX30101 and the MAX30102 modules. The firmware was implemented first on the motherboard prototype and then ported on the final version with few architecture dependent modifications. Some of the described features are only available in the final motherboard version. The implemented states are described below.

INIT The *init* state identifies the system during startup when the following tasks are performed:

- Clock configuration. The main system clock is initially set to 24 MHz for the startup phase.
- Configuration of interrupt priorities for the main process and the data collection job.

- RTC initialization.
- Configuration of the `LIS2DSH12` accelerometer mounted on the probe board using default settings.
- Initialization of the MAX30101 PPG sensor using a default configuration in which the ADC full scale is 8192 nA, the sampling frequency is 100 Hz, and the LEDs are supplied with currents of 10 mA. During the initialization phase the PPG sensor is programmed to operate in SpO_2 mode and it is configured in low-power mode.
- The auxiliary output of the `TPS62740` buck-converter is enabled in order to provide the power supply to the BLE module and the micro SD card.
- If the micro SD is mounted and the FatFS file system is initialized.
- Configuration of the additional sensors available on the motherboard (IMU and environmental sensors). During the initialization phase and the *idle* state, the sensors are kept in power-down state.
- Check for the correct configuration and initialization of the peripherals.

During the *init* state the onboard LED is illuminated with red color. If the initialization phase ends successfully, the system goes in the *idle* state.

IDLE When the system goes in *idle* state, the main clock is set to a frequency of 2 MHz and the microcontroller is configured to operate in low power run mode to optimize the energy consumption. The LED blinks with the blue color for 200 ms each 2 s and the system awaits for incoming commands through the BLE radio. If no device connects within 120 s, the system goes into *stop* mode, the lowest power consumption state. By means of specific commands, from *idle* state it is possible to initiate new streaming or log sessions.

STOP After 120 s in which the platform is in the *idle* state without receiving a connection from a client device, the system goes in *stop* mode. In this state, the Cortex core is stopped and the clocks are switched off while SRAM and register content are kept. The system can be awakened from the *stop* state through the tap feature of the onboard IMU.

LOG The *log* state can be reached by sending the `CMD_START_LOG` command. The system verifies whether the micro SD card is correctly mounted and has free space available, sensors are awakened and then the acquisition starts. A separate header file is saved in order to keep trace of the current acquisition settings (e.g. acquisition mode, sampling frequency, full-scales etc.). The saved file can be downloaded afterwards by accessing the memory through the USB connection.

STREAM A new streaming session can be started by sending the `CMD_STREAM` command. The sensors are awakened and the system transmits at the desired frequency the selected data through the radio connection. During the acquisition states (*log* and *stream*) the LED blinks with the green color at a frequency of 1 Hz. The streaming session ends whenever the specific command is sent or if the connection is lost.

ERROR The *error* state identifies a generic error during the system functioning. When the system goes in this state, the *stream* and *log* related commands are inhibited, therefore for a correct operation the system must be restarted by means of the specific `CMD_RESTART` command.

3.2.2 Communication protocol

Bluetooth Low Energy

Bluetooth Low Energy (frequently abbreviated with BLE) is a short-range wireless communication technology developed by the Bluetooth Special Interest Group (SIG) and integrated into Bluetooth 4.0 in 2009. It was designed for a wide range of applications, from healthcare to home entertainment. The Bluetooth Low Energy is independent from Bluetooth and it has no compatibility, but they can coexist. The main intent of this technology, as the name suggests, is to provide a considerably lower power consumption and a similar communication range with respect to the Classic Bluetooth. A power consumption as low as 0.01 mW makes this solution particularly suitable for applications that do not require a continuous data stream, but a constant accessibility to the device. The Bluetooth Low Energy is designed to work in the 2.4 GHz ISM (Industrial, Scientific and Medical) band. To enable a reliable operation, it leverages a frequency-hopping spread spectrum technique that transmits data over several channels. Devices change periodically the channel according to a pseudo-random sequence called "hopping sequence". At the application level, several profiles are defined. A profile is a set of specifications for how a device works in a particular application. The bigger part of low energy application profiles are based on the Generic Attribute Profile (GATT), a general specification for sending and receiving small pieces of data known as attributes [67]. Two different roles are defined: server and client. The former can contain attributes accessible by the client through the protocol. In other words, the server is a device that receives GATT commands and requests, and returns responses. On the other hand, a client initiates GATT commands and requests, and accept responses. Data made available by the server are structured as attributes. Attributes are the smallest data entity defined by GATT [68]. Each and every attribute contains information about the attribute itself and the actual data, organized according to the following parameters.

- **Handle** - It is a unique 16 bit identifier for each attribute on a particular GATT server. It is the part of each attribute that makes it addressable, and it is guaranteed not to change between transactions. The allowed range of handle values is `0x0001-0xFFFF`, because the value `0x0000` denotes an invalid handle.
- **Type** - It is a universally unique identifier (UUID) which determines the type of data contained in the attribute. This UUID can be 16 bit, 32 bit, or 128 bit long. Many kinds of UUIDs can be used to fill in the type. They can be standard that determine the GATT server's attribute hierarchy, profile UUIDs that specify the kind of data contained in the attribute, and proprietary, in which the meaning is assigned by the vendor.
- **Permissions** - They specify which operations can be executed on each particular attribute and with which specific security requirements.
- **Value** - The actual value of the attribute.

Figure 3.7 shows a schematic representation of the attribute structure.

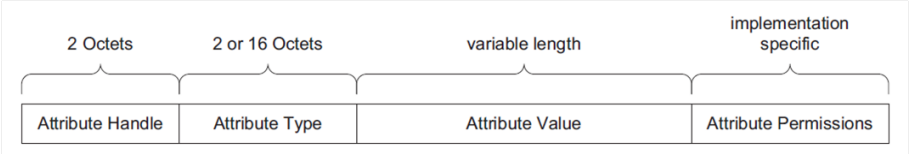

Figure 3.7 – GATT attribute structure.

GATT provides a hierarchy to organize the attributes in a practical manner and has a set of rules that constitute the framework for all GATT-based profiles. The attributes are grouped into services, each of which can contain a set of characteristics. Each characteristic can include descriptors which provide additional information about a characteristic. In this way, all GATT compliant devices acting as servers have attributes that fall necessarily in one of the three categories (service, characteristic, descriptor). A characteristic can be seen as a container for data, whereas a service groups a collection of semantically related characteristics, as depicted by the GATT hierarchy diagram shown in Figure 3.8.

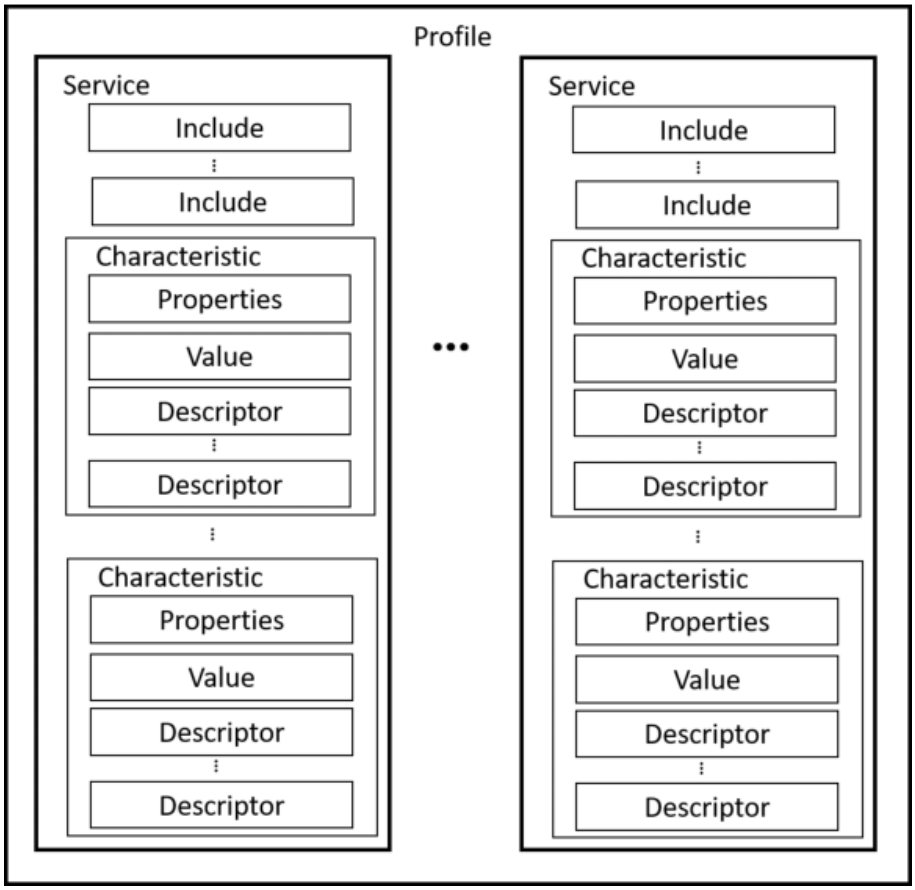

Figure 3.8 – GATT attribute hierarchy.

For the specific implementation of the wearable PPG sensor system different services and characteristics were implemented as depicted by the block diagram in Figure 3.9. In particular, "Communication Service" is a custom service containing a single characteristic used for the implementation of the communication protocol. By means of this characteristic, it is possible to send command and receive responses compliant with the communication protocol defined in the next section.

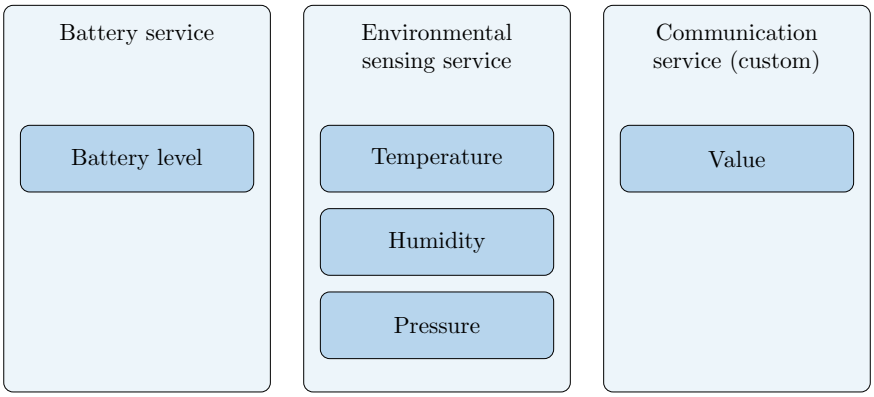

Figure 3.9 – BLE services and characteristics implemented on the wearable system.

Commands

The communication protocol developed for the PPG wearable platform follows the same TLV format described in Section 2.2.4 and depicted in Figure 3.10. The messages have a fixed-length header composed of the *Type* and *Length* fields which represent the request type and the parameters' length respectively. The next field, *Value*, contains the possible additional parameters.

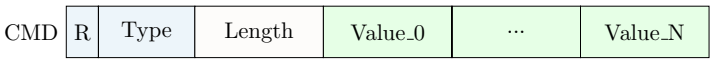

Figure 3.10 – Message in the TLV command format.

Each packet receives an ACK message, either positive (success) or negative (error), carrying information about the outcome in the same TLV format. The format of the ACK message is shown in Figure 3.11. The commands defined for the communication with the wearable PPG system are summarized in Table 3.4. Then, each command is documented in the following paragraphs.

Figure 3.11 – ACK message in the TLV command format.

Code	Command	Description	Access
0x02	CMD_STATE	Get/set the state of the system	R/W
0x03	CMD_RESTART	Restart the system	W
0x06	CMD_DATE	Get/set the date	R/W
0x07	CMD_STREAM	Start a streaming session	W
0x08	CMD_STOP_SESSION	Stop the current session (stream or log)	W
0x09	CMD_START_LOG	Start a log session	W
0x0A	CMD_PPG_CONFIG	Read/write a register of the MAX30101 PPG module	R/W
0x0B	CMD_ACC_FS	Get/set the accelerometer full scale	R/W

Table 3.4 – Commands list of the PPG wearable system.

CMD_STATE The state of the system can be get or set by means of the command ID 0x02. To get the state of the system, the command 0x82 must be issued with 0x00 as length and no payload. In case of ACK_SUCCESS, the payload will be 3 bytes long. The third byte reports the code associated with the actual state of the system.

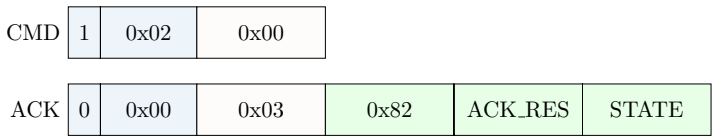

Figure 3.12 – State command (read) format.

To set the state of the system, the command 0x02 must be issued with 0x01 as length and with the code of the desired state as payload. This command is used only for debugging purposes as it can generate errors if unexpected transitions are performed.

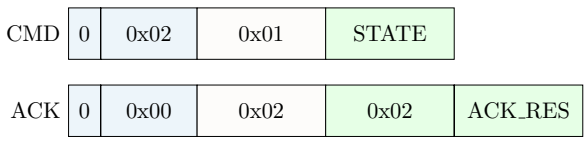

Figure 3.13 – State command (write) format.

The list of the possible states associated with their IDs is shown in Table 3.5.

Code	State
0x01	Startup
0x02	Idle
0x03	Stop
0x04	Stream
0x05	Log
0xFF	Error

Table 3.5 – State codes of the system.

CMD_RESTART A system reboot can be forced by means of the command core 0x03. The system will return ACK_SUCCESS or ACK_ERROR. In case of success, 2 seconds after the reception of the command, the system will restart and any Bluetooth connection will be lost.

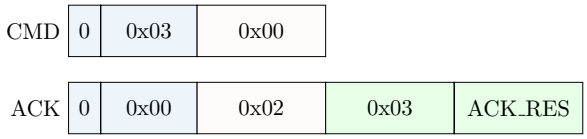

Figure 3.14 – Restart command format.

CMD_DATE The local date and time of the system can be set through the command code 0x06. To set the date, a command ID 0x06 must be issued with a payload length of 0x04. The 4 bytes payload is the Unix epoch represented with a 32 bit signed integer. The system will return either ACK_SUCCESS or ACK_ERROR.

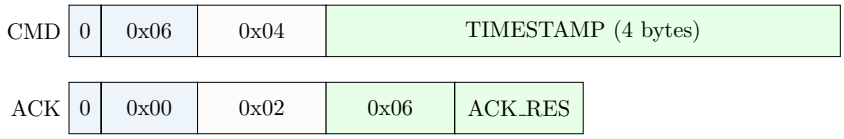

Figure 3.15 – Date command (write) format.

To obtain the actual date, a command code 0x86 must be issued with a payload length of 0x00. In case of success, the system will return a message containing as payload the Unix timestamp represented with a 32 bit signed integer.

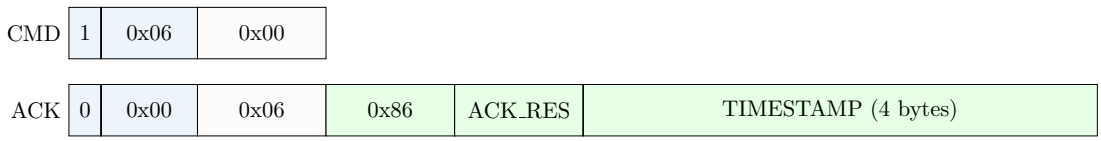

Figure 3.16 – Date command (read) format.

CMD_STREAM A streaming session can be triggered by means of the command code `0x07`. The payload length of the `CMD_STREAM` message is `0x03` and the payload represents the acquisition mode and the sampling frequency respectively. The byte which sets the acquisition mode complies with the format depicted in Figure 3.17.

bit	7	6	5	4	3	2	1	0
value	R_EN	/	IR_EN	/	G_EN	/	ACC_EN	/

Figure 3.17 – Structure of the `A_MODE` byte.

Each bit of `A_MODE` allows to enable or disable the acquisition of specific PPG channels or acceleration values; if the bit is set to one, the sampling is enabled, otherwise it is disabled.

CMD	0	0x07	0x03	A_MODE	FREQ (2 bytes)
ACK	0	0x00	0x02	0x07	ACK_RES

Figure 3.18 – Stream command format.

CMD_STOP_SESSION A streaming or log session can be stopped by means of the command ID `0x08`. The system will return `ACK_SUCCESS` and it will go into the *idle* state.

CMD	0	0x0F	0x00		
ACK	0	0x00	0x02	0x0F	ACK_RES

Figure 3.19 – Stop session command format.

CMD_START_LOG A log session can be started by means of the command code `0x09`. To start the sessione, the command must be issued with length `0x03` and the same payload described for the command `CMD_STREAM`.

CMD	0	0x09	0x03	A_MODE	FREQ (2 bytes)
ACK	0	0x00	0x02	0x09	ACK_RES

Figure 3.20 – Start log command format.

CMD_PPG_CONFIG The command ID `0x0A` allows to access and configure the MAX30101 registers. To set the value of a specific register, a command `0x0A` must be issued with payload length of `0x02`. The payload specifies the register address and the value to be set. The system will return `ACK_SUCCESS` or `ACK_ERROR`.

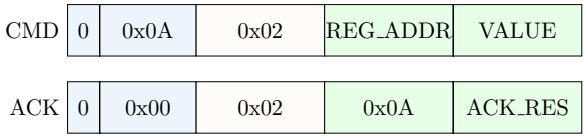

Figure 3.21 – PPG config command (write) format.

To get the value stored in a register, a command `0x8A` must be issued with `0x01` as payload length. The payload specifies the address of the register to be read. In case of success, the system will return a message with a payload length of 4 bytes reporting the address of the register and its content.

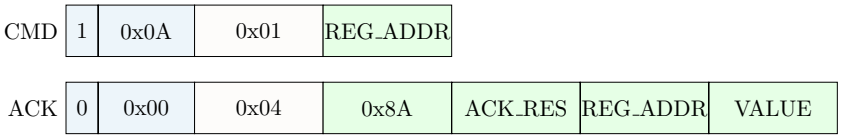

Figure 3.22 – PPG config command (read) format.

CMD_ACC_FS The full scale of the accelerometer mounted on the probe-board can be changed by issuing the command ID `0x0B`. The payload length must be `0x01` and the payload represents the full scale according to the values listed in Table 3.6.

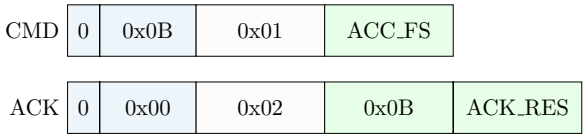

Figure 3.23 – Accelerometer full scale command (write) format.

Value	Full scale
`0x00`	±2 g
`0x10`	±4 g
`0x20`	±8 g
`0x30`	±16 g

Table 3.6 – Accelerometer full scale settings.

Similarly, the current full scale setting can be obtained by issuing the command code `0x8B`.

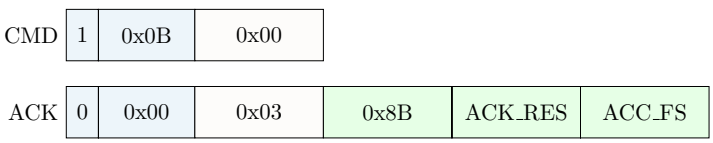

Figure 3.24 – Accelerometer full scale command (read) format.

3.3 Windows application

To facilitate the usage of the PPG system, a Windows application was developed. The software implements the high level API (Application Programming Interface) required for the interaction with the wearable platform. The application was developed in C# using the Windows Form GUI (Graphical User Interface) through the Visual Studio IDE. The graphical interface was implemented in order to provide a simple means with which the user is able to send commands to the system.

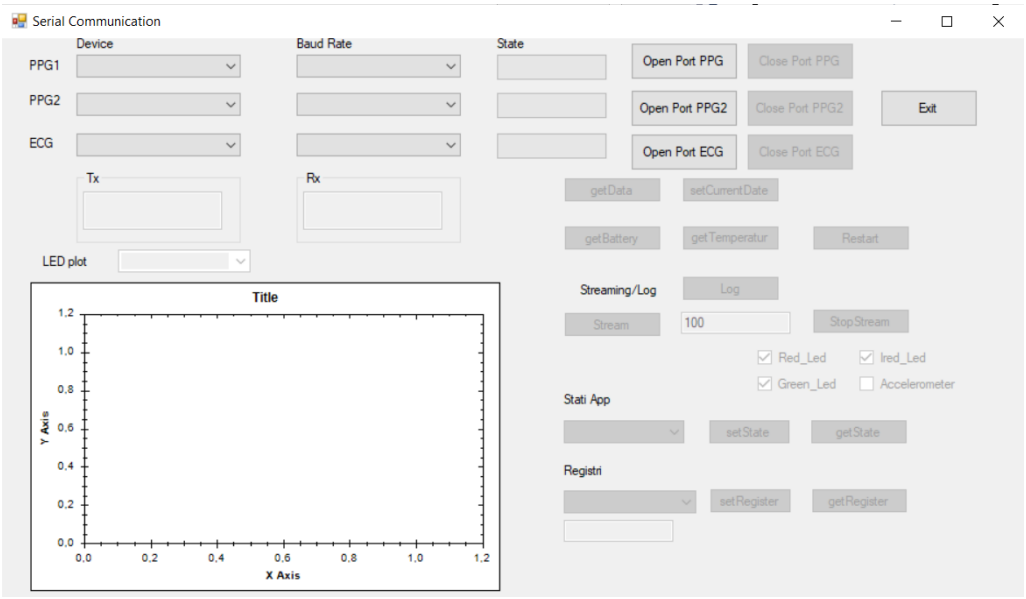

Figure 3.25 – Screen of the implemented Windows application.

Figure 3.25 shows the main screen of the developed application. To open a new connection, the device must be chosen using a dropdown menu and then, by selecting the "Open port" button, the connection can be established. When the connection is set, the state bar becomes green, otherwise an error message will appear. Once the wearable system is connected, all the buttons that allow to communicate with it are enabled. The main functions offered by the software are the following.

- Set and get the current date - The user can obtain the current date and time of the platform by clicking the corresponding button. The current value is then displayed in the status textbox. In a similar way, it is possible to synchronize the current value of the wearable system with the actual date and time of the client.

- Read temperature - The user can obtain the environmental temperature by clicking the corresponding button.

- Read state of charge - By means of this function it is possible to obtain the current state of charge value.

- Restart - The restart function allows to reboot the system.

- Read and write PPG registers - A specific function allows to read and write the registers of the MAX30101 PPG module.

- Start a streaming session - It is possible to select the channels to be enabled during the acquisition (red, IR, green) and if acceleration values have to be sampled. A textbox allows to set the sampling frequency and, by means of a dropdown menu, the user can decide which PPG channel to plot. Moreover, the software saves the streaming session in a log file to allow further offline data analysis.

- Start a log session - The command `CMD_START_LOG` was implemented to handle log sessions.

Figure 3.26 shows a flow diagram of a typical use case of the developed application.

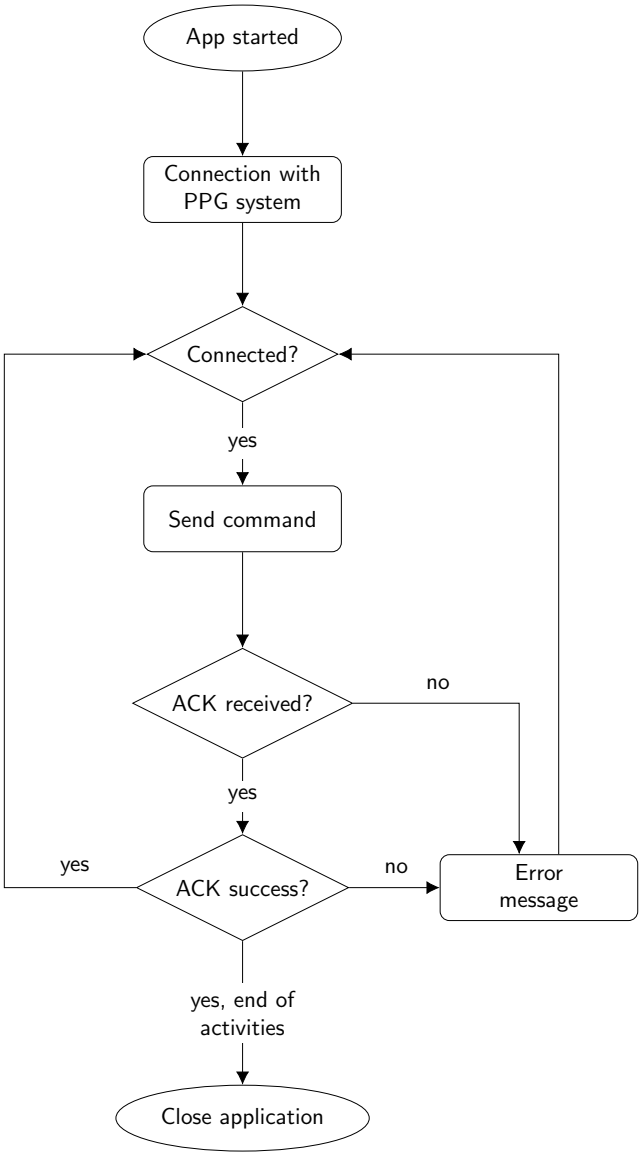

Figure 3.26 – Block diagram of the typical use case of the developed application.

3.4 Characterization and measurements

As described in Chapter 1, the photoplethysmographic waveform consists of a small AC component superimposed over a large DC component [23]. The DC component depends on the structure of the tissue and the average blood volume of arterial and venous blood, whereas the AC component shows changes in the blood volume occurring during the systolic and diastolic phases of the heart cycle. A measurement of the PPG signal performed by means of the presented wearable system is depicted in Figure 3.27; each waveform corresponds to a specific channel (red, infrared or green).

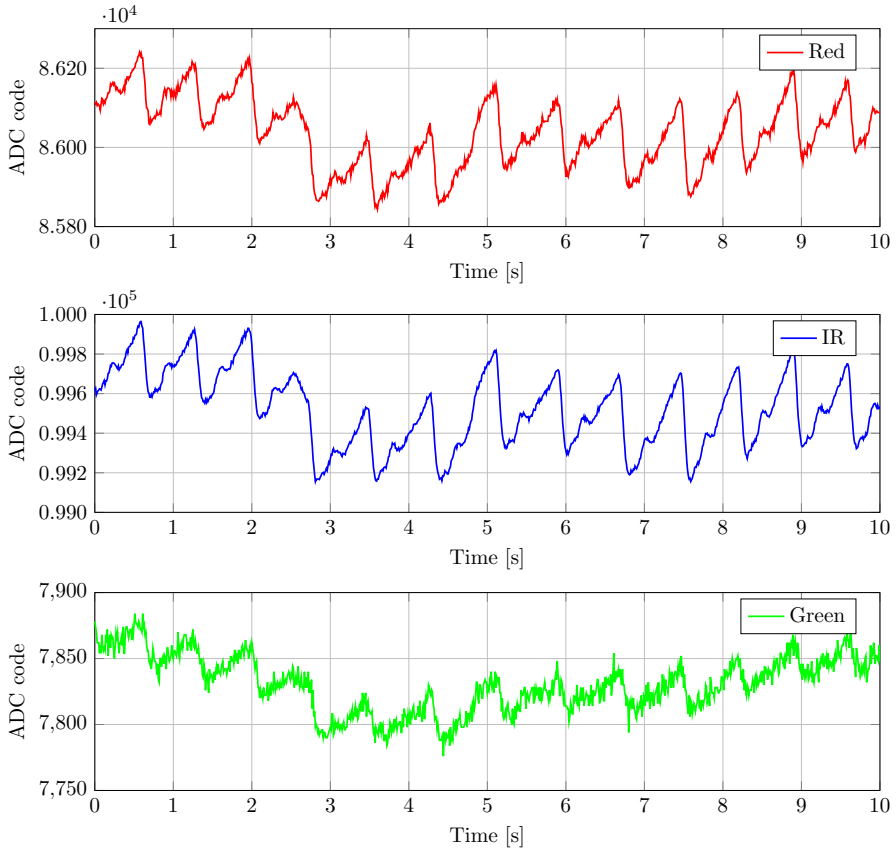

Figure 3.27 – Measurement of the PPG waveforms using three different wavelengths: red, IR and green.

There are several factors that affect the quality of the acquired traces. Among these, the interaction between the light and tissues, motion artifacts and probe contact force are the most crucial for optimal detection. This section provides additional details concerning the investigation carried out to address these potential problems and gives the results concerning the autonomy of the developed wearable system. It is important to notice that the PPG signal value of the y axis shown in different figures of the current chapter corresponds to the converted ADC code, therefore it is reported with no unit of measurement. This is because the amount of light detected has no direct physiological meaning, but it is relevant only its variation and the waveform that it produces.

3.4.1 Power consumption

After the firmware development, measurements were carried out in order to characterize the power consumption of the system in the different states. The system was supplied with a constant voltage of 3.7 V using a Keysight E3631 DC power supply and current measurements were carried out by means of an Agilent 34461A digital multimeter. The multimeter was set with an aperture of 0.02 PLC and at least 100000 values were averaged to compute the mean current drawn for each state. Table 3.7 summarizes the results of the measurements performed on the first motherboard prototype (*neMEMSi Xtreme*) and the improved power consumption on the final motherboard. The autonomy for each state is calculated by considering the battery capacity of 210 mAh. For the *log* and *stream* states, the power consumption is affected by the configuration of the PPG module, in particular by the LEDs supply currents. The optimal configuration was determined on the base of the considerations outlined in the next section.

Mode	First prototype			Final prototype		
	Current	Power	Autonomy	Current	Power	Autonomy
Stop	10.64 mA	39.37 mW	19 h	7 µA	26 µW	>30 000 h
Idle	24.75 mA	91.58 mW	8 h	660 µA	2.44 mW	318 h
Log (max f)	n/a	n/a	n/a	4.67 mA	17.28 mW	44 h
Log (100 Hz)	33.46 mA	123.80 mW	6 h	2.43 mA	8.99 mW	85 h
Stream	34.57 mA	127.91 mW	6 h	11.63 mA	43.03 mW	18 h

Table 3.7 – Power consumption measurements.

3.4.2 LED current

The initial characterization activities were focused on defining the best configuration leading to a good trade off between signal quality and power consumption. In this direction, initial data was collected from one subject in rest condition for different LED currents in the range between 2 mA and 50 mA. Table 3.8 summarizes the results by showing the average amplitude of the acquired signal at different LEDs supply currents, whereas Figure 3.28 gives a graphical representation of the same measurements. As it can be noticed, with low LEDs currents the amplitude of the PPG signal is limited and higher amplitudes can be achieved with higher supply currents. With increased LEDs currents, both AC and DC components increase, but not at the same rate. A good signal amplitude can be obtained with a LED current of 10 mA and a 4 % duty cycle. It is worth noting that, as the red and IR LED currents approach 25 mA of intensity, the related ADCs start saturating thus voiding the measurement. On the other hand, the green LED never saturates even at the maximum current of 50 mA. Moreover, the 10 mA value was chosen to limit power consumption.

Mode	PPG signal amplitude [ADC code]		
	Red	Infrared	Green
2 mA	73.59	142.14	56.33
4 mA	154.14	319.47	84.30
6 mA	240.41	504.00	83.30
10 mA	401.53	1024.50	116.67
15 mA	537.23	1160.03	135.42
20 mA	628.53	1491.00	226.31
25 mA	1216.10	2562.80	429.50
30 mA	–	–	478.23
40 mA	–	–	516.00
50 mA	–	–	631.70

Table 3.8 – Mean amplitude of the signals with different LED currents.

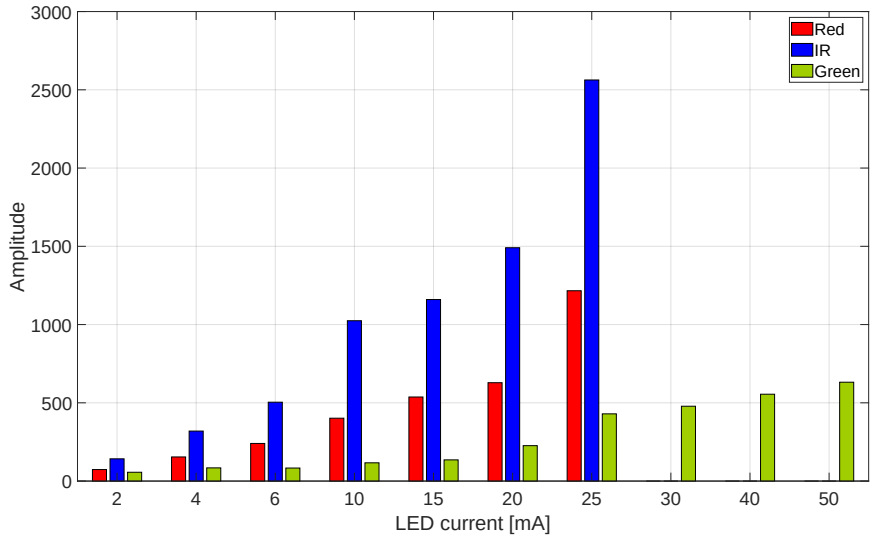

Figure 3.28 – Mean amplitude of the signals with different LED currents.

By knowing the amplitude and the DC value of the PPG signals it is useful to compute the perfusion index. The perfusion index is calculated as the ratio between the pulsatile blood flow and the non-pulsatile component and it can be computed as shown in Equation (3.1) [69]. This index is a relative measurement that allows to compare the quality of signals acquired using different wavelengths or measured at different body locations.

$$PI = \frac{\hat{x}_{max} - \hat{x}_{min}}{|\overline{x}|} \tag{3.1}$$

In the equation, $|\overline{x}|$ represents the statistical mean of the raw PPG signal and $\hat{x}$ is the filtered PPG signal. The perfusion index gives information about the pulse strength and, as depicted by Table 3.9 and Figure 3.29, the modulation is higher for the green LED if

compared to red and IR wavelengths.

Mode	Perfusion index [%]		
	Red	Infrared	Green
2 mA	0.51	1.03	6.30
4 mA	0.48	1.04	6.20
6 mA	0.48	1.06	6.00
10 mA	0.46	1.20	10.08
15 mA	0.41	0.89	2.93
20 mA	0.36	0.87	3.56
25 mA	0.56	1.17	5.65
30 mA	–	–	5.96
40 mA	–	–	5.87
50 mA	–	–	5.57

Table 3.9 – Mean perfusion index of the signals acquired with different LED currents.

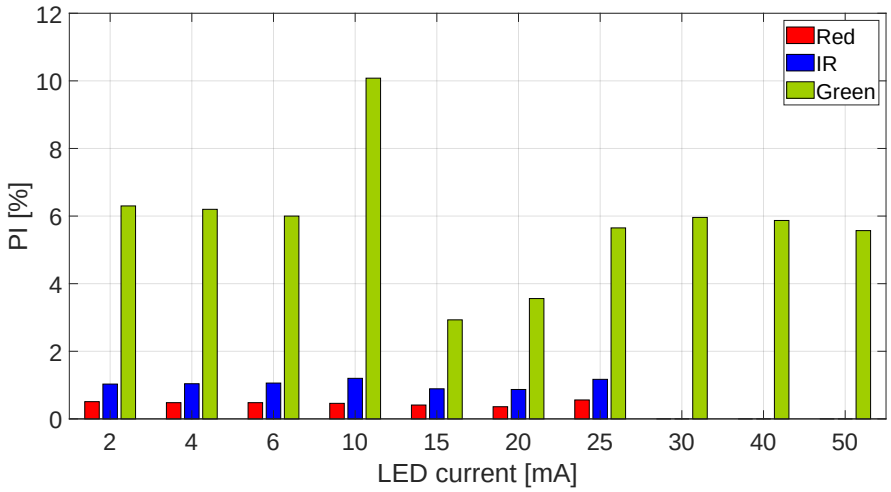

Figure 3.29 – Mean perfusion index of the signals acquired with different LED currents.

3.4.3 Measurement location

The measurement site is an important factor which determines signal quality and robustness against motion artifacts. Most PPG sensors working in reflectance mode use IR or green light sources to perform measurements. IR and near-IR wavelengths are suitable for measurements of blood flow in deep tissue such as the muscles, whereas green light enables measurement of the superficial blood flow in the skin. Although there are different sensors with different light source wavelengths, green light is the de-facto standard for wrist devices (e.g. smartwatches and fitness bands) since it provides the strongest modulation [70]. Wearable PPG sensors operating in transmission mode have limited body locations on

which they can be worn because the light must be able to pass through the tissue. In practice, only fingertip, earlobe, and toe are the possible candidates for this kind of measurements. Sensors working in reflectance mode can overcome this limitation and they can be theoretically placed on any site of the body, even though locations characterized by a high perfusion are the most appropriate ones. Several locations have been investigated in state-of-the-art systems: forehead [71], nasal bridge [72], fingers [73], wrist etc.

Measuring site	Red	IR	Green
Right thumb	0.31	0.71	2.99
Right forefinger	0.33	0.71	3.65
Right middle finger	0.30	0.67	3.78
Left thumb	0.30	0.67	3.46
Left forefinger	0.34	0.78	3.97
Left middle finger	0.32	0.73	3.38
Right wrist (posterior)	0.06	0.15	0.88
Right wrist (anterior)	0.05	0.06	1.07
Left wrist (posterior)	0.05	0.07	0.84
Left wrist (anterior)	0.07	0.11	0.96
Forehead	0.16	0.32	2.14
Nasal bridge	0.16	0.36	2.41
Right ear	0.22	0.51	2.31
Left ear	0.29	0.69	2.21
Right ankle	0.04	0.06	0.76
Left ankle	0.04	0.06	0.70
Manubrium	0.06	0.13	1.29
Xiphoid process	0.07	0.11	0.90

Table 3.10 – Perfusion index computed for the measurements acquired from 18 body locations.

In this work, 18 body sites were evaluated while performing measurements on 10 volunteers. The participants were in a sitting position and the measurements were performed at least after 15 minutes of acclimatization with a room temperature of 24±2 °C. For all the body location, except the ears, an adhesive medical tape was used to hold in place the probe board. The group was composed of 8 male and 2 female individuals with a mean age of 32.1 years (standard deviation 15.4) having a type II or III skin tone in the Fitzpatrick scale [74]. In order to compare the pulse strength at the different monitoring sites, the Perfusion Index (PI) was used. Recordings for each measurement site had a duration of at least 60 seconds and the PI was calculated over a 3 seconds-long moving window. Acquisitions were performed on the three PPG channels (red, IR, green) with a sampling frequency of 100 Hz. Table 3.10 shows the results averaged for all the individuals whereas Figure 3.30 depicts the perfusion indexes related to each monitoring site. Although the perfusion index can vary a lot between various individuals, it was possible to determine that some locations are more suitable for detecting a good quality PPG signal, in agreement with a previous study on basal perfusion of the cutaneous microcirculation [75]. Fingers, ears and nose reveal a much higher perfusion than other sites evaluated, and the PIs calculated on symmetric body positions are substantially the same. The choice of the most suitable light wavelength largely depends on the measurement site. Light with longer wavelengths penetrates more deeply into the tissue. For instance, the IR light has a relatively deep

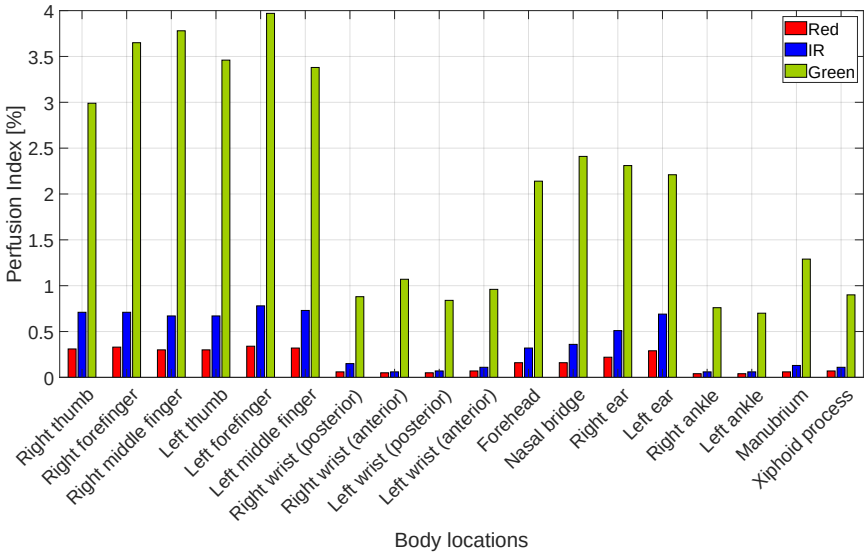

Figure 3.30 – Perfusion index calculated for red, IR and green wavelengths from measurements done on different body locations and with LEDs supply currents of 10 mA.

penetration (0.8 - 1.5 mm) into living tissue, whereas the penetration depth of green light does not exceed 0.6 mm. Wrist mounted PPG devices typically measure the blood in skin capillaries since the ulnar and radial arteries are located in the lateral and posterior section of the wrist and measuring the blood flowing in these vessels would require very precise placement of the sensor. On the other hand, green light is widely absorbed by melanin so it is harder to perform measurements on people with darker skin pigmentation. Ears are not the absolute best body locations in terms of signal quality, yet they still provide good positioned results. Moreover, the auditory canal offers a natural mechanic support that makes it possible to mitigate motion artifacts induced on the PPG signals by the sensor displacement. Particularly in consumer wearable systems, a device worn in the ear canal has the main advantage of not interfering with the current activity of the individual.

3.5 Algorithms for data analysis

After the initial investigation carried out in order to assess the performance of the wearable system, the work focused on the extraction of relevant parameters from the acquired traces. In particular, the main goal was the estimation of the following parameters: heart rate (HR), oxygen saturation (SpO_2), and heart rate variability (HRV). A first part of the work concerned with the development of an algorithm used for the processing of PPG signals acquired when the subject is in rest conditions. The aim was to design a lightweight analysis procedure suitable for integration within an embedded system. The second part of the study evaluated a different algorithm capable of tolerating the effect of artifacts when motion is experienced.

3.5.1 HR estimation in rest conditions

The PPG waveforms are acquired from the red and IR channels and they are sampled at a frequency of 100 Hz. The estimation is carried out in the time domain over rolling windows of 10 seconds with a 50 % overlap. The signals are detrended in the time domain by

subtracting low-pass filtered signals (LP) obtained at the output of a 2$^{\text{nd}}$ order Butterworth filter with a cutoff frequency of f_0 =0.5 Hz. Afterwards, the two preprocessed waveforms are combined as follows:

$$\hat{x}_{Red} = x_{Red} - LP(x_{Red}, f_0) \tag{3.2}$$

$$\hat{x}_{IR} = x_{IR} - LP(x_{IR}, f_0) \tag{3.3}$$

$$\hat{x}_{ppg} = \hat{x}_{Red} + \hat{x}_{IR} \tag{3.4}$$

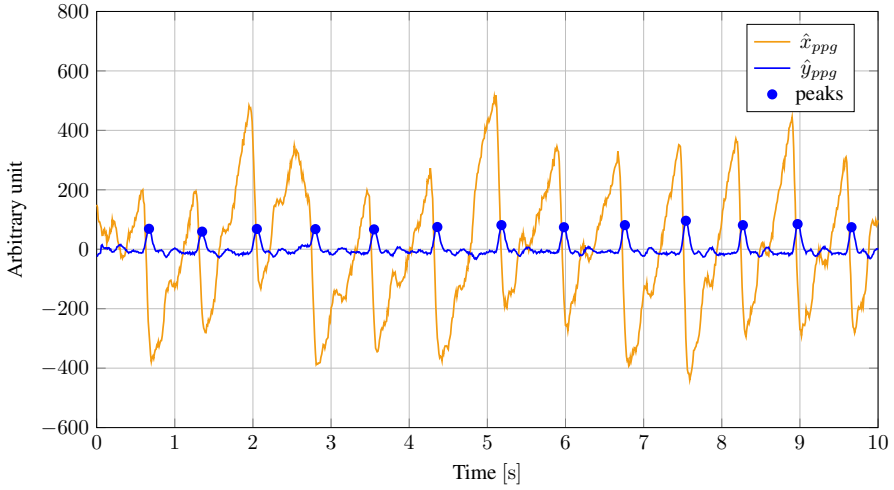

Figure 3.31 – HR estimation algorithm for PPG signals. The orange line represents the combined filtered PPG waveforms. The blue line shows the result obtained after the application of the differentiator filter and the inversion, whereas the markers highlight the peaks.

Then, the PPG signal is filtered by means of a 6$^{\text{th}}$ order FIR differentiator filter (DF):

$$\hat{y}_{ppg} = DF(\hat{x}_{ppg}) \tag{3.5}$$

The obtained $\hat{y}_{ppg}$ signal is inverted and the peaks are computed through a peak detection algorithm which keeps into account the following constraints:

- Minimum peak distance: it is the minimum distance between two peaks in order to be considered valid. The maximum detectable heart frequency (considering that the individual is in rest conditions) is equal to 200 bpm, so the minimum peak distance is fixed to 300 ms.
- Minimum peak prominence: it is the minimum amplitude allowed for a peak and it is empirically fixed as twice the standard deviation of $\hat{y}_{ppg}$ for the current window.
- Minimum number of peaks: when considering a particular window, the peak detection procedure could lead to a wrong estimation of the HR because of a low quality signal. For this reason, a minimum number of 7 points (corresponding to 42 bpm) must be detected in order to consider the window valid.

Given a specific window, the timespan t_i between two consecutive peaks is calculated and the heart rate is given by the following equation

$$HR_{ppg} = \frac{60}{\bar{t}} \tag{3.6}$$

$\bar{t}$ is the mean distance between the peaks detected in the evaluated window. Figure 3.31 depicts the preprocessed PPG waveform $\hat{x}_{ppg}$ and the differentiated signal $\hat{y}_{ppg}$ with the peaks detected in a specific window.

3.5.2 Discussion

In order to assess the performance of the developed algorithm for the HR estimation, 21 acquisitions with a duration of at least 60 s were carried out. The measurements were done on 11 volunteers aged between 18 and 57 years (mean 29.5 years, standard deviation 12.1 years), 5 males and 6 females. The validation was done by recording the ECG (electrocardiogram) traces of the limb leads by means of a wearable ECG system presented in the previous chapter. For each acquisition, the mean absolute error (MAE) is determined as the average absolute error between the HR given by the algorithm (HR_{ppg}) and the reference value obtained from the ECG traces (HR_{ECG}) for each window j, as reported by the following equation:

$$MAE = \frac{1}{n}\sum_{j=1}^{n} |HR_{ppg,j} - HR_{ECG,j}| \tag{3.7}$$

where n is the total number of windows. The average error of the developed algorithm is equal to 1.042 bpm, as depicted in Table 3.11, whereas Figure 3.32 shows the estimated HR compared to the ground truth given by the ECG (the estimation is updated each 5 s and the initialization phase requires 10 s).

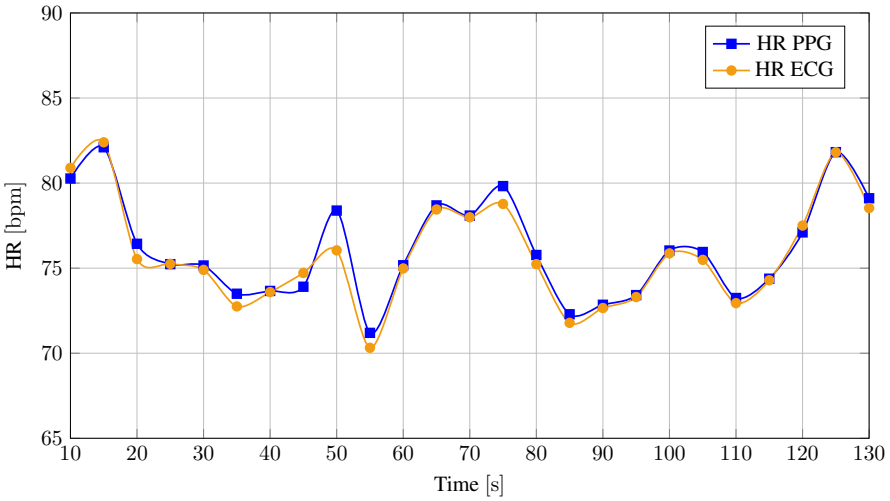

Figure 3.32 – Results of the HR estimation algorithm compared with the reference heart rate gathered from the ECG.

Subject	Age	Sex	Acq	Length [s]	HR [bpm]	MAE [bpm]
1	24	M	A	70	67.570	1.148
			B	70	68.879	1.352
2	48	F	A	70	86.882	0.838
			B	70	89.837	1.363
3	19	F	A	70	65.832	0.649
			B	70	67.750	0.649
4	23	F	A	70	68.263	1.201
5	25	M	A	60	95.340	0.628
			B	130	78.328	2.021
6	28	M	A	130	51.667	1.080
			B	130	53.013	1.085
7	31	F	A	130	78.108	1.693
			B	130	84.690	1.036
8	26	M	A	130	72.003	0.922
9	18	F	A	140	61.623	1.686
			B	140	59.679	0.398
10	57	F	A	200	67.858	0.117
			B	200	65.387	0.303
11	26	M	A	200	69.412	1.135
			B	200	71.463	1.528
			C	120	68.871	0.618
					Average	1.042

Table 3.11 – Results for the HR estimation algorithm in resting conditions.

3.5.3 SpO_2 estimation

Two different models were used for the estimation of the SpO_2 value. Hemoglobin (Hb) is an oxygen-transport protein in red blood cells (RBCs). The two main forms of Hb present in blood are oxygenated haemoglobin (oxyhaemoglobin, HbO_2) and deoxygenated haemoglobin (deoxyhaemoglobin, RHb). SpO_2 is the measurement of the peripheral capillary oxygen saturation. More specifically, SpO_2 is an estimate of the amount of oxygen in capillary blood and it is expressed as a percentage of the amount of oxyhemoglobin to total haemoglobin, expressed as follows:

$$SpO_2 = 100\frac{C[HbO_2]}{C[HbO_2] + C[RHb]} \tag{3.8}$$

where $C[HbO_2]$ and $C[RHb]$ are the concentrations of HbO_2 and RHb respectively. The first model used for the computation of the saturation is often used in literature in the context of medical devices and it is described by the following equation [23]:

$$SpO_2 = 100 - 25R \tag{3.9}$$

where R is determined as follows:

$$R = \frac{\frac{AC_{red}}{DC_{red}}}{\frac{AC_{IR}}{DC_{IR}}} \tag{3.10}$$

However, to obtain an accurate value of SpO_2, an empirical calibration of the ratio of ratios for the specific device is needed. In this context, Maxim Integrated made available another model and related guidelines to achieve better results. The calibrated model is defined by the following equation [76]:

$$SpO_2 = aR^2 + bR + c \tag{3.11}$$

a, b, and c are calibration coefficients and in the framework of the developed system, the default calibration coefficients without the optical shield provided by Maxim Integrated for the MAX30101 module were used (Table 3.12).

Default calibration coefficients			
	a	b	c
MAX30101	1.5958	-34.6597	112.6899

Table 3.12 – Default calibration coefficient for the MAX30101 module without optical shield.

3.5.4 HRV estimation

An algorithm was implemented to estimate the heart rate variability (HRV), also referred to "cycle length variability" or "RR variability". The HRV measures the variability in the time interval between heartbeats and can give important information about the neurocardiac functions of the patient. The clinical relevance of heart rate variability was first appreciated in 1965 when Hon and Lee noted that fetal distress was preceded by alterations in beat-to-beat intervals before any appreciable change occurred in the HR itself. The importance of HRV became evident it the late 1980s when it was confirmed that HRV was a strong predictor of mortality after myocardial infarction. There are different methods able to evaluate HRV; the selected one was the SDNN index, calculated as the standard deviation of the normal-to-normal interval.

3.5.5 HR estimation with motion compensation

A wearable system, to be defined as such, must be able to tolerate artifacts induced by motion. While the mechanical design and the form factor can help to reduce the impact of these disturbances, often this is not sufficient. The accelerations measured by the accelerometer mounted on the probe-board can be used to estimate and compensate the effects of motion on the PPG signals. The developed algorithm is based on an adaptive filtering technique and it was developed using Matlab R2019a software. The following procedure is applied in the frequency domain over moving windows having a timespan of 20 s (80 % overlap). The PPG waveforms (sampled at 500 Hz) are preprocessed in the same way described in the previous subsection. The acceleration magnitude is computed and band pass filtered (BP) by means of two cascaded HP+LP 4^{th} order Butterworth filter with a cutoff frequency of f_1 =0.5 Hz and f_2 =10 Hz respectively.

$$x_{acc} = \sqrt{a_x^2 + a_y^2 + a_z^2} \tag{3.12}$$

$$\hat{x}_{acc} = BP(x_{acc}, \omega_1, \omega_2) \tag{3.13}$$

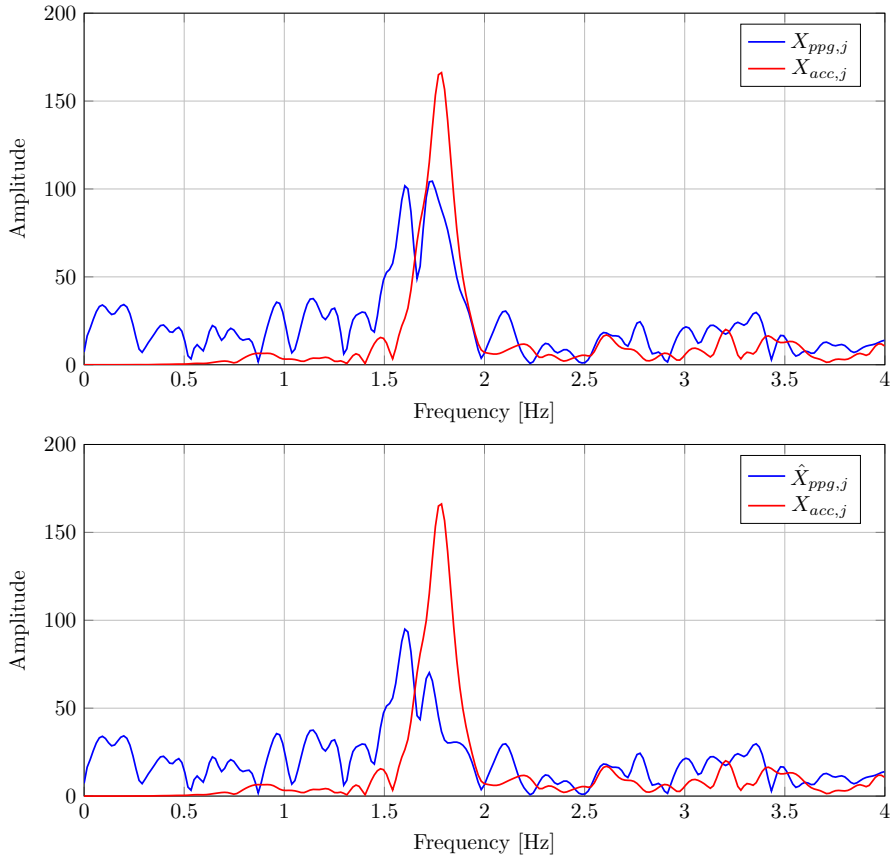

Figure 3.33 – Behavior of the algorithm when a motion artifact is detected. In the upper plot it is possible to observe the DFTs of the PPG signal and the accelerations: there are motion artifacts introduced on the PPG signal by the sensor displacement. The lower plot depicts the DFTs after the application of the adaptive filter on the PPG signal.

Considering the j-th window, the Discrete Fourier Transforms (DFTs) of the filtered PPG and accelerometer signals are computed. The DTFs $X_{ppg,j}$ and $X_{acc,j}$ are calculated by means of the FFT (Fast Fourier Transform) algorithm. The range considered for the HR estimation was between 42 and 240 bpm (corresponding to a frequency range of 0.7 - 4 Hz). The accelerations can amplify frequency components of the PPG signal, so a 2^{nd} order IIR notch filter can be applied to the PPG signal. The frequency of the filter is equal to the dominant frequency gathered from $X_{acc,j}$. The notch filter is computed and used only in presence of motion disturbances and only if they are degrading the quality of the PPG signal. When one of the following conditions is satisfied, the filter is not applied:

- there are no dominant frequencies connected to motion
- the dominant frequency of the PPG signal does not lie in an interval around the dominant frequency of the accelerations
- the dominant frequency of the PPG signal lies in an interval around the dominant frequency of the accelerations, but the amplitude of the second dominant component of the PPG signal is negligible

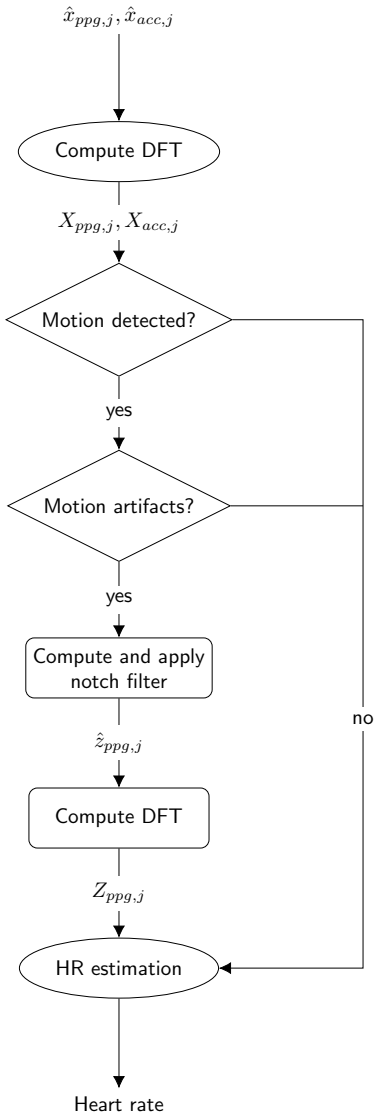

Figure 3.34 – Block diagram of the HR estimation with motion compensation algorithm.

After the application of the notch filter in the time domain that allows to obtain $\hat{z}_{ppg,j}$, the DFT on the PPG signal $Z_{ppg,j}$ is computed again. Finally, the dominant frequency of the filtered signal is selected as the HR estimation. In Figure 3.33 it is possible to observe the behavior of the described algorithm in presence of motion artifacts. A schematic representation of the main steps of the algorithm is presented in Figure 3.34. In order to assess the performance of the developed algorithm, 10 acquisitions with a duration of at least 100 s were carried out. The measurements were done on 7 volunteers aged between 25 and 57 years (mean 31.3 years, standard deviation 11.5 years), 5 males and 2 females. During the experiment, the subjects were asked to walk at low speed (around 50 steps per minute). The ECG traces were recorded and used as the ground truth for HR estimation. Figure 3.35 shows the estimated HR compared to the reference value obtained from the ECG and the results without the application of the motion compensation techniques. The average error of the presented algorithm was equal to 2.77 bpm as depicted by Table 3.13. Even though the experiments were conducted in a controlled environment, the results encourage to affirm that similar performances can be expected during daily activities and

with longer timespans. In this sense, preliminary measurements were performed when a volunteer was asked to wear the sensor system when driving a car: the algorithm was able to compensate the artifacts caused by the vehicle motion.

Subject	Age	Sex	Acq	Length [s]	HR [bpm]	MAE [bpm]
5	25	M	A	240	100.47	3.39
			B	240	100.07	3.88
12	26	M	A	200	69.45	2.04
11	26	M	A	260	94.01	3.11
6	28	M	A	150	67.20	1.94
			B	160	70.87	2.35
7	31	F	A	220	89.88	2.04
14	26	M	A	180	73.09	4.37
			B	180	75.43	2.05
10	57	F	A	110	90.42	2.53
					Average	2.77

Table 3.13 – Results for the HR estimation algorithm with adaptive motion filtering.

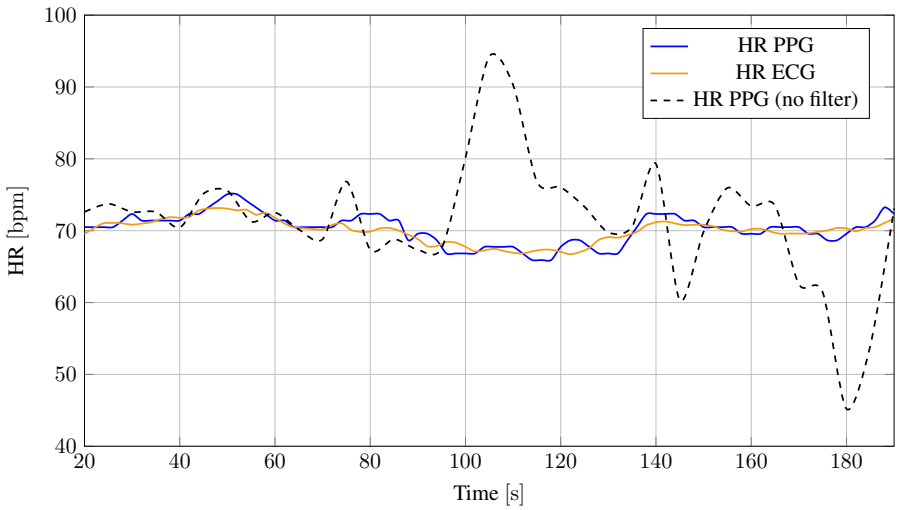

Figure 3.35 – HR estimation during a slow pace walk achieved by means of the presented algorithm.

3.5.6 Algorithms comparison

The developed algorithm for HR estimation with motion compensations can be used also for acquisition carried out in resting conditions. To demonstrate this, a new dataset was build by carrying out 13 acquisitions of 5 volunteers in resting conditions (mean age 24.6 years, standard deviation 3.3). As depicted by Table 3.14, the estimation obtained by means of the first presented algorithm (HR rest) gives better results with respect to the algorithm with motion compensation (HR MC). In each acquisition the results were compared to

the reference value obtained from the ECG traces. Even though the error is higher, the performance is still good and shows how the algorithm is suitable both for motion and resting conditions.

Subject	Age	Sex	Acq	Length [s]	HR rest	HR MC	ECG	MAE rest	MAE MC
11	26	M	A	135	74.829	75.074	74.613	0.216	0.549
			B	135	74.567	73.393	74.541	0.080	1.271
			C	195	69.812	69.490	69.682	0.184	0.465
13	27	F	A	140	81.879	80.960	81.639	0.273	1.658
			B	135	79.602	82.400	79.609	0.384	1.924
			C	190	75.917	75.889	75.793	0.228	1.324
16	26	F	A	135	61.421	61.499	60.091	1.932	0.802
			B	140	63.321	61.994	60.091	1.464	1.694
			C	190	62.799	61.428	61.734	1.148	1.050
12	26	M	A	140	60.353	62.121	60.263	0.199	1.859
			B	135	60.262	59.510	60.199	0.102	0.817
			C	195	60.124	63.447	59.915	0.210	3.725
9	17	F	A	135	64.472	64.217	64.275	0.199	2.308
							Average	0.509	1.496

Table 3.14 – Heart rate comparison between the results obtained with the two algorithms.

3.6 State-of-the-art

In this section, different systems for photoplethysmographic measurements are discussed. Several devices were considered, varying in the application, measurement location and commercial availability. Some of the discussed platforms were developed for specific research applications in the medical field. In this assessment, solutions that perform PPG measurements at ear level were preferred.

3.6.1 Cosinuss One

Cosinuss One (Cosinuss, Munich, Germany) is a commercial professional fitness tracker [77] able to monitor several vital signs during physical activities with a good degree of accuracy.

Figure 3.36 – Cosinuss One PPG device.

The main parameters measured are the heart rate, the heart rate variability, the respiration rate and the body temperature. Moreover, thanks to a Bluetooth Low Energy

radio, it is possible to display measurements on a smartphone with a dedicated app. The system performs PPG measurements in the external auditory canal and is characterized by a reduced form factor of 4 x 4 cm and a weight of only 6 g. The Cosinuss One is particularly suited for monitoring subjects during physical activities also because it is build with biocompatible materials that don't produce irritation to the skin. Figure 3.36 shows a photograph of the device.

3.6.2 Bragi Dash Pro

The Dash Pro (Bragi, Munich, Germany) is a wireless headset, equipped with sensor technology [78] that is able to provide real-time feedback of recorded movements and pulse rate. The system is constituted of left and right headphones that communicate wirelessly with each other. The Dash Pro is able to measure the heart rate in the external auditory canal using infrared light by reflection measurement. The device itself is available in one size, but can be fitted to the user's ear with interchangeable silicone caps. A photograph of the device is shown in Figure 3.37.

Figure 3.37 – Bragi Dash Pro PPG device.

3.6.3 Zheng et. al.

In 2012 Zheng et. al. presented an eyeglasses-based device [72] able to acquire photoplethysmogram (PPG) from the nose bridge. The main goal of this system is to provide a mean of monitoring which doesn't use uncomfortable clips frequently used in PPG measurements from finger and ear. The eyeglassess-based PPG device contains the following compoents: optical sensor, sample and hold circuit, MCU and Bluetooth module. The PPG signal is detected in reflective mode and the infrared wavelength was used to perform the measurement. A switching signal is applied on the LED and PD to reduce power consumption. The switching frequency is 125 Hz, whereas the pulse width of the switching signals for the LED and PD are 6 ms and 2 ms respectively. The PPG signal is digitized by the MCU integrated ADC with a 500 Hz sampling frequency and a 10 bit resolution. After processing, the signals can be transmitted to a connected client via the Bluetooth module. Experimental results showed that the eyeglasses-based device is characterized by better performance than PPG from finger and the same performance as PPG from ear in terms of HR monitoring. Moreover, this kind of system is more comfortable and convenient for daily use, since it mounts the sensors on the eyeglasses and does not need to introduce additional clips. Figure 3.38 depicts a block diagram of the eyeglasses-PPG measurement device.

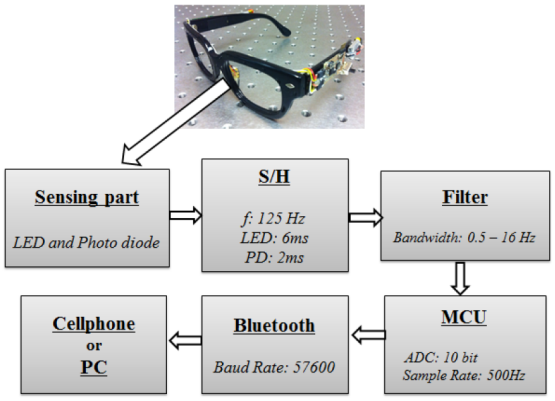

Figure 3.38 – Eyeglasses based PPG measurement device developed by Zheng et. al.

3.6.4 Choi et. al.

The paper authored by Choi et. al. (2018) presents a wearable wrist device [79] which allows to monitor the driver's stress through the measurement of PPG signals, galvanic skin response (GSR), acceleration, and rate of rotation. PPG was widely used for driver's monitoring, because cardiovascular activity that contains information of the autonomic nervous system (ANS) can be observed with this signal. The SFH7050 optical sensor was used as a light source and photodetector. The sensor was controlled by means of the AFE4404 analog front-end which allows to drive the LEDs and to perform analog-to-digital conversion. The measured samples are collected by an MCU and sent over a Bluetooth connection. The developed device is shown in Figure 3.39.

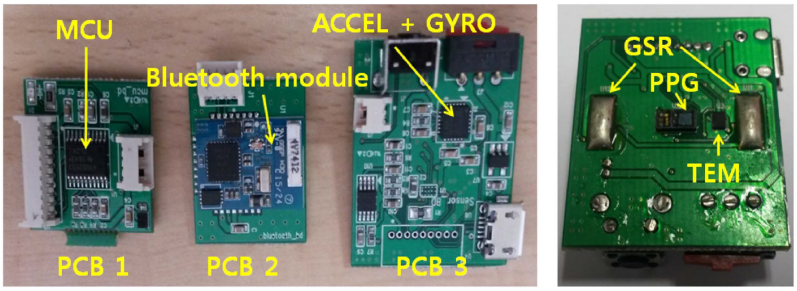

Figure 3.39 – Photograph of the PPG device presented by Choi et. al.

3.6.5 Tigges et. al.

The study of Tigges et. al. (2018) has as a main concern the assessment of the validity of in-ear photoplethysmography as a surrogate for electrocardiography in heart rate variability analysis [80]. The measurements of the PPG signals were conducted with an in-ear sensor system. The front-end consists of commercial components and it is composed of two parts: a miniaturized optical sensor that can be introduced in the ear canal and an analog front-end that performs analog signal conditioning, digitization and communication with a microcontroller through an SPI interface. The optical sensor is based on the OSRAM SFH 7051 which integrates three green LEDs with a matching PD. The sensor was integrated in a modified headphone earpiece, as shown by the photograph in Figure 3.40. The optical sensor is connected to the Texas Instruments AFE4490 analog front-end. The AFE4490 integrated a LED driver and a receive channel that performs signal conditioning and analog-to-digital conversion by means of a 22 bit ADC. The samples are then collected by

the microcontroller that stores all data and a micro-SD flash memory card. Concerning data analysis, HRV features from both the time and frequency domain were calculated from the in-ear PPG signal and a reference ECG signal. Results showed that the in-ear PPG is a viable alternative modality for continuous HRV monitoring when ECG is not applicable.

Figure 3.40 – Photograph of the PPG device presented by Tigges et. al.

3.6.6 Poh et. al.

In 2010 Poh et. al. presented an earring sensor and wireless earpiece for wearable photoplethysmography [81]. The miniaturized system can be worn comfortably on the earlobe and embeds an accelerometer to provide motion reference for adaptive noise cancellation.

Figure 3.41 – Photograph of the PPG device presented by Poh et. al.

The earring sensor is designed to measure the pulsation of the blood flow as well as motion of the ear. The sensor is kept in place on the earlobe thanks to nickel plated neodymium magnets. The PPG measurement is carried out by the CNB10112 reflective photosensor which integrates and infrared LED and a matched PD. After signal conditioning, the sampling is performed using the integrated ADC of the microcontroller. The digitized signals can be transmitted wirelessly to a laptop through the use of a pair of 2.4 GHz radio transceivers modules. The form factor and the shape of the system are favorable factors for unobtrusive and discreet monitoring. Moreover, the active noise cancellation algorithm

allows to obtain a good agreement with respect to the heart rate estimated from the ECG. Figure 3.41 depicts a photograph of the developed system.

3.6.7 State-of-the-art comparison

The system presented in this work was compared with representative commercially available devices and state-of-the-art solutions described previously. The most common available PPG systems are based on finger and wrist measurement sites. Although there are plenty of PPG-based devices, in-ear PPG systems are not yet deeply investigated and for this reason devices worn in other body locations were considered in this comparison. Several parameters were taken into account: the main ones are the autonomy of the system during normal operation, the wireless connectivity and the form factor. Results are summarized in Table 3.15. Among the evaluated systems, the presented platform has the best autonomy as it can operate for more than 3 days performing continuous monitoring. Like most of the devices, a wireless interface is available in order to control the operation of the system and to gather the acquired data. Additionally, the form factor of the system reduces the burden for the users and algorithms were implemented in order to address the effects of motion artifacts on the acquired signals. All these characteristics can make the device an attractive solution for wearable monitoring applications.

	Body location	LEDs wavelength	Battery [mAh]	Power cons. [mW]	Autonomy [h]	Sampling freq. [Hz]	Resolution [bit]	Wireless connectivity	Size $[mm^2/mm^3]$	Motion tolerant	HR est. error
[77][82]	In-ear	Green	50	n.d.	7	100	n.d.	BLE, ANT+	45 x 38 x 18 *	Yes	1.8 bpm
[78][82]	Ext. ear	IR	100	n.d	5	n.d	n.d	BLE	21.9 x 21.9 x 22.4 *	Yes	2 bpm
[72]	Nasal bridge	IR	n.d.	40 **	n.d.	500	10	BT	n.d	No	4
[79]	Wrist	Red, IR, green	140	50	10	100	24	BT	35 x 35 x 15	Yes	n.d.
[80]	In-ear	green	3000	110	27	250	22	BT	n.d.	No	n.d
[81]	Earlobe	IR	n.d.	n.d	n.d	400	12	RF 2.4 G	15 x 35	Yes	2.74 %
This system	In-ear	Red, IR, green	210	9	85	100 - 3200	19	BLE	32 x 20 x 10	Yes	2.77 bpm

* With housing
** Power consumption measured not including the current drawn of the radio module

Table 3.15 – Performance comparison between the presented PPG wearable system and the state-of-the-art solutions.

Conclusions

This thesis described the fundamental aspects of the development of two sensor systems useful to monitor several parameters of the cardiovascular system. In particular, the presented devices exploited two different measurement techniques: the electrocardiogram (ECG) and photoplethysmography (PPG). A complete overview of the design and development process for each sensor system was given from the following perspectives:

- Hardware
- Firmware
- User application
- System characterization and measurements
- Data analysis and algorithms

The wearable system for ECG measurement is capable of recording up to three ECG leads, the bioimpedance, the 3D accelerations, the body skin temperature, and the ambient temperature providing additional sensing capabilities with respect to the state-of-the-art systems. Moreover, a fully wearable prototype was developed by integrating the electronic device with a custom made t-shirt treated with conductive traces applied to the textile. Measurements demonstrated the capability to record good quality traces even during motion. For this reason, the system is widely used in different fields of application ranging from telemedicine to sport. Additionally, the flexible hardware architecture allows to increase the number of detectable leads up to 12 with a small amount of modifications.

On the other hand, the miniaturized PPG system was used to extract different parameters and, depending on the final application, it can be seen as alternative or complementary with respect to the ECG. The initial activities were focused on the definition of the design parameters and the characterization of the system. With this system it is possible to reach up to 85 hours of autonomy without the need of user interaction. Acquisitions with different LED currents were performed in order to determine the optimal configuration that guarantees a good trade-off between signal quality and power consumption. Different body locations were evaluated through measurements on several volunteers and results showed that the ear canal is a good candidate to perform PPG measurements. Moreover, the auditory cavity offers a natural steadiness during acquisitions and the location of the sensor does not interfere with user's normal activities. Two algorithms for HR estimation were developed: the former is a lightweight procedure particularly suitable for measurements carried out in rest conditions, whereas the latter features a motion compensation adaptive filter that allows to mitigate the effect of motion artifacts. Additional useful parameters were estimated, namely the heart rate variability (HRV) and then oxygen saturation (SpO_2). Even though there are plenty of PPG-based devices in scientific literature, in-ear PPG systems are not yet deeply investigated. Among the available devices, the presented platform has the best autonomy and is characterized by a form-factor compatible with the state-of-the-art systems.

Bibliography

[1] World Health Organization. *The top 10 causes of death*. May 2018. URL: https://www.who.int/news-room/fact-sheets/detail/the-top-10-causes-of-death (visited on 08/31/2020).

[2] Gianni Loasano. *Fisiologia cardiovascolare: un approccio integrato*. River Publishers, 2013.

[3] Dee Unglaub. Silverthorn. *Human physiology*. Pearson Education, 2013.

[4] Wikipedia. *Image - Diagram of the human heart*. URL: https://commons.wikimedia.org/wiki/File:Diagram_of_the_human_heart_(cropped).svg (visited on 04/05/2021).

[5] Wikipedia. *Image - Heart valves*. URL: https://en.wikipedia.org/wiki/File:2011_Heart_Valves.jpg (visited on 07/11/2020).

[6] *The Action Potential in Ventricular Cells - Phases*. Mar. 2018. URL: https://teachmephysiology.com/cardiovascular-system/cardiac-muscle/action-potential-ventricular-cells/.

[7] What when how. *Image - Ionic currents shape the cardiac action potential*. URL: http://what-when-how.com/cardiac-arrhythmias-new-considerations/the-cardiac-ion-channels-cardiac-arrhythmias-part-1/ (visited on 07/11/2020).

[8] cnx.org. *Image - Cardiac conduction*. URL: https://cnx.org/contents/nmLg_P9I@1.1:7zZXOBty@1/Cardiovascular-System-Module-4-Cardiac-Muscle-and-Electrical-Activity (visited on 08/22/2020).

[9] Wikipedia. *Image - Schematic diagram of normal sinus rhythm for a human heart as seen on ECG*. URL: https://en.wikipedia.org/wiki/Electrocardiography#/media/File:SinusRhythmLabels.svg (visited on 08/22/2020).

[10] Dr Araz Rawshani. *Pocket Guide to ECG Interpretation (PDF)*. Feb. 2020. URL: https://ecgwaves.com/pocket-guide-to-ecg-interpretation-pdf/.

[11] Maxim Integrated. *Introduction to Electrocardiographs*. May 2010. URL: https://www.maximintegrated.com/en/design/technical-documents/tutorials/4/4693.html (visited on 08/04/2020).

[12] Joseph D. Bronzino and Donald R. Peterson. *The biomedical engineering handbook*. CRC Press, 2015.

[13] Enrique Company-Bosch and Eckart Hartmann. *ECG Front-End Design is Simplified with MicroConverter®*. 2003. URL: https://www.analog.com/en/analog-dialogue/articles/ecg-front-end-design-simplified.html (visited on 08/04/2020).

[14] B. B. Winter and J. G. Webster. "Driven-right-leg circuit design". In: *IEEE Transactions on Biomedical Engineering* BME-30.1 (1983), pp. 62–66.

[15] Texas Instruments. *Application report SBAA 160A. Analog Front-End Design for ECG Systems Using Delta-Sigma ADCs*. Apr. 2010. URL: https://e2echina.ti.com/cfs-file/___key/telligent-evolution-components-attachments/00-58-01-00-00-22-60-03/Analog-Front_2D00_End-Design-for-ECG-Systems-Using-Delta_2D00_Sigma-ADCs.pdf (visited on 08/04/2020).

[16] Aymen A. Alian and Kirk H. Shelley. "Photoplethysmography". In: *Best Practice & Research Clinical Anaesthesiology* 28.4 (2014). Hemodynamic Monitoring Devices, pp. 395 –406. ISSN: 1521-6896. DOI: https://doi.org/10.1016/j.bpa.2014.08.006. URL: http://www.sciencedirect.com/science/article/pii/S1521689614000755.

[17] John G. Webster. *Design of pulse oximeters*. Informa, 1997.

[18] D. Castaneda et al. "A review on wearable photoplethysmography sensors and their potential future applications in health care". In: *International journal of biosensors & bioelectronics* 4.4 (2018), pp. 195–202. DOI: 10.15406/ijbsbe.2018.04.00125.

[19] John Allen. "Photoplethysmography and its application in clinical physiological measurement". In: *Physiological measurement* 28.3 (Mar. 2007). DOI: 10.1088/0967-3334/28/3/R01.

[20] T. Tamura, Y. Maeda, and M. Yoshida. "Wearable Photoplethysmographic Sensors - Past and Present". In: *Electronics* 3.2 (2014), pp. 282–302.

[21] F. Taffoni et al. "A Wearable System for Real-Time Continuous Monitoring of Physical Activity". In: *Journal of Healthcare Engineering* (Mar. 2018).

[22] M. Elgendi et al. "The use of photoplethysmography for assessing hypertension". In: *npj Digital Medicine* 2.1 (2019).

[23] Texas Instruments. *Application Report: How to Design Peripheral Oxygen Saturation (SpO2) and Optical Heart Rate Monitoring (OHRM) Systems Using the AFE4403*. Mar. 2015. URL: http://www.ti.com/lit/an/slaa655/slaa655.pdf (visited on 08/10/2020).

[24] Maxim Integrated. *Using reflectometry for a PPG waveform*. URL: https://www.maximintegrated.com/en/design/technical-documents/app-notes/6/6547.html (visited on 08/04/2020).

[25] STMicroelectronics. *STM32F411VE datasheet*. URL: https://www.st.com/resource/en/datasheet/stm32f411ve.pdf (visited on 07/15/2020).

[26] Texas Instruments. *TPS62740 datasheet*. URL: http://www.ti.com/lit/ds/symlink/tps62740.pdf (visited on 07/15/2020).

[27] Microchip. *MCP73831T datasheet*. URL: https://www.microchip.com/wwwproducts/en/en024903 (visited on 07/15/2020).

[28] STMicroelectronics. *STM6600 datasheet*. URL: https://www.st.com/resource/en/datasheet/stm6600.pdf (visited on 07/15/2020).

[29] Texas Instruments. *ADS1298R datasheet*. URL: https://www.ti.com/lit/gpn/ads1298r (visited on 07/15/2020).

[30] STMicroelectronics. *LIS2DH12 datasheet*. URL: http://www.st.com/resource/en/datasheet/lis2dh12.pdf (visited on 08/20/2020).

[31] Meina Li, Keun-Chang Kwak, and Youn Kim. "Estimation of Energy Expenditure Using a Patch-Type Sensor Module with an Incremental Radial Basis Function Neural Network". In: *Sensors* 16 (Sept. 2016), p. 1566. DOI: 10.3390/s16101566.

[32] TDK. *B57861S104F40 datasheet*. URL: https://www.tdk-electronics.tdk.com/inf/50/db/ntc/NTC_Mini_sensors_S861.pdf (visited on 07/15/2020).

[33] Panasonic. *ERTJ1VS104FA datasheet*. URL: https://www.tdk-electronics.tdk.com/inf/50/db/ntc/NTC_Mini_sensors_S861.pdf (visited on 07/15/2020).

[34] STMicroelectronics. *M41T62LC datasheet*. URL: https://www.st.com/resource/en/datasheet/m41t62.pdf (visited on 07/15/2020).

[35] STMicroelectronics. *Bluetooth Classic BT 3.0 modules*. URL: https://www.st.com/resource/en/product_presentation/blue_modules_ug_nov_2013.pdf (visited on 07/15/2020).

[36] Cypress. *S25FL256S datasheet*. URL: https://www.cypress.com/file/448601/download (visited on 07/15/2020).

[37] STMicroelectronics. *Description of STM32F4 HAL and low-layer drivers*. URL: http://www.st.com/resource/en/user_manual/dm00105879.pdf (visited on 07/18/2020).

[38] STMicroelectronics. *STM32CubeMX for STM32 configuration and initialization C code generation*. URL: https://www.st.com/resource/en/user_manual/dm00104712-stm32cubemx-for-stm32-configuration-and-initialization-c-code-generation-stmicroelectronics.pdf (visited on 07/20/2020).

[39] Massimo Carli. *Android 6: guida per lo sviluppatore*. Apogeo, 2016.

[40] Google. *Introduction to Activities*. URL: https://developer.android.com/guide/components/activities/intro-activities (visited on 07/25/2020).

[41] Google. *Fragments in Android*. URL: https://developer.android.com/guide/components/fragments (visited on 07/25/2020).

[42] Google. *Understand the Activity Lifecycle*. URL: https://developer.android.com/guide/components/activities/activity-lifecycle (visited on 07/25/2020).

[43] Google. *Bluetooth overview: Android developers*. URL: https://developer.android.com/guide/topics/connectivity/bluetooth (visited on 07/27/2020).

[44] Rigel medical. *Rigel 333 user manual*.

[45] M. K. Delano and C. G. Sodini. "A long-term wearable electrocardiogram measurement system". In: *2013 IEEE International Conference on Body Sensor Networks*. 2013, pp. 1–6.

[46] I. Wang et al. "A Wearable Mobile Electrocardiogram measurement device with novel dry polymer-based electrodes". In: *TENCON 2010 - 2010 IEEE Region 10 Conference*. 2010, pp. 379–384.

[47] S. Lee and W. Chung. "A robust wearable u-healthcare platform in wireless sensor network". In: *Journal of Communications and Networks* 16.4 (2014), pp. 465–474.

[48] Hristijan Gjoreski et al. "Telehealth using ECG sensor and accelerometer". In: May 2014, pp. 270–274. ISBN: 978-953-233-077-9. DOI: 10.1109/MIPRO.2014.6859575.

[49] E. Valchinov et al. "Wearable ECG system for health and sports monitoring". In: *2014 4th International Conference on Wireless Mobile Communication and Healthcare - Transforming Healthcare Through Innovations in Mobile and Wireless Technologies (MOBIHEALTH)*. 2014, pp. 63–66.

[50] E. Spano, S. Di Pascoli, and G. Iannaccone. "Low-Power Wearable ECG Monitoring System for Multiple-Patient Remote Monitoring". In: *IEEE Sensors Journal* 16.13 (2016), pp. 5452–5462.

[51] S. P. Preejith et al. “Wearable ECG platform for continuous cardiac monitoring”. In: *2016 38th Annual International Conference of the IEEE Engineering in Medicine and Biology Society (EMBC)*. 2016, pp. 623–626.

[52] Zephyr Anywhere. *Zephyr website*. URL: https://www.zephyranywhere.com/ (visited on 07/30/2020).

[53] Alive technologies. *Alive technologies website*. URL: https://www.alivetec.com/pages/alive-bluetooth-heart-activity-monitor (visited on 07/30/2020).

[54] STMicroelectronics. *STM32F407IE datasheet*. URL: https://www.st.com/resource/en/datasheet/stm32f407ie.pdf (visited on 08/20/2020).

[55] Texas Instruments. *TPS799 datasheet*. URL: https://www.ti.com/lit/gpn/tps799 (visited on 08/20/2020).

[56] STMicroelectronics. *L6924D datasheet*. URL: https://www.st.com/resource/en/datasheet/l6924d.pdf (visited on 08/20/2020).

[57] STMicroelectronics. *LSM9DS0 datasheet*. URL: https://www.mouser.it/datasheet/2/389/lsm9ds0-955023.pdf (visited on 08/20/2020).

[58] STMicroelectronics. *STM32L475RG datasheet*. URL: https://www.st.com/resource/en/datasheet/stm32l475rg.pdf (visited on 08/20/2020).

[59] Maxim Integrated. *MAX17048 datasheet*. URL: https://datasheets.maximintegrated.com/en/ds/MAX17048-MAX17049.pdf (visited on 08/20/2020).

[60] STMicroelectronics. *LSM6DSL datasheet*. URL: https://www.st.com/resource/en/datasheet/lsm6dsl.pdf (visited on 08/20/2020).

[61] STMicroelectronics. *HTS221 datasheet*. URL: https://www.st.com/resource/en/datasheet/hts221.pdf (visited on 08/20/2020).

[62] STMicroelectronics. *LPS22HH datasheet*. URL: https://www.st.com/resource/en/datasheet/lps22hh.pdf (visited on 08/20/2020).

[63] STMicroelectronics. *SPBTLE-RF datasheet*. URL: https://www.st.com/resource/en/datasheet/spbtle-rf.pdf (visited on 08/20/2020).

[64] Analog Devices. *ADP166 datasheet*. URL: https://www.analog.com/media/en/technical-documentation/data-sheets/ADP165_166.pdf (visited on 08/20/2020).

[65] Maxim Integrated. *MAX30101 datasheet*. URL: https://datasheets.maximintegrated.com/en/ds/MAX30101.pdf (visited on 08/20/2020).

[66] Maxim Integrated. *MAX30102 datasheet*. URL: https://datasheets.maximintegrated.com/en/ds/MAX30102.pdf (visited on 08/20/2020).

[67] Kevin Townsend et al. *Getting Started with Bluetooth Low Energy*. URL: https://www.oreilly.com/library/view/getting-started-with/9781491900550/ch04.html.

[68] Bluetooth SIG. *GATT Specifications | Bluetooth technology website*. URL: https://www.bluetooth.com/specifications/gatt/ (visited on 08/20/2020).

[69] M. Elgendi. “Optimal Signal Quality Index for Photoplethysmogram Signals”. In: *Bioengineering (Basel)* 3.4 (Dec. 2016), p. 21.

[70] Alexei Kamshilin and Nikita Margaryants. “Origin of Photoplethysmographic Waveform at Green Light”. In: *Physics Procedia* 86 (Feb. 2017), pp. 72–80. DOI: 10.1016/j.phpro.2017.01.024.

[71] R. P. Dresher and Y. Mendelson. “Reflectance Forehead Pulse Oximetry: Effects of Contact Pressure During Walking”. In: *2006 International Conference of the IEEE Engineering in Medicine and Biology Society*. 2006, pp. 3529–3532.

[72] Y. Zheng et al. “A clip-free eyeglasses-based wearable monitoring device for measuring photoplethysmograhic signals”. In: *2012 Annual International Conference of the IEEE Engineering in Medicine and Biology Society*. Aug. 2012, pp. 5022–5025. DOI: 10.1109/EMBC.2012.6347121.

[73] Sokwoo Rhee, Boo-Ho Yang, and H. H. Asada. “Artifact-resistant power-efficient design of finger-ring plethysmographic sensors”. In: *IEEE Transactions on Biomedical Engineering* 48.7 (2001), pp. 795–805.

[74] T. B. Fitzpatrick. “The validity and practicality of sun-reactive skin types I through VI”. In: *Archives of Dermatology* 124.6 (1988), pp. 869–871.

[75] Ethel Tur et al. “Basal Perfusion of the Cutaneous Microcirculation: Measurements as a Function of Anatomic Position”. In: *Journal of Investigative Dermatology* 81.5 (1983), pp. 442 –446. ISSN: 0022-202X. DOI: https://doi.org/10.1111/1523-1747.ep12522619. URL: http://www.sciencedirect.com/science/article/pii/S0022202X15432312.

[76] Maxim Integrated. *Guidelines for SpO2 measurement using the Maxim MAX32664 sensor hub*. URL: https://www.maximintegrated.com/en/design/technical-documents/app-notes/6/6845.html (visited on 08/22/2020).

[77] Cosinuss GmbH. *Cosinuss One technical data sheet*. URL: https://www2.cosinuss.com/en/products/one (visited on 06/25/2020).

[78] Bragi. *Dash Pro technical specifications*. URL: https://support.e-use.com/hc/en-us/articles/115003121785-The-Dash-Pro-Technical-Specifications (visited on 06/25/2020).

[79] M. Choi et al. “Wearable Device-Based System to Monitor a Driver’s Stress, Fatigue, and Drowsiness”. In: *IEEE Transactions on Instrumentation and Measurement* 67.3 (2018), pp. 634–645.

[80] Timo Tigges et al. “Assessment of In-ear Photoplethysmography as a Surrogate for Electrocardiography in Heart Rate Variability Analysis”. In: *World Congress on Medical Physics and Biomedical Engineering 2018*. Ed. by Lenka Lhotska et al. Singapore: Springer Singapore, 2019, pp. 293–297. ISBN: 978-981-10-9038-7.

[81] M. Poh, N. C. Swenson, and R. W. Picard. “Motion-tolerant magnetic earring sensor and wireless earpiece for wearable photoplethysmography”. In: *IEEE Transactions on Information Technology in Biomedicine* 14.3 (2010), pp. 786–794.

[82] S. Passler, N. Müller, and V. Senner. “In-Ear Pulse Rate Measurement: A Valid Alternative to Heart Rate Derived from Electrocardiography?” In: *Sensors (Basel)* 19.17 (Aug. 2019), p. 3641.